A Computational Model for Pulmonary Microcapillary Blood Flow

by

Amit S. Dhadwal

Bachelor of Science in Mechanical Engineering
(University of California, Irvine, 1993)

Submitted to the Department of Mechanical Engineerig in partial fulfillment of the requirements for the degree of

Master Of Science in Mechanical Engineering

at the

MASSACHUSETTS INSTITUTE OF TECHNOLOGY

May, 1995

Author .....
Amit S. Dhadwal
May, 1995

Certified by .....
Dr. Roger D. Kamm
Professor of Mechanical Engineering
Thesis Supervisor

Accepted by .....
Dr. Ain A. Sonin
Chairman, Departmental Committee on Graduate Studies

A New Model for Pulmonary Capillary Blood Flow

by

Amit S. Dhadwal

Submitted to the Department of Mechanical Engineering on May 9, 1995, in partial fulfillment of the requirements for the degree of Master of Science in Mechanical Engineering

Abstract

The pulmonary alveoli or 'air sacs' of thin tissue constitute the gas-blood interface for gas exchange with blood in the alveolar septum - a network of compliant capillaries between adjacent alveoli. Blood-flow through the septum is a function of septum physiology and morphology, blood and alveolar pressures, blood rheology, and lung volume. The goal of this thesis is to include these features to model blood-flow in the septum.

Two models that include the effects of breathing, blood rheology, spatial variability in septal compliance and septal height at zero transmural pressure (α and h_o), were developed. A previous model by Fung in which blood flow is simulated as occuring in the space between two compliant sheets was extended to include breathing by transforming the equations from an Eulerian to a Lagrangian frame; where breathing was assumed to change the lateral dimensions of the septum isotropically, varied as the cube root of lung-volume. A second model was developed to facilitate the analysis of red blood cell and neutrophil transit through the pulmonary capillaries. The 'tube-model' was developed for a square array (of side 75 μm) of 60 segments, 32 junctions, and 5x5 cylindrical, distensible 'posts'. The lateral septal (and post) dimensions were assumed to change isotropically during breathing; post-height was varied assuming a constant post volume.Quasi-steady inertia-free flow was assumed. Spatial variability in h_o and α was imposed by a random selection from a normal distribution. Pressure was imposed on the boundaries.Results from the revised Fung's model compared well with earlier analytic predictions. Flow rates from the 'tube-model' were in good agreement with Fung's model. A friction factor was computed that was in good agreement with exact analysis by Weinbaum et. al. The model was used to explore the effects of breathing and pulsatility in boundary pressures, the effects of spatial variability in h_o and α, and the effects of capillary blockage. It was shown that breathing had a significant impact on local capillary resistance, with oscillations as high as 45% of the mean value. Neither capillary blockage nor spatial variability, coupled with breathing changed the nature of flow- oscillations in the capillaries, only the mean values. Pulsatility in boundary pressures had little affect on the flow-rate oscillations. The static cases demonstrated that spatial variabilily in h_o and α resulted in preferentially perfused regions, with variability in h_o dominating the effect of variability in a. Capillary blockage resulted in local flow disturbances, with its effect diminishing with increasing variability in h_o and α. The study of RBC & PMN transit is therefore an important application of the 'tube-model'.

Thesis Supervisor: Professor Roger D. Kamm.
Title: Professor of Mechanical Engineering

Acknowledgements

I am most grateful to Prof. Roger D. Kamm for being an understanding advisor, an inspiring teacher and a great mentor. I thank him for his guidance in always pointing me in the right direction, for his invaluable scientific insight, and for his confidence in my abilities even at times when I found my progress stagnating. Many thanks to Dr. Barry Wiggs for providing me with his time, patience, motivation and knowledge in the completion of this thesis, and for his distinctive sense of humor in making MIT a more fun place to be. A special note of thanks to Dr. Derek Dunn-Rankin at UC Irvine for being an inspiring mentor and for encouraging me to attend MIT.

"The MIT experience" has been an enriching one - one filled with challenge, hard work, learning, and fun. Thanks to the unique Fluid Mechanics Lab Community for adding a colorful perspective to graduate student life, and for being supportive friends in times of need. Thanks to James "Mr. Gold" Shin, Edwin "B" Ozawa, Art, Serhat, Frank, and MG for being motivating friends and good human beings. I would specially like to acknowledge MG and Serhat for their computer help (and answering the high order of magnitude telephone calls !)- my buddies Hemant, Vishnu and Sankar "Mr. Perspective" Sunder for their support and advice.

Special thanks to Samina Choudhury, for being a mature, understanding, and loving friend, even at times when work demanded precedence over our friendship- thank you for your time, your unconditional support, and your car :).

I am indebtted to my father, my mother, and brother for always supporting me, cutivating an interest in science in me, guiding me toward engineering, and for being a motivating and caring family. Thank you for always being there, despite our physical separation of 20,000 miles !

Lastly, I would like to dedicate this thesis to my father for always being a mentor and a best friend, and to my mother, whose relentless ailment with acute bronchitis for the past 18 years has often left me frustrated, and has motivated me to understand and fight pulmonary disease.

This work is dedicated to my parents.....

..... Thankyou

Table Of Contents

List Of Figures

List Of Tables

Chapter 1

Introduction

1.1 Overview

The human lung is a complex organ with over twenty-three generations of airway branching beginning at the trachea and culminating at the alveoli. The walls of the alveoli or "air-sacs" (figure [1.1]) form a thin gas-blood across which oxygen and carbon-dioxide are exchanged. A partial pressure-gradient across the interface drives the gas exchange by diffusion and approximately 300 million alveoli provide over 100 square meters of surface area for this exchange (West, 1974). A highly interconnected capillary network (figure [1.1]) between adjacent alveoli conveys blood through the interface for gas exchange; the focus of this thesis is to model the blood-flow in this network.

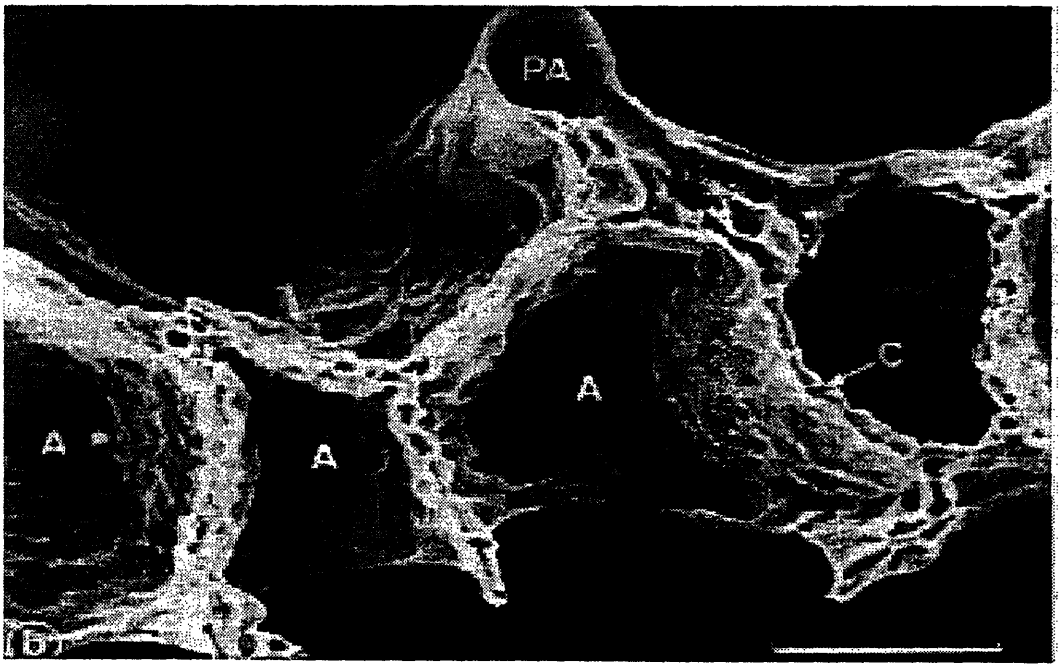

Figure 1.1: Connection between pulmonary artery (PA), capillary network(C) and alveolar walls (A) in a perfusion-fixed rabbit lung. Scale marker:50 μm. Taken from "The Lung, Scientific Foundations", [5].

1.2 Pulmonary blood vessels

The anatomy of the capillary vessels (fig [1.2]) makes the lung an efficient organ for gas exchange. Blood in the pulmonary capillary network is conveyed from the pulmonary arterioles to the venules, with gas exchange occurring during this transit. The alveolar septum, which contains the microcapillary region, consists of a highly interconnected network that lies in the plane of the septum. Separating the blood from alveolar gas are the vascular endothelium, a narrow interstitial space, the alveolar epithelium, and the alveolar liquid layer. This entire distance from blood to alveolar gas across the gas-blood barrier may be as small as 0.5 μm, thus greatly enhancing the rate of gas exchange. Each red blood cell spends about 3/4 sec in the capillary network, in which time it traverses about two or three alveoli and achieves nearly complete equilibration of exchanged oxygen and carbon-dioxide (West, 1974).

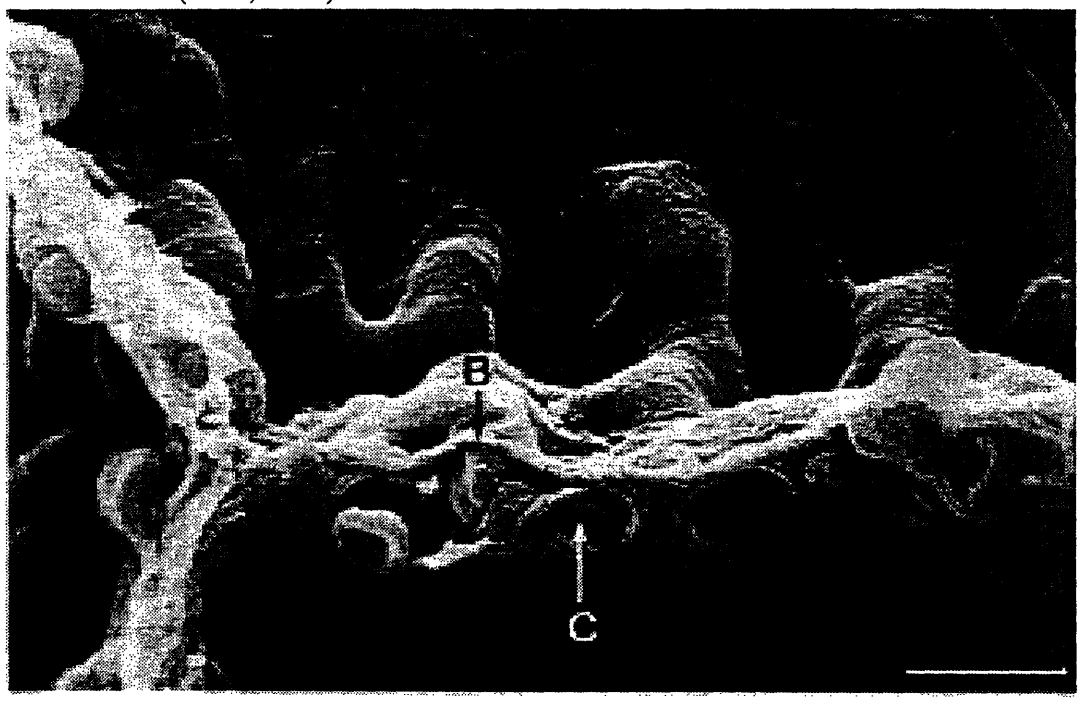

Figure 1.2: Scanning electron micrograph of the alveolar wall in the human lung. Scale marker: 10 μm. (From ref. [5]).

Since the pulmonary capillaries in the lung lack the surrounding tissue found in the systemic vessels, the walls of the pulmonary vasculature are more compliant than those of relatively high pressure systemic circulation [11]. As an example, while the blood capillaries in the systemic blood vessels show a negligible change in diameter with changes in pressure, the pulmonary capillary height varies linearly with changes in the transmural pressure [12], changing approximately 0.1 μm for every 1 cm H_2O change in transmural pressure (based on compliance measurements, Fung & Sobin ([14]). This high compliance causes the relationship between blood flow and arteriolar-venular pressure differences to be non-linear.

The lung vasculature is a low pressure system, ranging from a right ventricular pressure of about 12 mm Hg to a left atrial pressure of 2.5 mm Hg (Fung, 1984), and approximately 34% of this pressure difference is thought to occur across the pulmonary capillaries (Hakim, 1981).The variability in capillary pressures can be considerable however, owing to such factors as hydrostatic gradients, viscous pressure drops, and breathing. The flow per unit volume increases in the direction of gravity since gravity affects the hydrostatic head of the blood pressure; gravity thus plays an important role in the blood flow distribution in the lung (West, 1974).

Bhattacharya [3], in his editorial article, has discussed the issue of determination of microvascular pressures in the lung. While it was earlier the belief that a single value for the microvascular pressure was sufficient for the description of filtration data, Bhattacharya et al [4] and Kadowitz et al. [20] have shown that the pressure varies markedly across the microvascular bed. One important aspect of the microvascular pressures concerns the question of how these microvascular pressures are controlled. Bhattacharya [3]

has pointed out that recent findings indicate that arterioles and venules vasoconstrict independently, thus allowing for independent control of arteriolar and venular resistance to flow.

1.2.1 Flow distribution in the whole lung

Gravity plays an important role in the distribution of pressures and flows in the entire lung. The effect of the hydrostatic head due to gravity may be seen in figure [1.3])(taken from West), that shows a vertical gradient of blood flow-rate within the lung.

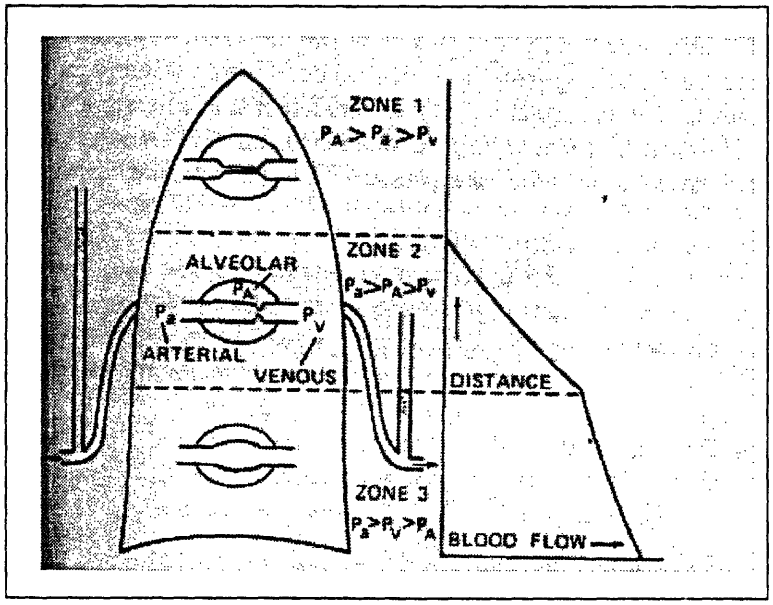

Figure 1.3: The influence of gravity on the pressure distribution in the lung.Model to explain the uneven distribution of blood flow in the lung, based on the vertical pressure-gradient due to gravity.[Taken from West, 1990].

Since the pressures in the upper regions of the lung are relatively lower than the pressures in the lower regions (Figure [1.3]) due to the hydrostatic head, the upper regions are less-perfused than the lower regions of the lung. Currently available data suggest that the greater part of the cardiac output passes through the gravitationally dependent regions of the lung ([19]; West 1990), thus leaving many of the upper lung capillaries unperfused

or underperfused. Also, the capillary diameters in the upper regions of the lung are smaller than the ones in the lower, more perfused regions of the lung. This variation in capillary size and degree of perfusion is important for the transit of RBC's and other cells in the blood (e.g. PMN's). It is known that a large vertical gradient of RBC transit times exits in the lung, with the RBC's taking longer to traverse through regions of low perfusion ([40])

1.3 Blood flow in the pulmonary microvasculature

Blood is a suspension of cells in plasma. The plasma, a solution of proteins, electrolytes and other substances, is an incompressible, virtually Newtonian fluid [41] with a viscosity of approximately 1.2 cP. The cellular fraction contains red blood cells (erythrocytes), white blood cells (leukocytes), and platelets. The volume fraction of red blood cells (hematocrit) is about 45% in humans, and therefore has a key influence on the blood's flow properties.

Mechanical and viscous properties of human red blood cells have been extensively studied, and are probably known better than those of any other cell type (Skalak, 1976; Hochmuth and Waugh, 1987). A thin membrane surrounds the cytoplasm and this membrane exhibits viscoelastic properties. The elastic shear modulus is several orders of magnitude lower than the modulus of isotropic dilation and this results in the membrane shearing readily but resisting changes in area. Also, the bending resistance is small unless very small radii of curvature are involved (Evans, 1983) and the membrane primarily exhibits shear viscosity in transient deformation (Secomb, 1984).

In the absence of external stresses, a human RBC is a biconcave disk, approximately 8 microns in diameter and 2 microns thick. Due to the fluid interior of the cell, and the low resistance of the membrane to shear and bending deformations, it is highly deformable, as

long as changes in surface area and volume are not required; this allows RBC's to pass through capillaries with diameters as small as 2.8 microns (Halpern and Secomb, 1989).

The mechanical and viscous properties of blood are modified in several diseases, including sickle cell anemia, malaria, and diabetes. Blood acidity and oxygenation also influence the mechanical properties of blood. Perhaps one of the most extensively studied mechanical property of blood is the viscosity of blood in different environments.

1.3.1 Blood Viscosity

The viscosity of blood traversing through a microvessel has been studied extensively. Starting with Martini et al. (1930) and Lindqvist (1931), numerous studies have been made regarding the viscosity of blood. Since blood does not behave as a continuum for flows in vessels with diameters below 300 microns (Fahraeus Lindqvist effect), the viscosity of blood depends on the size and shape of the vessel and is characterized by either the 'apparent viscosity, μ_{app}', or the "relative apparent viscosity, μ_{rel}", which are complex functions of several parameters such as the flow hematocrit (% RBC content by volume), size of the vessel etc. These parameters are described in relation to the pressure drop that would occur in Poiseulle's Law for a tube of length L, and diameter, D, and are defined as:

$$\mu_{app} = \frac{\pi \Delta p D^4}{128 L} \tag{1.1}$$

$$\mu_{rel} = \frac{\mu_{app}}{\mu_{plasma}} \tag{1.2}$$

The study of blood and blood viscosity in small capillaries and larger vessels has been a subject of great interest. As stated earlier, blood is a suspension of cells in plasma. As the size of vessels decrease (diameters < 300 microns), the apparent viscosity of blood at first

decreases (Fahraeus-Lindqvist effect). However, a reversal of this trend occurs in very small microvessels (< 5-7 microns in diameter), where the apparent viscosity of blood tends to infinity as the diameter approaches a critical value of about 2.8 microns. Amongst other things, blood hematocrit and shear-rate also influence apparent viscosity, but the effects of shear-rate are usually small compared to those of vessel diameter and blood hematocrit ([24]).

The direct measurement of apparent viscosity of blood in actual capillary beds, while technically challenging, has been accomplished recently by Pries et. al. (1990). One important finding from their work was that there was a large discrepancy between *in-vivo* and *in-vitro* apparent viscosities of blood, and it was observed that the models (e.g. Pries, 1990) and experiments through glass tubes with corresponding diameters tend to under-predict the resistance of the capillary bed.

In addition, Kiani et. al. [16] have shown that the axial diameter variability along a microvessel has a large effect on the pressure drop calculation as opposed to calculating the pressure drop based on a mean diameter; and that the effect is larger for smaller vessels. All of the above considerations play a key role in the transit of RBC's through capillary networks.

1.3.2 RBC transit through capillary networks: distinction between the Capillary flow and Sheet flow approaches

The motion of blood cells through a network of microvessels is a complex problem. Historically, one of two approaches have been adopted for the treatment of RBC motion through systemic capillaries, namely the tube-flow and the sheet-flow approaches. The first treats the capillary network as a network of interconnected segments, while the latter

treats the capillary blood flow as flow between as two compliant walls, incorporating the effect of resistance due to connective tissue in terms of a net friction factor.

Capillary flow approach

The first approach has been to treat blood as suspension of cells in plasma (or as two distinct phases); the plasma, a solution of proteins and other substances, and the cells such as RBC's, WBC's (White blood cells), and platelets. However, as stated previously, since normal human blood has about 45% RBC's by volume, they generally exert a dominant influence on the flow properties of blood.

In the capillary flow model, the transit of blood 'suspension' is assumed to occur through a network of cylindrical tubes. The work of Lighthill [28] and Barnard [2] on the motion of axisymetric RBC's through capillaries using lubrication theory provided the groundwork for this approach. These models were further developed by the work of others (Secomb and Gross, 1983, Secomb et al, 1986, Zarda, Chien and Skalak, 1977). Under these approaches, the RBC's are treated as a relatively flexible, highly deformable membrane surrounding the cytoplasm. This deformability allows the RBC to pass through tubes much smaller than its diameter, the minimum capillary diameter being 2.8 microns. Models of flow through networks of such capillary segments require an expression for the apparent viscosity of blood that accounts for dependence of blood viscosity on the capillary diameter, and reflects the increase in viscosity as the capillary diameter approaches the critical value of 2.8 microns.

Sheet flow approach

The second approach, the sheet-flow model developed by Fung & Sobin (1969) was utilized to better capture the characteristics of flows through networks with a high degree

of interconnectedness such as the ones in the lung or the retina. In this case, blood flow is modelled as flow between two compliant "sheets" attached to each other by "posts" of connective tissue. The interaction of the RBC's with the wall in this case is represented by two parameters; one that accounts for the effect on flow-resistance due to the presence of the posts (connective tissue between the sheets) and another representing the effect of the confining of RBC's within the sheets. A separate parameter characterizes the mechanical distensibility of the alveolar sheet, also known as the sheet compliance. This was determined experimentally by Fung and Sobin (1972a) [14]. Using the sheet-flow model, Fung was able to make analytic predictions of flow velocities and pressure distributions in the alveolar septum. The model was developed for the case of a stationary septal wall, thereby neglecting the effect of septal wall motion due to breathing; further, in its present form, the capillary networks are represented as having single-input single-output flow conditions and uniform properties.

1.4 Solution methods for capillary network problems

Based on either approach taken in the two models described in the above sections, blood flow in interconnected networks may be analyzed by developing computational models in order to simulate blood-transit. While the behavior of blood in microvessels larger than 10 microns is a complex phenomenon, theoretical studies of the motion of cells through thinner tubes will be useful to the modelling approach. Further, since there is a large degree of heterogeneity in microvascular networks, simulations must be able to account for this.

In the past, network studies have been performed by taking into account the effects of segments and bifurcations; at any junction of two or more segments, the distribution of RBC content by volume (hematocrit) in the daughter segments has been derived as a func-

tion of various parameters of the bifurcation and the parent hematocrit ([34] & [35]). Under this approach, with mass being conserved at every junction and the flows being specified in terms of segment pressures, a linear system of nodal pressures is obtained. However, in a more rigorous approach, including the effect of bifurcations and relating the resistances to the red cell content which in turn depends on the flows, one obtains either a computationally intense problem or a non-linear problem that must be solved iteratively ([39], [35]). Pries et.al. (1990) made a comparison of hemodynamic properties between results obtained experimentally and results from heterogenous network model; they made the comparison for the hematocrits and velocities in networks of rat mesentry containing 383 to 913 segments. They concluded that the flow resistance was underpredicted by the models and that the actual apparent viscosities were substantially higher than those observed in glass tubes. The cause of this discrepancy is unknown, but several possible explanations were offered: the effect of WBC resistance that are often removed from glass tube experiments, a layer of macromolecules that line the inner lumen of the vessels which might reduce the cross section available for flow, asymmetric radial distributions of red cells within microvessels *in vivo*, and finally, the irregularity of the interior of the microvessels *in vivo*.

Before proceeding to develop one such model, one needs to have an idea of the morphology of the capillary network and its properties, knowledge of the behavior of blood in small capillaries, and estimates of pressure (and flow) distributions within the lung.

1.5 Neutrophil (PMN) transit in the pulmonary microvasculature

Neutrophils are a type of leukocyte found in blood and are known to "reside" in the pulmonary microvasculature; studies in several species indicate that the pulmonary microvas-

culature is a large site of marginated or "stored" neutrophils ([1], [6]); the concentration of neutrophils in the capillary network being 30-100 times higher than the concentration found in larger systemic capillaries([4],[14]). The increased concentration of neutrophils in the lung is thought to be the result of longer transit times required for the neutrophils compared to the RBC's traversing the capillary network, where the capillary size is typically comparable to or smaller than the RBC and PMN diameters ([47]). It is believed that this relatively longer PMN transit time may be due to two primary reasons; the difference in deformability between RBC's and PMN's, and the ability of PMN's to behave actively by a rearrangement of cytoskeletal components, cytoplasmic organelles, or action of adhesion molecules on the endothelium, thereby changing viscoelastic properties.

The difference in deformability may be attributed to a difference in geometric and mechanical properties of RBC's and PMN's. The RBC's are shaped as biconcave disks, which makes them more deformable than spherical PMN's of comparable diameters. In addition, PMN's are mechanically more rigid than RBC's and undergo mechanical deformations less readily ([47]). Several investigators have pointed out that this difference in deformability can explain why an RBC can enter smaller capillaries much more quickly than the less deformable neutrophils [38].

Factors, other than deformability, also influence the tendency for PMN's to marginate in the capillary network is their ability to behave actively (adhesion molecules on the cell surface, rearrangement of cytoskeletal components etc.). These mechanisms are also thought to alter the viscoelastic properties of the PMN's, thereby influencing the response of neutrophils to external forces. As a result, time-dependent pressure gradients (due to breathing) and viscous forces in the septum play a key role in the mechanics of neutrophil transit through the capillary network.

Some recent work on modelling neutrophil margination exists, and comparisons have been made with experimental results; however, there are discrepancies between experimental studies and predictions from computational models. For example, videomicroscopic studies by Lien et al.([24], [25]) showed that 40-45% of neutrophils were able to pass through the pulmonary capillary bed with a transit time similar to that of RBC, while the remaining 55-60% stopped at least once, and that the neutrophils had longer transit times than RBC's. A computer simulation of PMN transit, however, predicted that 55-60% of PMN's stop at least once if only 1-2% of the segments presented obstructions to the PMN's ([18], [29]); if a larger percentage (>1-2%) of capillaries provided obstruction to PMN transit, the percentage of delayed neutrophils would be even more. Morphometric measurements, however, reveal that more than 60% of capillary segments are narrower than PMN's and would therefore obstruct the motion of a neutrophil. This discrepancy between the computational prediction and videomicroscopic studies coupled with morphometric measurements showing that more than 60% of the capillary segments are narrower than a neutrophil diameter suggests that neutrophil transit must be facilitated in some way in order to overcome the obstruction due to capillary size.

While PMN's are less easily deformed than RBC's, they can change shape. The deformation of neutrophils while traversing the capillary bed was quantified by measuring the longest diameter and the diameter perpendicular to the longest axis using intratracheal instillation of glutaraldehyde; it was observed that while neutrophils in suspension were close to spherical, the ones in the capillary network were elongated substantially ([8]). It is believed that the neutrophils take longer to deform than do RBC's while entering capillary segments with a diameter narrower than the neutrophil diameter ([8],[47]). Further, the

multi-segmented geometry of the pulmonary bed provide several parallel pathways to allow the faster moving RBC to stream around slowly deforming neutrophils that are temporarily obstructing a capillary.

Pressure gradients across a neutrophil in a capillary segment will influence the time required for neutrophil deformation and eventual passage through a narrower capillary as has been shown in *in-vitro* experiments.([9],[38]). However, pressures used in these experiments are considerably greater than those that would exist across a single capillary segment in the lung and the times for neutrophils to enter and traverse the micropipets are therefore less than observed i*n vivo* ([32]).

In summary, RBC and PMN transit in the septum needs to be addressed in order to understand phenomena associated with their transit (margination, transit time etc.). The first step in this direction is to develop a comprehensive model that incorporates the septal anatomy and morphology, as well as blood rheology and neutrophil mechanics. The influence of the effects of breathing, the effects associated with anatomical and morphological variability in septal properties on the pressures and perfusion patterns in the septum are not well known.

The primary motivation for the current work is the simulation of RBC and neutrophil transit through the pulmonary capillary bed in the lung. In particular, we seek to better understand the role of neutrophil mechanics in determining transit times through a network of capillaries, given a computed flow field and blood pressure distribution in the capillary bed. We would like to be able to tie the mechanics of neutrophil transit with the fluid mechanics of the capillary bed as well as the solid mechanics of the alveolar septum and septal posts.

1.6 Problem Statement

The goal of this thesis is to develop a computational model for pulmonary capillary blood-flow that incorporates the morphometrics and the mechanical properties of the alveolar septum and the viscous characteristics of blood in order to simulate flow through the septal capillary network. Subsequently, this study will address transport of RBC's and PMN's through the capillary network. In particular, our aim is to the compute and quantify the time-dependent pressure gradients and flow velocities that exist within the alveolar septum, taking into account the effects of septal stretching resulting from breathing.

This thesis presents two different approaches to the problem of blood flow through a single septum. First, it looks at the sheet-flow model developed by Fung & Sobin, and then modifies the equations to include the effects of breathing and variability in septal properties. The solution under this approach is based on spatial finite-point discretization and standard finite differencing methods for time integration.

In the second approach, a capillary network model is developed in which the alveolar septum is represented as a dynamic network of collapsible tube segments. The effects of breathing are still incorporated into the modelling; in addition, the model incorporates a time dependent segment geometry and is capable of incorporating statistical variability in the sheet properties. With the help of this model, we hope to be able to demonstrate the effects of breathing on the flow in the capillary bed, the effect of statistical variability in the properties of individual segments on the flow in the capillary bed, and also couple the above in order to simulate a realistic scenario of blood flow in the septum. The solutions obtained may then be used to simulate RBC transit times through the capillary bed.

Chapter 2

The Sheet Flow Model

2.1 Introduction: Fungs sheet flow model

This Chapter presents the pulmonary microcirculation model developed by Fung ([13]). In addition, modifications to Fung's sheet-flow model that incorporate the effects of breathing are also described.

Fung's sheet-flow model views blood flow in the alveolar septum as passing between two compliant membranes (of fixed overall dimensions) which are connected by 'posts' of connective tissue (Figure [2.1]). The two membranes make up the space between adjacent alveoli across which gas exchange takes place, the walls of each alveolus being shared by a network of capillary blood vessels. Together these comprise the 'interalveolar septum', a sheet of capillary blood vessels exposed to air on both sides.

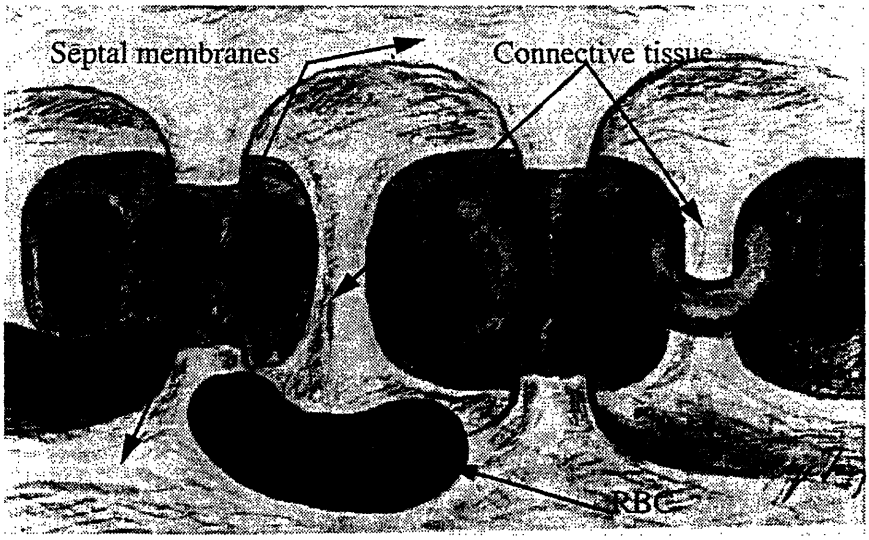

Figure 2.1: Schematic of an 'Interalveolar Septum'

The membranes (alveolar septae i.e) continually undergo cycles of stretching and relaxation due to the expansion and contraction of the lung during a breathing cycle. Here I

extend Fung's model to include the effects of breathing by allowing the septae to stretch (and relax) due to the expansion (and contraction) of the lung during breathing.

In the sheet flow approach, Fung et al.(1969) incorporated the effects of the flow-passage geometry as well as the rheological characteristics of blood. Flow within the alveolar septum with the exact geometries and mechanical properties of the septum is a complex problem to characterize and solve. Fung's model incorporates the effect of the posts as a lumped resistance friction factor. With these assumptions, Fung's model treats the flow in the septum as the flow between two compliant membranes as shown in figure [2.2]. The equations characterizing the flow are developed using dimensional analysis combined with empirically-based laws describing mechanics of the septum.

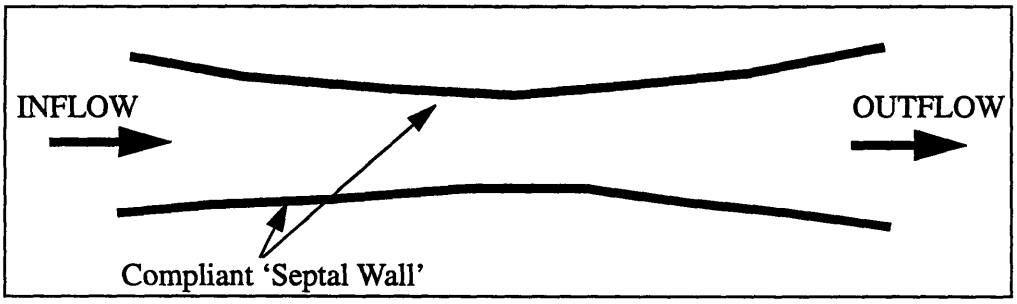

Figure 2.2: Simplified Sheet flow Model

This chapter presents Fung's model, and then revises it to incorporate the effects of breathing. The revised equations utilize a coordinate transformation from an Eulerian to a Lagrangian frame of reference. The transformation equations and boundary conditions are derived and cast in non-dimensional form. The finite difference scheme and computational procedure are then presented. Finally, Fung's sheet model is compared to the revised model.

2.2 Fungs sheet flow model

2.2.1 Pulmonary microvasculature in the sheet model

Fung's model idealized the pulmonary capillaries as two compliant membranes separated by equally spaced "posts" depicted here as a collection of hexagonal elements with a cylindrical post at the center of each (Figure [2.3]).

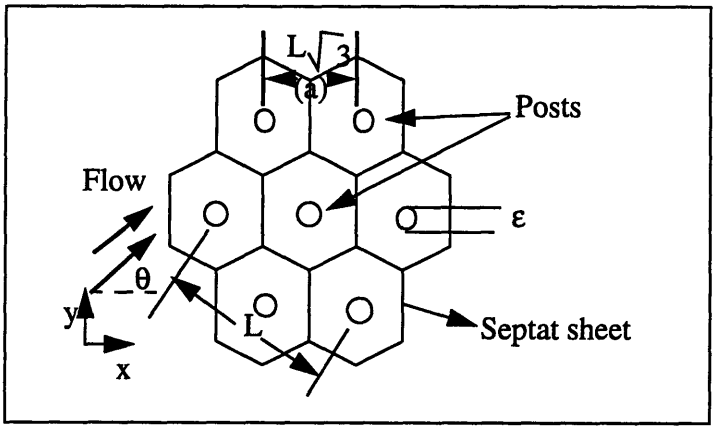

Figure 2.3: Sheet flow model: Septal geometry in the plane of the sheet

2.2.2 Development of Modelling equations

The geometry of the 'sheet' microvascular system and the mechanical properties of the septum are described by the following parameters:

- The VSTR, or the vascular space to tissue ratio. This defines the ratio of Vascular lumen volume to the volume of connective tissue between the connective tissue.The VSTR is assumed to be independent of the sheet height, and reduces to the fractional area occupied by blood in the XY cross sectional plane (Fig. [2.3]).
- The post diameter ε.
- The blood Hematocrit, *H*.
- The spacing between the posts, *a*
- The width of the sheet, w.

- The red cell diameter, D_c
- The elastic modulus of the red cell membrane, E_c.
- The orientation of the mean flow with respect to a reference line (X axis) defining the postal pattern, θ.
- The characteristic angular frequency of oscillation (breathing or heart rate) is given by ω.
- Blood viscosity given by μ_o.

The variables of the sheet flow model are the local fluid pressure, *P*, the local fluid velocity components *U (*in the x direction*)* and *V* (in the y direction*)*, the local sheet height, *h*.

Based on this set of variables and using results for viscous flow between parallel plates, the following dimensionless groups may be obtained (Fung 1984).

$$\frac{h^2}{\mu_o U}\nabla P = F\left(\frac{D_c}{h}, \frac{\mu_o U}{E_c h}, N_r, \frac{h}{2}\sqrt{\frac{\omega\rho}{\mu_o}}, H, \frac{w}{h}, \frac{h}{\varepsilon}, \theta, VSTR\right)$$

Where:

$\frac{h}{2}\sqrt{\frac{\omega\rho}{\mu_o}}$ = Womersly number

$\frac{\mu_o U}{E_c h}$ = cell strain parameter

$\frac{Uh\rho}{\mu_o} = N_r$ (Reynolds number)

For blood flow in the septum, both the Reynolds number and the Wormersley number are much smaller than 1, and thus inertial effects may be neglected (Fung 1984). This implies that the density is unimportant and the flow is quasi-steady. In order to investigate the function, *F*, Lee and Fung(1968), Lee(1969), Fung(1969), and Yen and Fung(1973)

conducted theoretical and experimental studies on particulate flow in the alveolar sheet. These papers argued that the dependence of F could be described as a product of three factors, namely, *F'*, *k*, and *f*:

$$\nabla P = -\frac{\mu_o U}{h^2} F'\left(\frac{D_c}{h}, \frac{\mu_{oU}}{E_c h}, H\right) k\left(\frac{w}{h}\right) f\left(\frac{h}{\varepsilon}, \frac{\varepsilon}{a}, \theta, VSTR\right) \tag{2.1}$$

The function *F'* accounts for the RBC geometry and mechanical properties and their net effect on the flow, *k* incorporates the effect of finite sheet width, while *f* represents the effects of septal geometry and flow orientation.

The above equation may be abbreviated as

$$\nabla P = -\frac{U}{h^2}\mu_{app} kf \tag{2.2}$$

Where μ_{app} stands for the apparent viscosity of whole blood. The function *k* is given by the following expression (Purday, 1949).

$$k = \frac{12}{\left(1 - 0.63\frac{h}{w}\right)} \tag{2.3}$$

for h/w<0.2

The function *f* is called the geometric friction factor and depends on the bed geometry, the orientation of the flow, the distribution of the connective tissue 'posts' within the septum and the post geometry (Lee 1969).

2.2.3 Analytic Formulation of the modelling equations

Since the flow solution incorporating the individual posts, red cells, membrane deflections

and other effects is difficult to solve, a simpler approach utilizing 'averaged' equations was developed by Fung (1984). The idea behind this approach is to separate the flow field into a local disturbance component and a relatively smooth "mean flow", and to incorporate the effect of the posts by a lumped resistance (f and k). Consider the cartesian frame described in Figure [2.3]. The velocity field is integrated along the z direction (from limits $z=0$ *to* $z=h$) in order to yield a 2 dimensional velocity field.

The idea behind this formulation is to seek the local mean velocities and local mean pressures ($P(x,y)$). Based on the dimensional analysis approach developed by Fung(1984) in section [2.2.2], the following equations may be derived.

Conservation of Momentum

$$\frac{\partial P}{\partial x} = -\frac{\mu U}{h^2} kf \tag{2.4}$$

$$\frac{\partial P}{\partial y} = -\frac{\mu V}{h^2} kf \tag{2.5}$$

These equations may be written in vector form as

$$\nabla P = \left(\frac{\mu kf}{h^2}\right) \hat{V}_{fluid} \qquad \text{(in 2-D)} \tag{2.6}$$

Where is the gradient a two-dimensional operator given by (2.7)

$$\nabla = i\frac{\partial}{\partial x} + j\frac{\partial}{\partial y} \tag{2.8}$$

Conservation of Mass (Equation of continuity)

Conserving the net mass inflow with the net mass outflow and the net mass stored in a control volume of height h, one obtains the following (Fung 1984).

$$\frac{\partial}{\partial x}(Uh) + \frac{\partial}{\partial y}(Vh) = -\frac{\partial h}{\partial t} \tag{2.9}$$

assuming negligible mass flux through the alveolar septum.

Constitutive P-h relationship

The following linear constitutive P-h relationship, based on experimental data obtained from cats, was introduced by Fung and Sobin (1972a,b),

$$h = h_o + \alpha (P - P_o) \tag{2.10}$$

Here, P is the local blood pressure, h is the local sheet height, P_o is the alveolar gas pressure, h_o is the sheet height when the local blood pressure equals alveolar pressure, and α is the compliance of the septum.

In reality, the compliance, α,is a function of location on the septal membrane, and also a function of lung volume. Yen and Fung [41] determined the spatial variation of the compliance of arterioles and venules in human lungs using silicone elastomer preparations, indicating that venules ('venules' of order 1 fall in the 18 micron range for their work) have a higher compliance than the arterioles of similar sizes. Fung and Sobin [14] have derived the following expression for the dependence of α on the properties (geometric and mechanical) and the tension, T, along the septal wall.

$$\alpha = \frac{\partial h_p}{\partial p} + \frac{c^2}{4\Gamma T}(2K_2K_3 - K_2 + \Lambda K_2K_3) \tag{2.11}$$

Here h_p is the height of the posts; c, K_1, K_2, K_3, Λ and Γ describe the sheet geometry and size, and T is the membrane tension.(Note as T approaches infinity, the second term in eq [2.11] approaches zero).

(for a full description of the variables of equation [2.11], refer to Fung and Sobin [14])

Equation [2.11] shows that the sheet gets 'stiffer' to changes in height with increasing tension (for example at high lung volumes). This equation, however, was never used in the actual models of alveolar blood flow. Instead, the model relied on experimentally-determined values of sheet compliancel *[12]*.

When the compliance is determined from experiments, equations [2.6]-[2.10] completely define the sheet flow model

2.3 Transformation of the sheet-flow equations

2.3.4 Coordinate transformation

Beginning with Fung's model for septal flow at a fixed lung volume, the equations may now be modified to simulate breathing and other sources of time-dependent behavior. The first stage is to model the septum as a square sheet of length *L(t)* (Fig [2.4]).

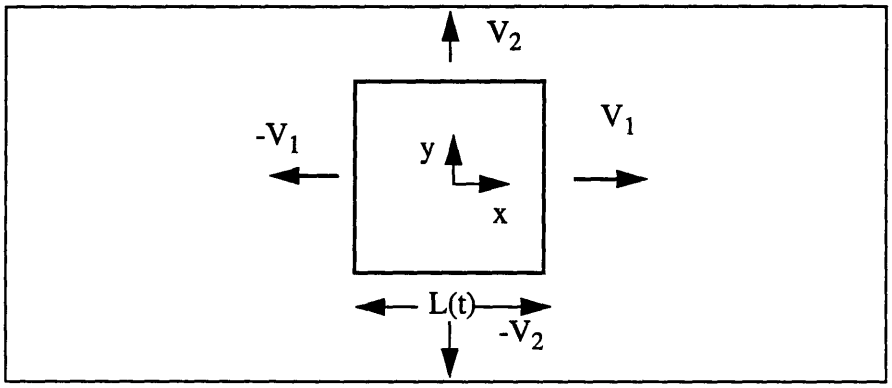

Figure 2.4: Septal sheet geometry and sheet motion

V_1 and V_2 are the velocities of the edges of the sheet in the x and y directions respectively with respect to a fixed point at the origin (fig. [2.4]). L(t) is the length of the sheet.

The equations are transformed from the Eulerian coordinate system (x,y) to the Lagrangian frame (ξ,η) fixed to the moving septum wall. The variables in these two frames are related by the following

$$x=L(t)\xi \tag{2.12}$$

$$y=L(t)\eta \tag{2.13}$$

Therefore

$$\left(\frac{\partial x}{\partial t}\right)_{\xi} = \xi V_1 \tag{2.14}$$

$$\left(\frac{\partial x}{\partial \xi}\right)_{t} = L(t) \tag{2.15}$$

Based on these equations, the partial derivative of any quantity Z(x,t) is:

$$\left(\frac{\partial Z}{\partial \xi}\right)_{t} = L\left(\frac{\partial Z}{\partial x}\right)_{t} \tag{2.16}$$

$$\left(\frac{\partial Z}{\partial t}\right)_{\xi} = \xi V_1\left(\frac{\partial Z}{\partial x}\right)_{t} + \left(\frac{\partial Z}{\partial t}\right)_{x} \tag{2.17}$$

2.3.5 Transformation Equations

The equations are non-dimensionalized using the following parameters. Variables sub-scripted 'c' imply characteristic values.

$$\xi=X/L(t) \tag{2.18}$$

$$\eta=Y/L(t) \tag{2.19}$$

$$h^*=h/h_c \tag{2.20}$$

$$U^*=(U-\xi V_1)/U_c \tag{2.21}$$

$$V^*=(V-\eta V_2)/U_c \tag{2.22}$$

$$\alpha^*=\alpha/\alpha_c \tag{2.23}$$

$$h_o^* = h_o/h_c \tag{2.24}$$

$$P^* = (\alpha_c/h_c)P \tag{2.25}$$

$$P_o^* = (\alpha_c/h_c)P_o \tag{2.26}$$

$$t^* = t/(L_c/U_c) \tag{2.27}$$

Note that the '*' quantities are non-dimensional,

2.3.6 Transformed Equations

The governing equations are transformed using equations [2.12]-[2.26]. The resulting equations are given below.

Equation of continuity

$$\frac{L_c}{L_1}\frac{\partial}{\partial\xi}(U^*h^*) + \frac{L_c}{L_2}\frac{\partial}{\partial\eta}(V^*h^*) + \left(\frac{L_c}{U_c}\right)\left(\frac{V_1}{L_1} + \frac{V_2}{L_2}\right)h^* = -\frac{\partial}{\partial t^*}h^* \tag{2.28}$$

Equation of Conservation of Momentum

$$U^* = -\frac{h_c^3}{U_c\alpha_c\mu kfL_1}\frac{\partial}{\partial\xi}P^* \tag{2.29}$$

$$V^* = -\frac{h_c^3}{V_c\alpha_c\mu kfL_2}\frac{\partial}{\partial\eta}P^* \tag{2.30}$$

By defining U_c and V_c appropriately (given by equation [2.31]), to be as follows:

$$U_c = \frac{h_c^3}{\alpha_c\mu kfL_1} \quad , \quad Vc = \frac{h_c^3}{\alpha_c\mu kfL_2} \tag{2.31}$$

The momentum equation reduces to:

$$U^* = -\frac{d}{d\xi}P^* \tag{2.32}$$

$$V^* = -\frac{d}{d\eta}P^* \tag{2.33}$$

Constitutive law (Fungs P-h Law)

The dimensionless form of Fung's P-h las is

$$h^*(\xi, \eta, t) = h^*_o(\xi, \eta, t) + \alpha_c(\xi, \eta, t)\,(P^* - P^*_o) \tag{2.34}$$

Equation [2.34] gives the generalized form of Fungs constitutive P-h law, and it allows for h_0 and α to vary spatially and with time as will occur when breathing is simulated.

Equations [2.28]-[2.34] complete the formulation of the transformed dimensionless equations.

Justification for a time-dependent *h* under the 'quasi-static' assumption: characteristic time constant associated with the equilibration of a pressure disturbance.

Flow in the septum is 'quasi-static', which essentially means 'very slow'. We used this assumption by neglecting the inertial in the momentum equation. The 'quasi-static' assumption implies that at each time-step, the solution may be obtained by assuming the flow to be 'static' at that step, meaning that the fluid acceleration is negligibly small (or zero). Since our system is not rigid, the resulting velocities and pressures from the solution of the 'static' momentum equation are integrated in time to obtain the updated displacements; and this is the reason for the time-integration in the continuity equation even though we have assumed a 'quasi-static' flow. In fact, a characteristic time constant, given by the following equation, may be estimated based on scaling of the continuity equation.

This time-constant represents the characteristic time for a pressure disturbance to equilibrate.

$$\tau = \mu k f \alpha_c \frac{L_c^2}{3h_o^3} \tag{2.35}$$

Using μ=0.02E-4 Cm(H_2O)-sec (value for whole blood at large diameter ~ 6 μm), k=12, f=2, α=0.127 μm/cm(water), h_o=3.5 μm, and L_c=75 μ, we obtain that τ=2.7E-3 seconds. This time constant is much smaller that the time scale associated with breathing (~5 seconds), thus the flow indeed is quasi-static. Further, the small time-constant would predict negligible phase-lags in pressures in the septum.

2.4 Parameters of the transformed sheet-flow model.

2.4.7 Viscosity

Blood viscosity, μ, is a function of the local sheet height, and the discharge hematocrit H_d (see figure [2.5]). The following expression has been proposed by Kiani, M [24]

$$\mu = \frac{\mu_p}{\left[1-\left(1-\frac{\mu_p}{\mu_c}\right)\left(1-2\frac{\Delta}{h}\right)^4\right]\left(1-\frac{D_m}{h}\right)^4} \tag{2.36}$$

μ_p = apparent viscosity of plasma in cP

μ_c=core apparent viscosity for a large tube (>300 microns)

Δ=width of marginal layer in microns (from marginal zone theory) ([24])

h=sheet height in microns

D_m = effective diameter of a single RBC in a small tube

Equations [2.37] & [2.38] are empirically determined curve-fits ([24]) with:

$$\Delta = 2.03 - 2.0H_d \quad [\mu m] \tag{2.37}$$

$$\mu_c = e^{(0.48 + 2.35Hd)} \quad [cP] \tag{2.38}$$

$$\mu_p = 1.7 \text{ Centipoise} \tag{2.39}$$

$$D_m = 2.7 \text{ microns} \tag{2.40}$$

A discharge hematocrit of 40% is used. The Capillary hematocrit in peripheral blood in a male varies between 45-55%

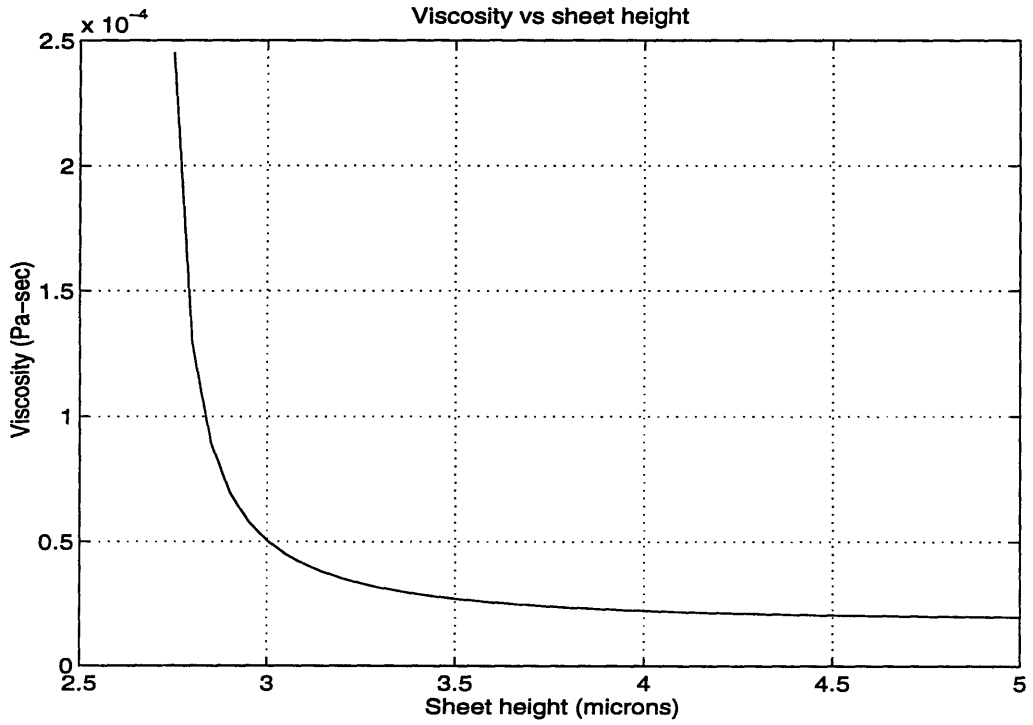

Figure 2.5: Viscosity as a function of local sheet height

2.4.8 Sheet Length, L(t)

The length of the sheet changes with time during breathing. The current model assumes a 75 micron square sheet, with 5x5 posts evenly separated by a distance of 15

microns. The length of the septum is assumed to vary as the cube root of the lung volume. Therefore, if V(t) is the volume of lung given by the expression:

$$V(t) = V_m + \frac{V_t}{2}\sin(\omega t) \tag{2.41}$$

Then the sheet length is given by

$$L = Lo\left(1 + \frac{V_t}{2V_m}\sin(\omega t)\right)^{1/3} \tag{2.42}$$

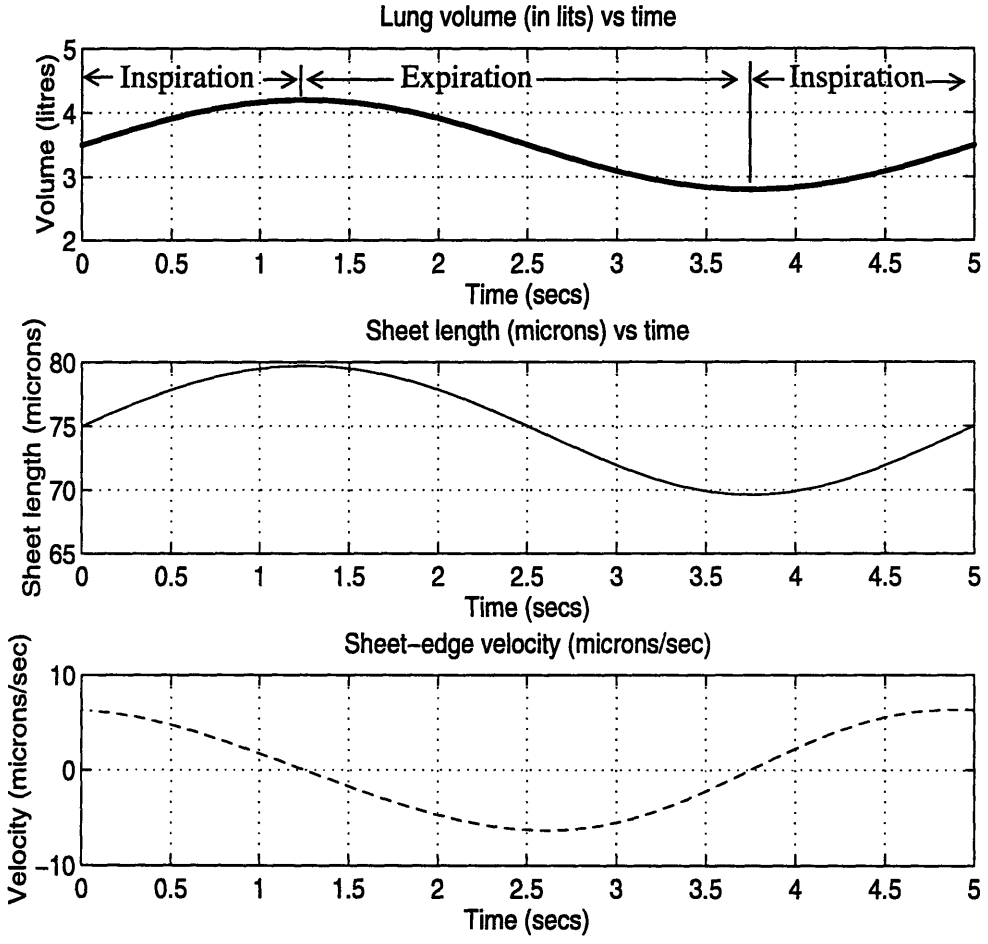

Figure 2.6: Phase relationship between lung volume, L(t) and sheet-edge velocity

Figure [2.6] shows the phase relationship between lung volume and sheet length determined from the lung volume. The sheet is assumed to distend isotropically; this implies that the change in length per unit length between any two points is constant.

2.4.9 Alveolar Pressure, $P_0(t)$

Changes in alveolar pressure impose a pressure gradient for air-flow into and out of the lung during inspiration and expiration; falling below atmospheric pressure during inspiration and rising above atmospheric pressure during expiration. In normal subjects, the change in alveolar pressure is only about 1 cm of water above and below atmospheric pressure[45] (it may be many times that in patients with airway obstruction). Figure[2.7] below (taken from West, 1990) shows the phase relationship between alveolar pressure and breathing.

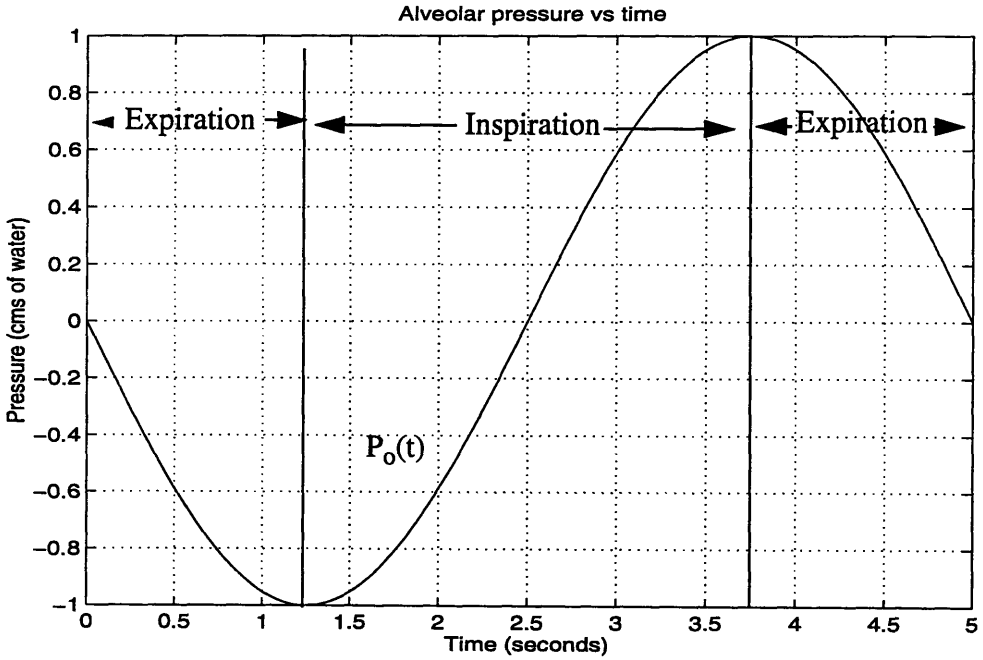

Figure 2.7: Alveolar pressure variation during breathing

2.5 Computational Procedure

Equations ([2.28]-[2.34]) are solved numerically to simulate both static and time-varying cases. The former is compared to Fung's solutions to validate the numerical procedure.

Computational grid

The transformation of coordinates to a Lagrangian or 'material' frame allows for a stationary computational grid, i.e. the set of coordinates (ξ,η) appear stationary in the Lagrangian frame of reference. Figure [2.8] shows a schematic of the computational grid in Lagrangian coordinates.

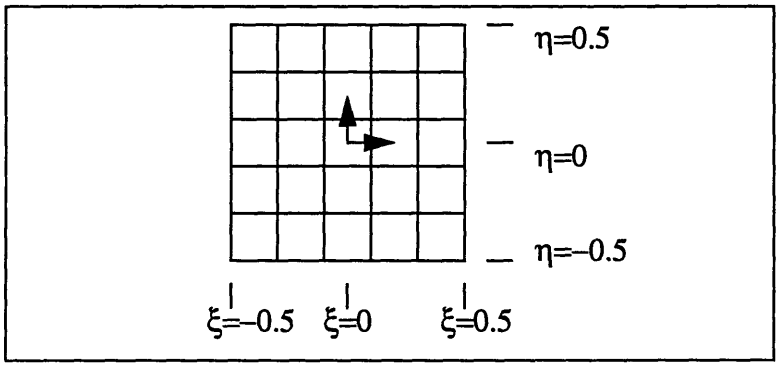

Figure 2.8: Computational Grid

Numerical discretization

Second order accurate spatial finite differences and a third order accurate Adams - Bashforth scheme (for time integrations) is used.

$$\frac{\partial \Phi}{\partial \xi} = \frac{\Phi_{i+1} - \Phi_{i-1}}{2\Delta\xi} + O\left(\Delta\xi^2\right) \qquad \text{Central difference}$$

$$\frac{\partial \Phi}{\partial \xi} = \frac{-3\Phi_i + 4\Phi_{i+1} - \Phi_{i+2}}{2\Delta\xi} + O\left(\Delta\xi^2\right) \qquad \text{Forward difference}$$

$$\frac{\partial \Phi}{\partial \xi} = \frac{3\Phi_i - 4\Phi_{i+1} + \Phi_{i+2}}{2\Delta\xi} + O\left(\Delta\xi^2\right) \qquad \text{Backward difference}$$

Adams-Bashforth scheme:

For a system comprising of y'=f(y)

$$y_{n+1} = y_n + \left(\frac{\Delta t}{2}\right)(55f_n - 59f_{n-1} + 37f_{n-2} - 9f_{n-3}) + O\left(\Delta t^3\right)$$

Boundary conditions

η=–0.5 defines boundary 1. ξ=0.5 defines boundary 2. η=0.5 defines boundary 3. ξ=–0.5 defines boundary 4.

Boundary conditions may either be specified in terms of pressure along the 4 edges or a 'solid wall' condition of zero normal velocity at either of the edges, or a mix of the two.

Numerical Scheme

The procedure used in the calculations is as follows:

- The equation of continuity is used to update the sheet height at every location on the grid. This is performed by time integration using a third-order Adams-Bashforth scheme.
- The new sheet height values are then used to compute the local Pressures
- The updated pressures are then used in order to determine the local fluid velocities
- The sheet length, viscosity, alveolar pressure are then updated as the values of the next time step.
- Boundary conditions are finally imposed and the process is repeated

2.6 Comparison of the Current model with Fungs sheet-flow model

The current model is essentially an enhancement of the model developed by Fung(1984), with the differences summarized in Table [2.1].

Table 2.1: Comparison of Fungs sheet flow model with the current model

Current Model	Fungs Model
Obtains a time dependent solution	Static Analytic solution

Table 2.1: Comparison of Fungs sheet flow model with the current model

Current Model	Fungs Model
Model capable of incorporating time-varying μ,α,k,f	Analysis limited to constant values of μ,α,k,f
Incorporates the effect of the motion of the septal walls.	Applicable to a stationary septum sheet
Capable of incorporating a time-varying alveolar pressure.	Constant alveolar pressure
The inlet and exit are along the entire width of the sheet.	The flow inlet and exit are assumed to be single openings into/out of the septum
The current model is general purpose as far as boundary conditions are concerned - it is also capable of handling pulsatile arteriole and venule pressures	Ignores the pulmonary pulsatility in the arteriole and venule pressures.

Chapter 3

The Tube Flow model

3.1 Introduction

While the sheet flow model provides useful insights into the fundamental aspects of pulmonary capillary flow, some assumptions of the model limit its applicability. Although, as shown in the previous chapter, the sheet-flow model can be revised to incorporate the motion of the alveolar septum due to breathing, it fails to capture some physical details that characterize the complexity of the septal bed. First, the sheet flow model incorporates the effect of the posts as a 'lumped resistance' parameter in the form of the geometric friction factor, k. The resistance parameter should ideally change both spatially and with time during a breathing cycle since the compliant sheet changes its dimensions; this variability is not incorporated in the sheet flow model. Second, Kiani et al. [23] have demonstrated that the diameter variability along a microvascular vessel has a significant effect on the pressure drop within the vessel; consequently, we would like to develop a model that takes into account this axial variability in diameter. Third, although we modified the sheet flow model so as to incorporate spatial variability of parameters, specifying such variability makes the problem computationally intense in terms of the density of discretization required to capture the essential physical details. This problem is eliminated in the tube model for reasons discussed later in this section.

Our ultimate objective in modelling flow through the alveolar septum is to demonstrate the effect of spatial variability in the sheet parameters and to simulate RBC and PMN transit times in the alveolar septum. While the sheet-flow model developed by Fung [13] is capable of predicting RBC transit time distributions based on the computed veloc-

ity of blood, the assumptions implicit in the sheet model preclude it from an accurate portrayal of important physical details. A more realistic transit time simulation depends on the tortuous path and the dimensions of individual capillary segments that either a RBC or a PMN would have to pass through while traversing the capillary bed. With this motivation in mind, the tube-flow (or capillary matrix) model was developed.

The capillary bed in the tube-flow model is modelled as a network of interconnected distensible tubes. Based on this idea, the capillary bed is then divided into "segments" and "junctions" (Figure [3.1]). The segments are the inter-connected capillaries, while a junction is defined as the region where three or more segments meet. The posts and the compliant alveolar membrane essentially define the geometry of the segments. Since the distance separating the alveolar septal walls and the post dimensions change continuously with time, the geometry of the segments is time-dependent. This further causes the flow-resistance, which depends upon such physical parameters as post and septal dimensions, to vary as with time as well.

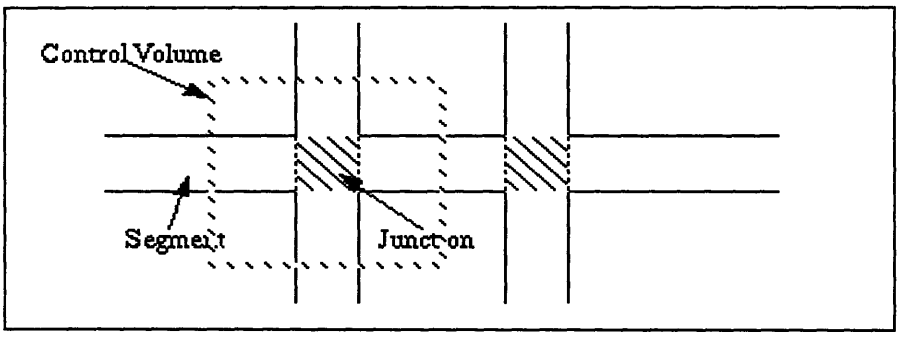

Figure 3.1: Segments and Junctions in the tube model

3.2 Derivation of tube flow equations

3.2.1 Assumptions of the model

As in the sheet flow model discussed in the previous chapter, the capillary network is

assumed to span a square of side 75 microns, with junctions separated by a distance of 15 microns. Every half-segment is characterized by a distensibility (capacitance) and every junction is characterized by a distensibility distinct from the adjoining half-segments. The pressure within a given control volume is assumed to be uniform and distinct from the pressure in adjacent control volumes. The local hematocrit is a function of the local septal distension (hydraulic diameter). Since the Reynolds number and the Womersly number are both much smaller than 1, a quasi-steady inertia-free flow approximation is used just as in the sheet flow model. The dependence of hemodynamic properties on bifurcations at junctions ([36] & [38]), for example the split of red cell flux at a bifurcation depending on bifurcation geometry and bifurcation angle, are not incorporated in the current model.

3.2.2 Development of the modelling equations

A schematic of the tube network skeleton is represented in figure [3.2] below

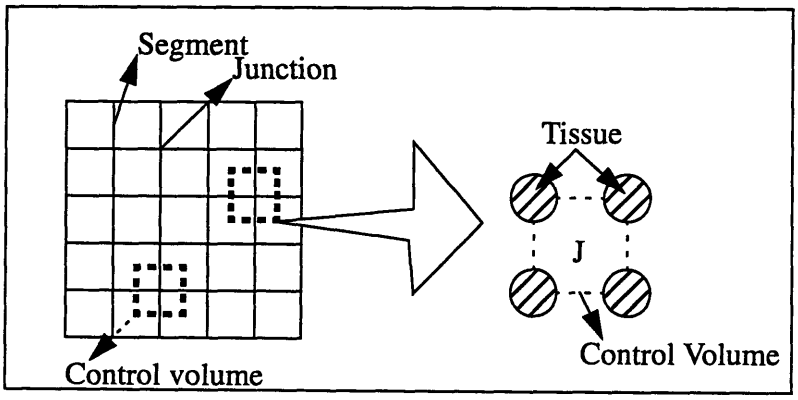

Figure 3.2: Tube network skeleton

The tube network is analyzed by analogy to an RC network, the electrical circuit parameters (R's and C's) corresponding to the fluidic system parameters (flow resistance and distensibility). A control volume is defined that encompasses one junction and one-half of each of the neighboring capillary segments. Flow passes between adjacent control volumes through segments characterized by their flow-resistance. A uniform 'mean pres-

sure' is assumed over the entire control volume for the purpose of determining junction and segment dimensions; the pressure differences between adjacent junctions driving the flow in the connecting segments. The final equations in the fluidic domain are derived with junction pressure, volume flow rates and hydraulic diameters being the fluidic variables.

3.2.3 RC Circuit analogy.

Every junction and the adjacent 4 'half-segments' comprising of a control volume is analyzed using an electrical analog.Each half-segment is characterized by a resistance and a capacitance (distensibility).

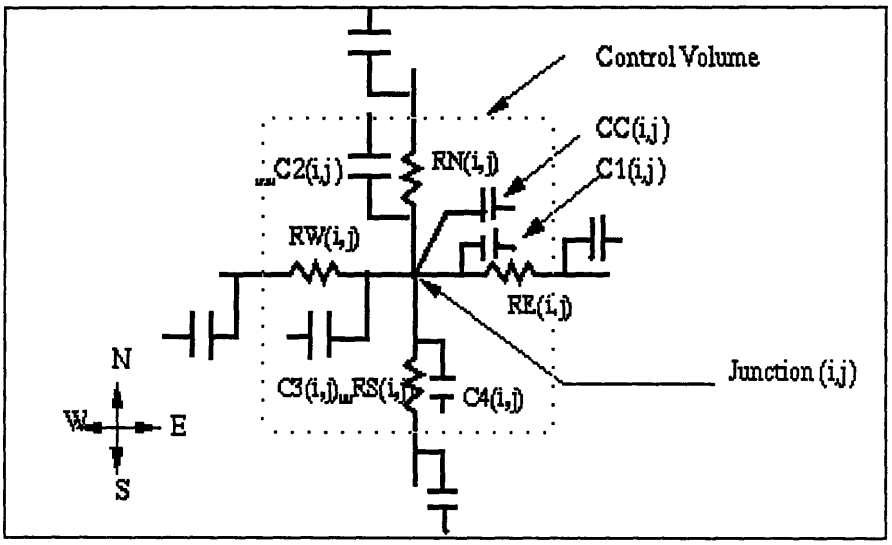

Figure 3.3: RC circuit model for the tube network

Since one of the assumptions of the fluidic model is to work with a 'mean junction pressure' which has an electrical analog of a junction voltage, all the capacitors within the control volume are connected in parallel, as shown in figure [3.3] (between the junction voltage and a voltage corressponding to the alveolar pressure). This provides a simplification in the circuit analysis in that all the capacitors connected in parallel can then be

reduced to a single capacitance C(i,j) at every junction. As a result, the junctional unit can be reduced to the network of circuit elements in Figure [3.4].

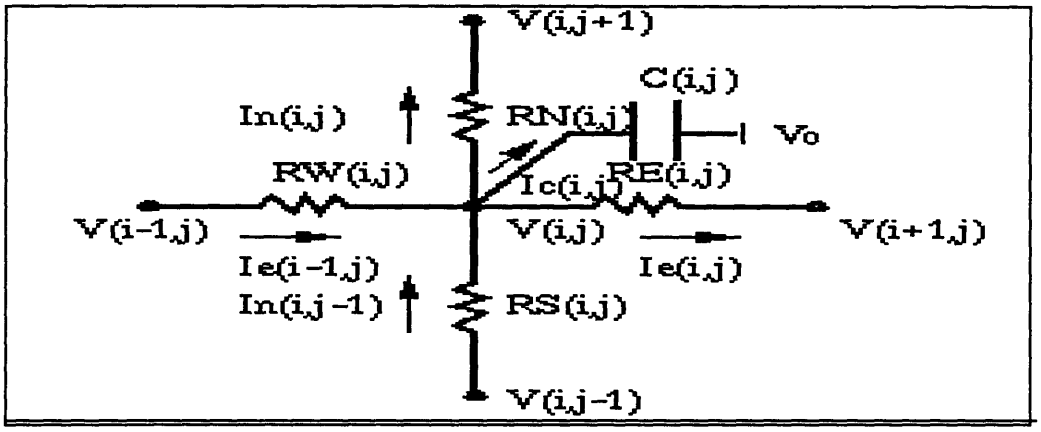

Figure 3.4: Equivalent RC circuit

The equivalent capacitance is then given by the following expression

$$C(i,j)=C_1(i,j)+C_2(i,j)+C_3(i,j)+C_4(i,j)+CC(i,j) \tag{3.1}$$

This simplification has important consequences since it allows us to collapse all the capacitance (or compliance for the fluidic model) into the junction.

3.2.4 Equivalent fluidic model: Governing equations

Let Q_1, Q_2, Q_3 and Q_4 represent volume flow rates into and out of a control volume, as defined in figure [3.5].

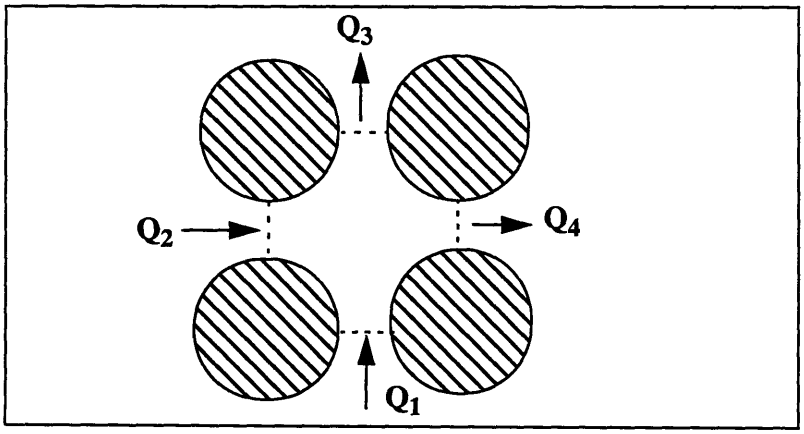

Figure 3.5: Conservation of mass for a given control-volume

Conservation of Mass at a junction

Let $V_c(i,j)$ be the volume of a given control volume. Then, by conservation of mass in the control volume, we must have that:

$$Q_1 + Q_2 - Q_3 - Q_4 = \frac{dV_c}{dt} \tag{3.2}$$

Segment Equation

Pulmonary capillary flow is modelled as inertia free (Fung, 1984), locally fully developed flow through a pipe with variable hydraulic diameter,D_h

$$Q = \frac{\pi}{8\mu_{app}}\left(\frac{\partial P}{\partial s}\right)\left(\frac{D_h}{2}\right)^4 \tag{3.3}$$

Where *'s'* is the coordinate direction parallel to the segment axis (See fig [3.7]),

Constitutive law for the Pressure-Volume relationship

An equation is required that relates the volume of the junctional unit, V_c, to the transmural pressure. While the relationship has not been measured, Fungs P-h law can be used to derive a P-V (transmural pressure - volume) law for purposes of the simulation. The sheet-flow model describes Fungs linear P-h (transmural pressure - height) law. The capillary matrix modelling equations and the RC circuit analogy allow for the entire compliance in the control volume to be lumped and represented by a single value. As a result, we may write Fungs linear p-h law for a given junction with the lumped compliance, α_{eff}, in the following way.

$$h(i,j)=h_o(i,j)+\alpha_{eff}(i,j)(P(i,j)-Po) \tag{3.4}$$

with *h* being the separation distance between the septal walls and P being the 'mean junction (transmural) pressure'.

In order to be consistent with Fungs linear relationship that we have adapted for the tube flow analysis, one may obtain a corresponding P-V law. The resulting equation has the following form:

$$V(i,j,t)=V_o(i,j,t)+\beta(i,j,t)(P(i,j,t)-P_o(t)) \tag{3.5}$$

The parameters V_o and β are described later in this chapter.

Flow Resistance due to segments and junctions

Since the flow is inertia free, the locally-fully developed flow approximation may be used in order to integrate equation [3.3] along the length of a segment in order to obtain a 'segmet resistance' (located between two junctions with pressures P_1 and P_2) defined by the following expression

$$R_{segment} \equiv \frac{\Delta P_{segment}}{Q} = \frac{8}{\pi} \int_0^{D(t)} \frac{\mu(x)}{\left(\frac{D_h(x)}{2}\right)^4} dx = \frac{P_1 - P_2}{Q} \tag{3.6}$$

where *D(t)* is the total length of a given segment. Note that viscosity is written as a function of axial distance because the hydraulic diameter (as well as the hematocrit) is a function of x.

The model must also account for the resistance to flow offered by a junction. An exact expression for the flow resistance due to a junction,especially when statistical variability is included, is too complex for this approximate analysis, the resistance is instead approximated by utilizing the expressions for flow between parallel plates. This may be demonstrated in the following way. From theory for 1-D flow between parallel plates, one may obtain the following expression for flow "resistance":

$$\frac{\Delta P}{Q} \equiv R = \frac{12\mu}{wh^3}\Delta x \tag{3.7}$$

Where Q is the volume flow rate, μ the fluid viscosity, *h* the channel height, *w* the channel width, and Δx the channel length (see figure [3.6]).

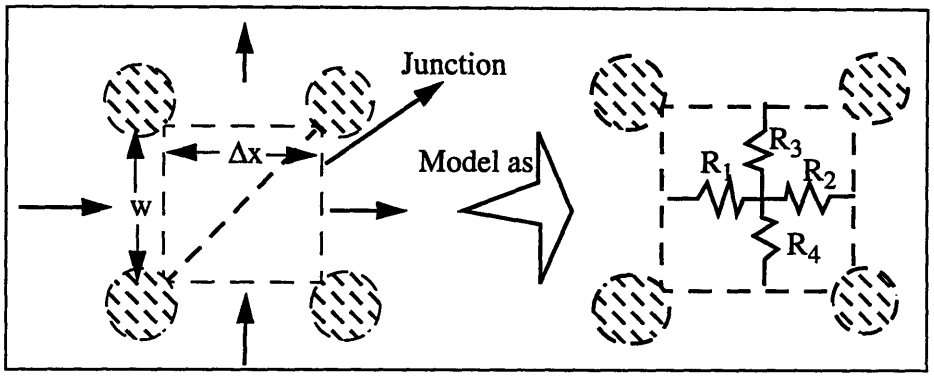

Figure 3.6: Estimation of junction resistance

Consider two cases: the first being that of 1-D flow from left to right, and the second being a 2-D flow with the equal flows entering the left and lower sides, and leaving the upper and right sides (as shown in fig [3.6]). The first case yields an upper bound on the resistance to the flow. Therefore, R is an upper estimate for the total junction-flow resistance. Under the second condition, one may deduce from the symmetry of inflow and outflow that the diagonal shown in the figure above is a "symmetry" streamline. Assuming the resistance per unit length to be constant, one may obtain the mean resistance of each "half junction" by integrating over the "half junction" divided by the symmetry streamline approximately given by R_{half}=0.5*1.414R. This provides a lower bound for the junction resistance.

We would like to associate the total junction resistance with the resistances of the neighboring capillaries by distributing it as a network shown by R_1, R_2, R_3, and R_4 in Figure [3.6]. For the first case, we can assume the total 1-D resistance, R, to be equally distributed over two resistors R_1 and R_2; thus for the first case, R_1=R_2=0.5R. For the second case, the approximate resistance of each half-junction may be distributed equally over

each of the two resistors in the "half-junction". Thus, in this case, $R_2=R_4=0.5R_{half}=R_1=R_2=0.35R$. With upper and lower bound estimates for the junction resistance, an arbitrary resistance of K_pR (with $0.35R<K_pR<0.5R$) was assigned to each of four resistors (R_1, R_2, R_3 and R_4). For the results presented in the thesis, K_p was set to 0.4 arbitrarily. Each of these four resistances were then combined in series with the resistances of the four adjacent capillaries to give R_e, R_w, R_n, and R_s in equation [3.8] given below.

3.2.5 Tube network equation.

Based on the equations developed in section [3.2.4], the following expression may be derived for a given junction:

$$\beta\frac{\partial P}{\partial t} = P\left(-\frac{1}{Re}-\frac{1}{Rw}-\frac{1}{Rs}-\frac{1}{Rn}-\frac{\partial\beta}{\partial t}\right)+\frac{Pe}{Re}+\frac{Pw}{Rw}+\frac{Pn}{Rn}+\frac{Ps}{Rs}+\frac{\partial}{\partial t}(P_o\beta)-\frac{\partial V_o}{\partial t} \tag{3.8}$$

Where P represents pressure in the $(i,j)^{th}$ junction, and R, resistances. The subscripts e,w,n and s correspond to locations east, west, north, and south of the (i,j)th junction. Note that the flow resistance in any segment is given by equation [3.6]. The system of equations described collectively by equation [3.8] may be represented as a first order, non-linear, ordinary differential system given by:

$$\dot{\underline{P}} = A(\Omega)\,\underline{P} + B(\Omega,\chi) \tag{3.9}$$

Where Ω is a function of sheet geometry, viscosity and mechanical properties of the septum. χ in general depends on the boundary conditions imposed along the sheet; for the present study, a pressure boundary condition is imposed along the edges of the sheet.

This completes the formulation of the tube-flow (capillary-matrix) model equations.

3.3 Parameters of the Tube-Flow model.

The parameters of the tube flow model for the simulation are obtained in the same way as the parameters for the Sheet flow model. Segment and junction geometry is shown in figure [3.7].

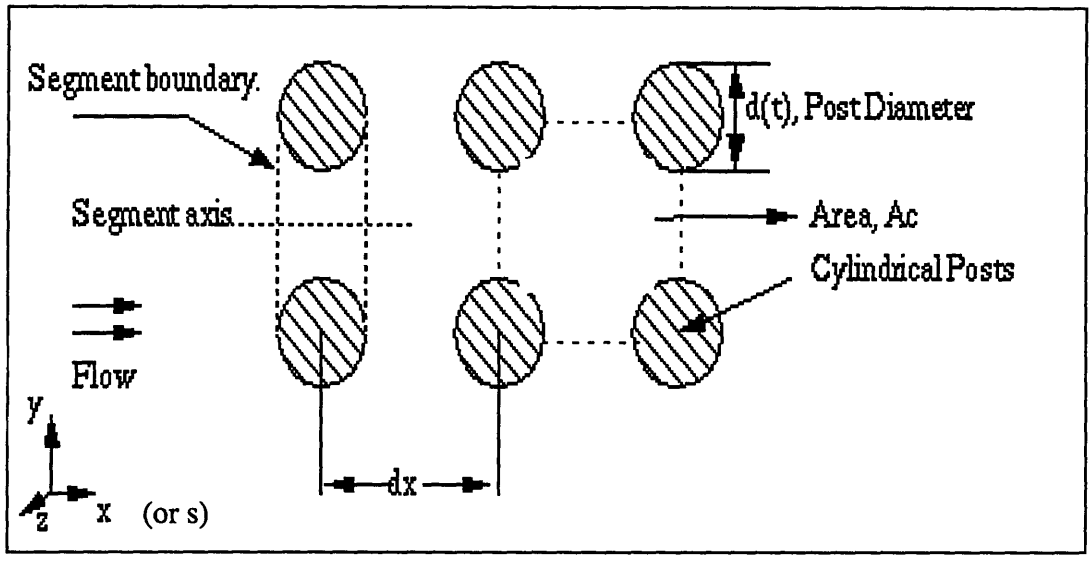

Figure 3.7: Schematic of the septal geometry for the tube network

Viscosity

The viscosity is obtained in the same way as it was determined for the sheet- flow network. However, using eq [2.38] based here on the local tube hydraulic diameter, D_h.

$$\mu = \frac{\mu_p}{\left[1-\left(1-\frac{\mu_p}{\mu_c}\right)\left(1-\frac{2\Delta}{D_h}\right)^4\right]\left(1-\frac{D_m}{D_h}\right)} \tag{3.10}$$

$$\Delta = 2.03 - 2.0H_d \tag{3.11}$$

$$\mu_c = e^{(0.48 + 2.35H_d)} \tag{3.12}$$

$$\mu_p = 1.7\text{Centipoise} \tag{3.13}$$

$$Dm = 2.7\text{microns} \tag{3.14}$$

H_d is again the discharge hematocrit.

Septal-wall extension

Septal dimensions are assumed to change isotropically in the plane of the septum. This implies that the change in length per unit length is a constant so that the actual distance between any two material points located at (ξ_1,η_1) & (ξ_2,η_2) changes according to:

$$\Delta x(t) = L_1(t)\,\Delta\xi \tag{3.15}$$

$$\Delta y(t) = L_2(t)\,\Delta\eta \tag{3.16}$$

$$\text{Where } x(t)=\xi L_1(t) \text{ and } y(t)=\eta L_2(t) \tag{3.17}$$

The above expressions allow one to compute the segment lengths and post diameter, both as functions of time during breathing. The cylindrical posts of connective tissue (assumed to be incompressible connective tissue) are also assumed to expand and contract laterally in an isotropic fashion.

Time-dependence of $h_o(t)$

The parameter h_o in Fungs linear P-h law is the local 'sheet' separation distance when alveolar pressure equals local blood pressure, and by analogy, may be viewed in the present model as the height of the cylindrical posts at zero transmural pressure. On the assumption of constant post-volume mentioned above, changes in h_o result from changes in lung volume (or L(t)) and can be described by:

$$ho(t) = h_{o,nom}\frac{d^2_{o,nom}}{d(t)^2} = h_{o,nom}\frac{L_o}{L^2(t)} \tag{3.18}$$

Where nominal values of h_0 and the post diameter, d_0, are given by $h_{o,nom}$ and $d_{o,\,nom}$ ($h_{o,nom}$ = 3.5 μm (from Fung, 1972a), and L_o=75 μm). The parameter h_0 may also be viewed as the 'sheet separation' distance at zero transmural pressure. The value of h_0 for each junction in the tube model may then be associated with a distinct post in order to approximate the spatial as well as time-dependence of h_0 at that junction.

Junction area, A_c.

The junction area A_c is approximated by the following expression (based on fig. [3.7]):

$$A_c(t) = L_p(t)^2 - \frac{\pi}{4} d(t)^2 \tag{3.19}$$

V_0(t) and the P-V compliance, β(t).

The theoretical P-V compliance is obtained using Fungs linear P-h law and the sheet geometry. The theoretical expression for the sheet compliance is obtained by writing an approximate expression for the volume of the control volume in terms of the sheet geometry and Fungs linear P-h law.

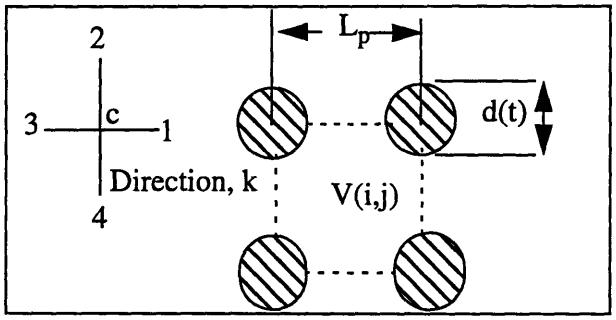

Figure 3.8: Control volume

Based on the control volume and directions shown in figure [3.8], the following expression may be derived for the volume of the $(i,j)^{th}$ control-volume. Note that h_0, which refers to the junction height at any given junction, is assumed to be spatially invariant for that control-volume.

$$V_{i,j} = Vo_{i,j} + \beta_{i,j}(P_{i,j} - Po) \tag{3.20}$$

Where

$$V_{o(i,j)} = h_o A_c + \sum_{k=1}^{4} \frac{\pi}{8} d\,(2L_p - d)\,h_{o,k} \tag{3.21}$$

(Note that $h_{o,k}(i,j) = h_o(i,j)$ in the current model)

$$\beta = \alpha_c A_c + \sum_{k=1}^{4} \frac{\pi}{8} d\,(2L_p - d)\,\alpha_k \tag{3.22}$$

The volumes of the 4 adjacent half-segments are each approximated by the volume of a solid-cylinder with a variable elliptical cross sectional area.See Appendix [B.1]

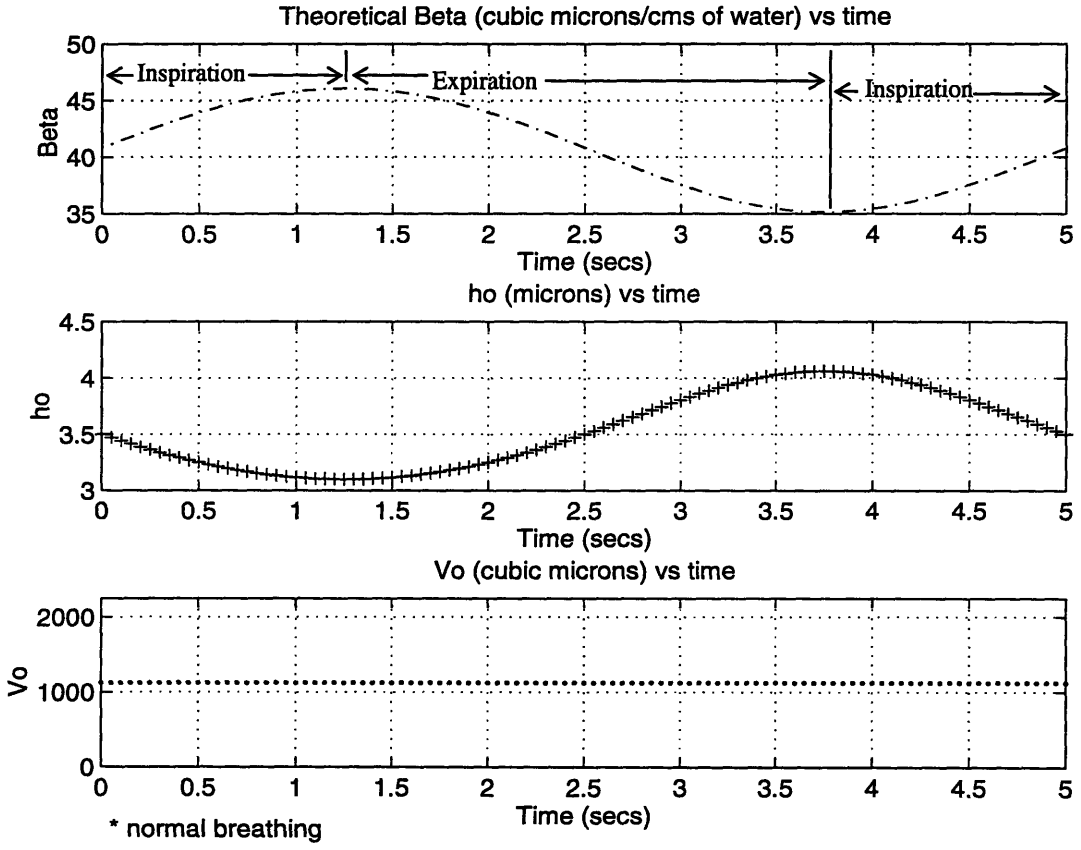

Figure 3.9: Theoretical β, h_o and V_o as functions of time

Figure [3.9] shows the variation of β, h_o, and V_o with time (during a normal breathing cycle). Although the volume-compliance is not a measured quantity that is available in the literature, its behavior with breathing seems counter-intuitive, since one would expect the compliance to decrease during inspiration (increasing resistance to increase in volume with changes in pressure). While the current modelling technique predicts this behavior in the compliance derived analytically, future work with the model will include experimental data from morphometric measurements in order to incorporate the true nature of the volume compliance.

V_o remains constant during a breathing cycle. This seems consistent with our modelling assumption of constant post-volume; however, morphometric measurements would be needed to ascertain the true nature of the variation of V_o with breathing.

3.4 Determining segment geometry and segment flow-resistance

The geometry of a given segment and the dependence of the viscosity on the geometry allows us to determine the resistance of that segment. Each segment is viewed in the present model as the space between two adjacent posts, as shown in figure [3.7].Note that in future work, the segment geometry will be dictated by morphometric studies and will therefore be of arbitrary shape. With this in mind, we adopt the following procedure for computing the segment resistance which can be applied to any segment geometry; any given geometry may be divided discretely (stations 1-5,say) as shown in Fig [3.10]

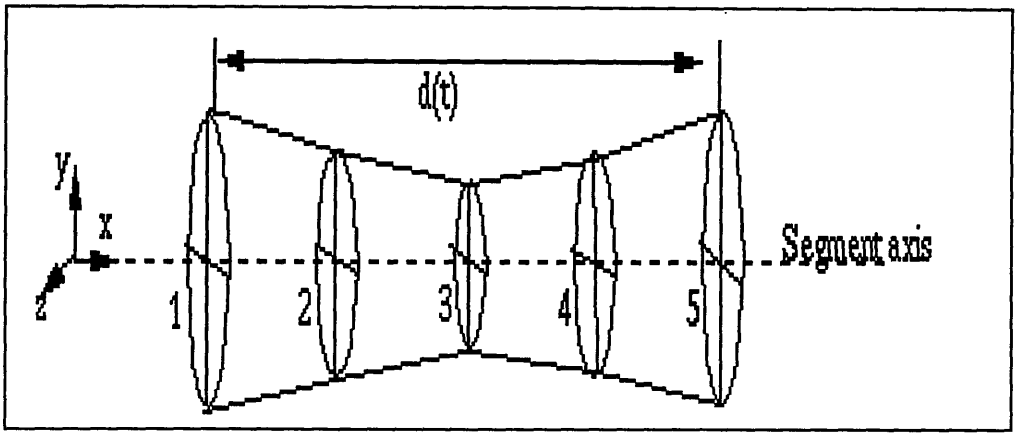

Figure 3.10: Capillary 'segment' geometry: discretization into 5 stations for resistance computation

Each of the five stations (1 thru 5) is characterized by two orthogonal dimensions along the y and the z directions (table [3.1]). These dimensions at each station further characterize an elliptic cross section (of major and minor axis a and b, say). Based on these axis dimensions, the hydraulic diameter, D_h, (at each of the five stations) is computed using the following expression:

$$D_h = \frac{4\,(\text{Area of cross section})}{Perimeter} = \frac{4ab}{(0.5)\,(a+b) + \sqrt{0.5\left(a^2+b^2\right)}} \qquad (3.23)$$

a= major axis (along the z direction)

b=minor axis (along the y direction)

The major and minor axes are determined at each of the sections in the following way. (h_i is the y dimension at the ith station, determined by Fung's P-h law)

Table 3.1: Computation of Major and minor axis

	2a	2b
station 1	$L_p(t)$	h_1
station 2	$(2L_p\text{-}d)/2$	h_2

Table 3.1: Computation of Major and minor axis

	2a	2b
station 3	L_p-d	h_2+h_4
station 4	$(2L_p$-$d)/2$	h_4
station 5	$L_p(t)$	h_5

Based on the local major and minor axis, a hydraulic diameter, D_h, is computed for each of the five sections in every segment. Note that the expression for resistance is based on the hydraulic diameter approximation for an ellipse which at high aspect ratios becomes less good an approximation. Then, equations [3.10]-[3.12] are used to compute the effective viscosities at each of the 5 stations. Finally, equation [3.6] is numerically integrated in order to yield the resistance of an individual segment. The approximated resistance of a junction, described in previous sections in this chapter as four resistors, is incorporated by placing each of the four resistors in series with capillary resistances in each of the four neighbouring capillaries for that junction.

3.5 Statistical spatial variability in h_0 and Sheet compliance, α.

The time dependence of h_0 has been discussed earlier in this chapter. One of the primary motives for developing the tube-flow model is to explore the effect of spatial statistical variability of the sheet parameters on the distribution of blood flow in the septum. In order to achieve this, a random selection for the spatial distribution was made based on the assumption that the variables (h_0 and α) were distributed normally, with specified means and standard deviations. The extent of spatial variability in the sheet compliance is a quantity that has not been explored experimentally in the past. As a result, we specified the normal distribution for the compliance by a mean value (experimentally determined, Sobin et al. (1979)) and a standard deviation as being a fixed percentage of the mean. Somewhat

better estimates for the spatial distribution in h_0 were available from experimental studies (Doerschuk et.al,[8]) where means and standard distributions for capillary diameters were obtained from experimental data. Although these were not experimentally determined distributions for h_0, we used the percent variability in the capillary diameters and assumed it to be representative of the percent variability in experimentally determined values for h_0 (Sobin et. al (1979)). The justification for this assumption is that the capillary diameters are closely related to h_0, and that this seemed a reasonable estimate in view of the limited amount of relevant morphometric data currently available.

While this approach of a specifying normal probability distribution yielded a random selection with zero spatial correlation (by definition), it was also possible to specify a non-zero covariance matrix in order to choose a random selection with a non-zero spatial correlation. The non-zero spatial correlation is important since in reality, even though the parameters of the sheet are randomly distributed, it is likely that some degree of spatial correlation exists physiologically.

3.6 Boundary conditions and solution method

The boundary condition for the capillary-matrix is given in terms of a specified pressure profile along the 4 boundaries of the septum. It is also possible to include a time-dependent pressure boundary condition to simulate pulsatility. One such pressure profile is shown in the figure [3.11]

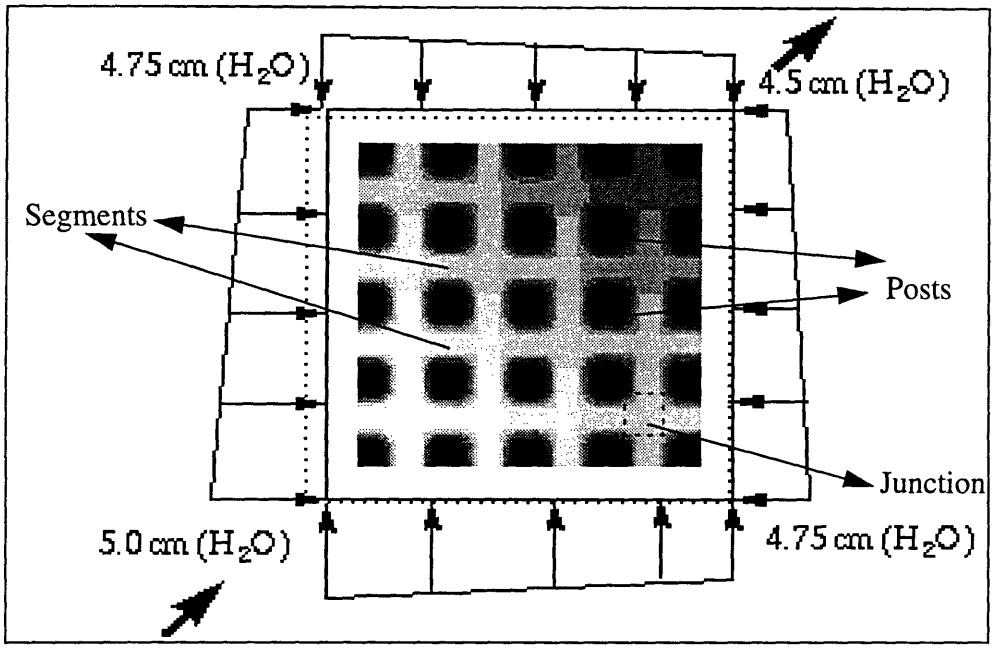

Figure 3.11: Typical pressure profile imposed for boundary condition. The septum is shown with shading representing a typical set of computed pressures.

The dynamic system of first-order non-linear differential equations given by eq[3.9] is numerically integrated on MATLAB, using 4th and 5th order accurate automatic step-size Runge-Kutta algorithms. The MATLAB program written for the solution of this system was designed to utilize several of the math subroutines available on MATLAB, and incorporate several user-defined subroutines to perform the integration. Further, the code was completely vectorized, resulting in a drastic decrease in computational time. For a complete description of the code, refer to Appendix[B.2]

Chapter 4

Results and Discussion

4.1 Introduction

This chapter presents the computational results obtained from each of the two models discussed in the previous chapters, namely, Fungs sheet model (with the addition of the effects of breathing) and the Tube-flow model.

The primary goal of this thesis is to develop a computational model for the pulmonary capillary blood-flow in order to:

1. Simulate breathing by causing the septal dimensions to change with time, and demonstrate the effect of breathing on the capillary blood flow. In particular, the objectives are to:

- Quantify the dynamic blood-pressure changes induced as a result of breathing.
- Quantify the changes in blood flow-rates induced as a result of breathing.

We anticipate that these dynamic changes in blood-pressure and flow rates, induced from breathing, will be important in determining the RBC (and PMN) transit times

2. Demonstrate the effect of spatial variability in the sheet compliance and h_o to ask the following questions:

- Does variability in the parameters play a key role in determining the blood-flow pattern in the network? Does variability lead to the presence of 'preferential pathways' for RBC transit through the septum?
- How sensitive is the blood-flow distribution to the degree of variability of each of the parameters?

3. Explore the effect of segment blockage on the resulting flow-rate distribution. Segment blockages may be used to simulate the effect of missing capillary segments or segments temporarily obstructed by PMN's.

4. Couple the dynamic effects induced from breathing with statistical spatial variabil-

ity in the parameters with blockage to simulate a realistic scenario of blood flow in the septum, and with the results obtained, move in the direction of calculating RBC transit-times based on the computed flow-rates in the septum.

Computational results from Fungs model are first compared to theoretical results in order to validate the numerical model.

4.2 Results for Fung's sheet-flow model

Fung has obtained the following analytic expressions for the sheet height profile, $h(x)$, and the volume flow-rate per unit width, Q, for 1-D flow between compliant sheets under static conditions [12]; these results are used to validate the numerical scheme for the static case.

$$h(x) = \left[h_a - \left(h_a^4 - h_v^4\right)\frac{x}{L}\right]^{\frac{1}{4}} \tag{4.1}$$

$$Q = \frac{\left(h_a^4 - h_v^4\right)}{48\mu_{eff}\alpha L} \tag{4.2}$$

$$\mu_{eff} = \mu f \tag{4.3}$$

(Under the assumption that μ,α,f,L being constant (f being the friction factor)).

Results from the numerical formulation of the sheet-flow model (see Chapter 2) for the sheet height, h, and the volume flow rate per unit width, Q, were compared with the above analytic expressions in order to validate the numerical scheme (Figure [4.1]). By imposing a uniform pressure on the two opposite boundaries of the sheet, and by setting a zero normal velocity on the other two, 1-D flow was obtained. Sheet-height profiles were computed for static cases under 3 different pressure conditions listed in table [4.1]. The volume flow-rate comparison was made by keeping the inlet pressure fixed at 10 cm (water) and varying the exit pressure for different cases listed in table [4.2].

Case	Inlet pressure (cm H_2O	Exit Pressure (cm H_2O)
1	12.5	10.0
2	12.5	6.0
3	12.5	3.0

Table 4.1: Validation of numerical scheme. 3 test cases for sheet ht. comparison.

P_{inlet} cm (water)	P_{exit} (cm of water)	P_{exit}/P_{in}
10.0	9.5	0.95
10.0	8.0	0.8
10.0	6.0	0.6
10.0	4.0	0.4
10.0	2.0	0.2

Table 4.2: Numerical validation. 5 test cases for the flow-rate comparison

(f=4.0, μ=0.0186E-3 cm (H_2O)-sec, L=75 μm, and α=0.127 μm/cm (H_2O) were used).

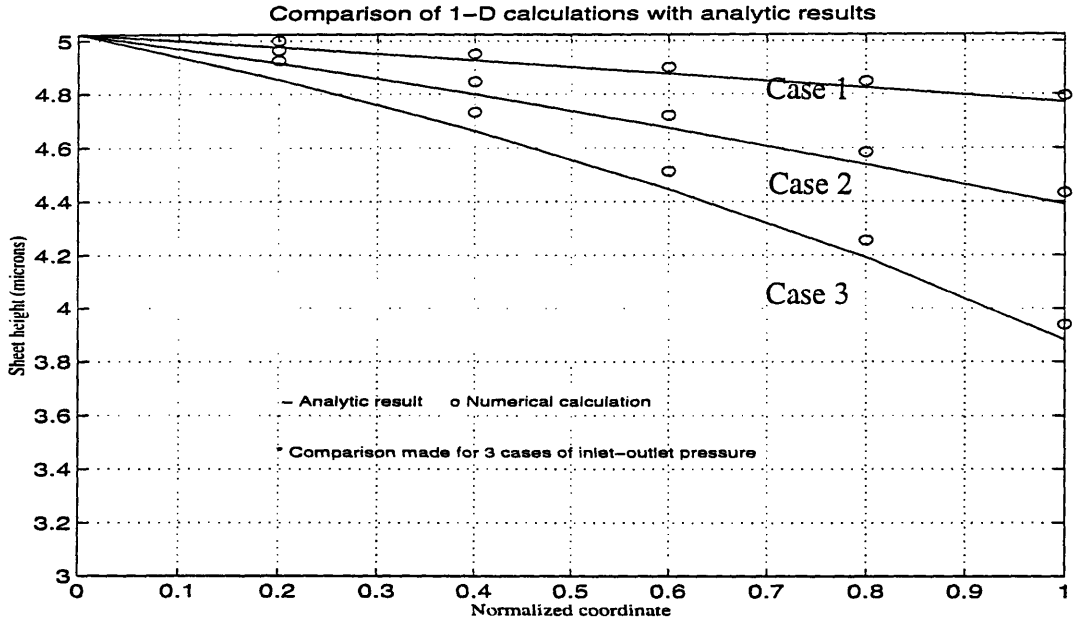

Figure 4.1: Validation of numerical scheme for Fung's model: Comparison of numerical results for h(x) with Fungs analytic solution for the 1-D static case

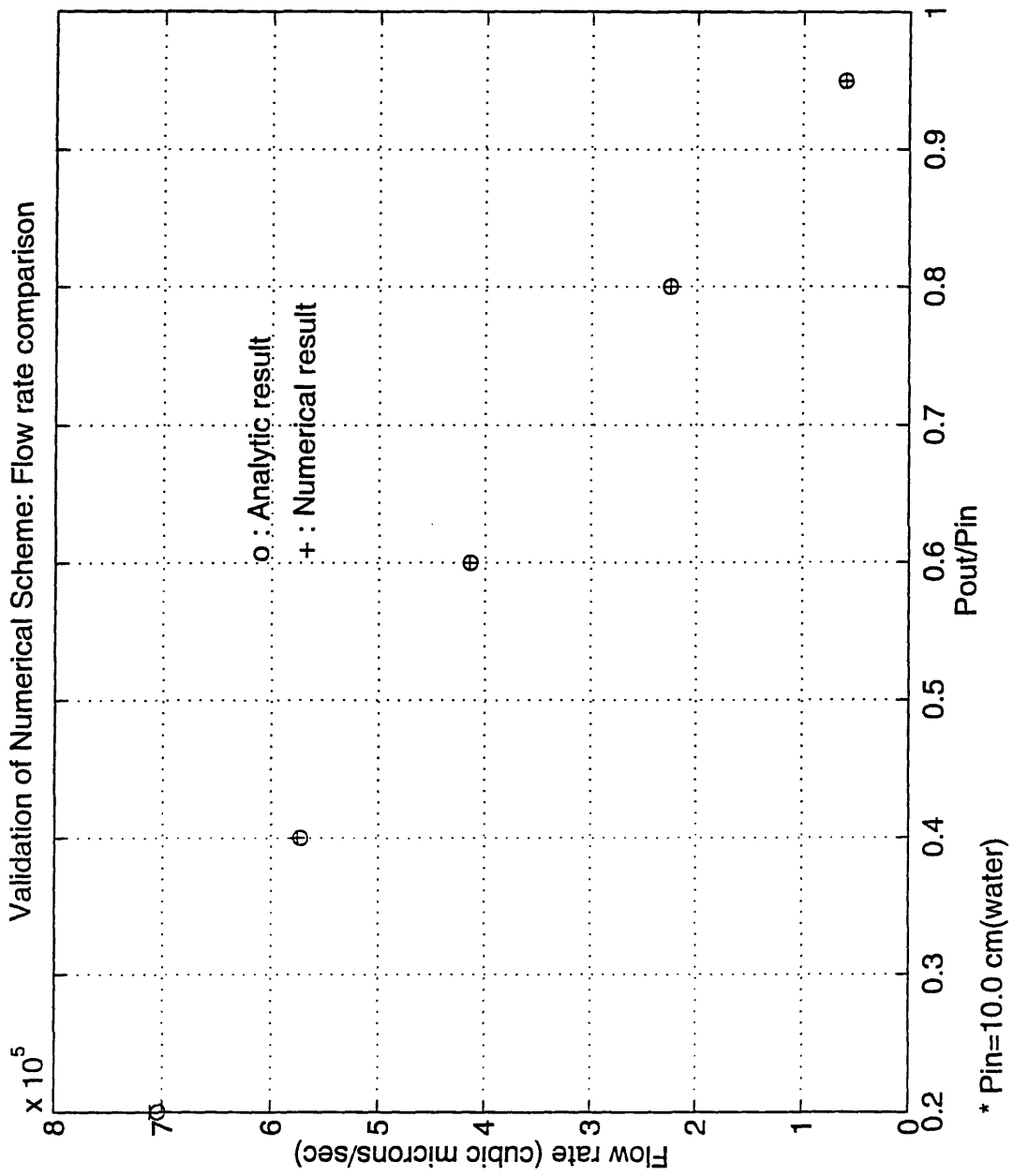

Figure 4.2: Validation of numerical scheme for Fung's model. Flow-rate comparison with Fung's analytic result for 1-D flow. 5 cases of inflow-outflow pressures.

The static results obtained from the numerical formulation of Fungs model show a good comparison with the analytic expressions obtained by Fung for the 1-D case, as seen

in figure [4.1]. The error in the sheet height was less than 1.5%, and the error in flow-rates was less than 1% of the prediction from analytic results.

Despite this close agreement between our numerical formulation and the theoretical predictions for Fung's model, and that we have incorporated the effects of breathing, for reasons given below, Fungs sheet-flow model is not appropriate for our ultimate goal to study phenomenon at the length scale of RBC's and capillaries, i.e. the phenomenon of RBC and PMN transit as they take a tortuous path while traversing the septum.

First, we are interested in studying the transit of RBC's and PMN's through a capillary bed composed of pathways (segments, junctions) and 'septal posts', and would like to capture the physics (viscous friction between the plasma and the septal walls, effects due to septal geometry, etc.) associated with the presence of these physical characteristics.

Second, our objective to study the effect of spatial variability in the parameters and explore the presence of preferentially perfused pathways as a result of this variability is not easily met by the sheet-model, which incorporates the effect of posts and channels by a lumped resistance to flow. In addition, introducing a variability in the parameters for the dynamic sheet-flow equations makes the equations computationally intense (the time step being determined by the length scale of variability).

4.3 Results for the Tube-flow model.

4.3.1 Validation of the Tube-flow model: comparison with other models.

Comparison with Fung's sheet model

Fung has obtained an expression for the volume flow rate per unit width for a static one dimensional case, given by equation [4.2]. Volume flow-rates are also obtained as a

result of calculations from the tube-flow model. In order to make a comparison between the calculations of the tube-flow model with the analytic 1-D results of Fung's model, we simulated an "approximately 1-D" flow in the tube model by imposing a uniform pressure along 2 "opposite" edges of the network, and a linear pressure gradient along the adjacent sides connecting the inflow (left edge) and outflow (right edge). Under this configuration of boundary conditions, we observed that the flow was "approximately 1-D" (from left to right), with less than 2% "flow-leakage" from the other two "farfield" edges (above and below). Thus, with the dominant direction of flow being from left to right, we were able to maintain one-dimensionality and compute the flow-rate to make the following comparison. (f=1 was used to compute the volume flow rate for Fung's model. This was estimated from results obtained by Yen and Fung (1973) (corresponding to the ratio sheet ht/post diameter~5/7 from the tube model)..

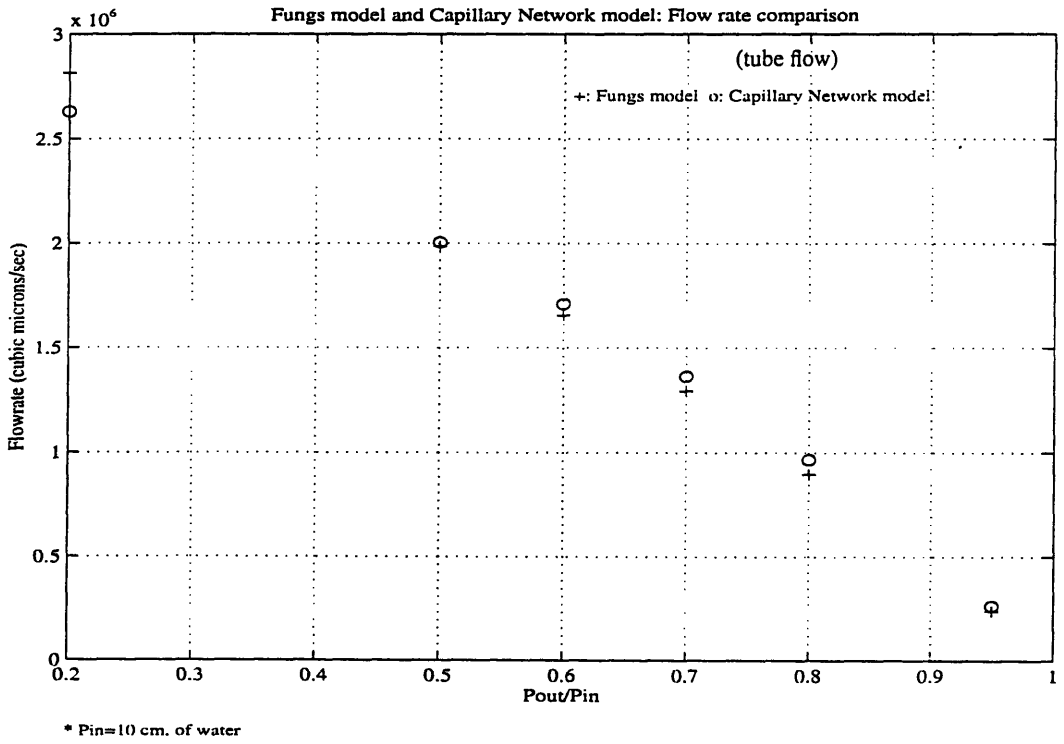

Figure 4.3: Volume flow-rate comparison: Fungs sheet model and Tube-flow model

Figure [4.3] shows a comparison of the volume flow-rates calculated by the two models, which confirms the good agreement. The advantage for us being that the tube-flow model is more appropriate for our objectives.

Friction factor comparison with Weinbaum's model.

Viscous flow is a channel with periodic cross-bridging fibres forming an infinite staggered array has been analyzed by Tsay and Weinbaum ([44]), who have obtained exact solutions for the flow-field in the array. While Lee and Fung (1969) developed theory for flow around a single fible, Weinbaum's model was an extension of their work that successfully described the transition from the Hele-Shaw potential flow limit (aspect ratio B<<1) to the viscous two-dimensional limiting case (B>>1, Sangani & Acrivos, 1982). Weinbaum's model also proposed an interpolation formula for the drag coefficient, f, in order to describe the transition of flow from the B<<1 case to the B>>1 case that successfully described the flow in the B~O(1) regime. This section aims at making a comparison between Weinbaum's ionterpolation formula and results for the drag coefficient for the current model.

The geometry of the idealized tube-network is similar to the geometry of the channel in Weinbaum's work, with the cylindrical posts of connective tissue being analogous to the cross-bridging fibres; however, the networks are somewhat different since the channel in Weinbaum's work is rigid with a staggered layout of 'cylindrical posts' with respect to the flow direction, as opposed to the tube-model with compliant network with a uniform layout of cylindrical posts (figure [4.4]). Nevertheless, it is possible to make a comparison of the tube model by setting the compliance to a very small number (reduce by a factor of

100, say) and by superimposing results obtained from the tube model in order to mimic the staggerdness of Weinbaum's network..

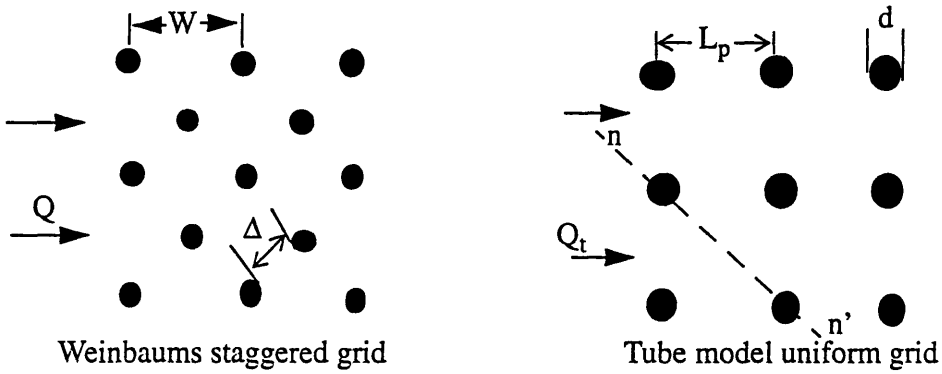

Figure 4.4: Schematic of Weinbaum's staggered grid and the tube-model's uniform grid

Flows at low Reynolds number are additive. Since the Reynold's number in the septum is of order 1, it is possible to add (as vectors) two solutions in order obtain a third solution that also satisfies conservation of mass and momentum at low reynolds number. We make use of this property to mimic Weinbaum's staggeredness from the uniform grid of the tube model by summing two similar 1-D flows, one from left to right and the other from bottom to top under the same pressure condition. It may be observed that summing the two solutions vectorally, and viewing the resulting flow about the line *nn'* in figure [4.4], one obtains the staggered-flow condition in Weinbaum's solution.

Weinbaum has obtained expressions for the drag coefficient, f, for a channel with staggered layout of cross-bridging fibres. Since we were able to mimic the staggerdness, we may compute f from the tube model and compare it to Weinbaum's results.The drag coefficient, f, is described by the following equations:

$$\overline{\nabla P} = -3\mu f \frac{\overline{U}}{B'^2} \tag{4.4}$$

$$\frac{Q}{2B'W\overline{U}} = 1 \tag{4.5}$$

Where Q is the total flux and 2B' is the vertical separation (or post height) of the channel. The overbar denotes an average over a region which is small compared with the macroscopic lengthscale, yet large enough to level off the microscopic hetrogeneity; for the channel, the average is taken over one periodic unit.

Based on the above expressions, we may obtain modified "effective variables" and compute the drag coefficient for the tube-model. Let Q_t be flow-rate obtained from a 1-D calculation (say in the left-right direction). Let $\overline{P}_x$ be the pressure imposed for this 1-D calculation. Similarly, let $\overline{P}_y$ be the pressure gradient imposed on the tube-model to obtain a 1-D flow (in the bottom-top direction) in order to obtain the same mass flux Q_t, now in the bottom-top direction. Since $Q_{tx}=Q_{ty}=Q_t$, we must have that $P_x=P_y$ in magnitude. Thus, if we were to sum the two flow's, the total flow-rate across the *nn'* line would be $2Q_t$,. Similarly, the magnitude of the pressure gradient would be the magnitude of the vector sum of the gradients $\overline{P}_x$ and $\overline{P}_y$,. Thus,

$$\left\|\overline{\nabla P}_{eff}\right\| = \sqrt{2}P_x = \sqrt{2}P_y \tag{4.6}$$

$$Q_{eff} = 2Q_t \tag{4.7}$$

$$W_{eff} = \sqrt{2}L_p \tag{4.8}$$

Thus, based on the above quantities and equations [4.9]-[4.10], one may obtain a value for *f* from the tube model that mimics a staggered-grid in Weinbaum's model..

$$\frac{Q_{eff}}{2B'W_{eff}\overline{U}_{eff}} = 1 \tag{4.9}$$

$$f = \frac{\nabla P_{eff} B'^2}{3\mu \bar{U}_{eff}} \tag{4.10}$$

In general, the drag coefficient, f, is computed as a function of fibre volume fraction S, defined as the ratio of fibre volume to total volume, the aspect ratio B, given by the ratio of the channel height to post diameter, and the flow configuration. Tsay and Weinbaum (1991) have obtained an interpolation formula for the friction factor, f, described by the following equations:

$$f = \left(f_{2D}^n + f_{3D}^n \right)^{\frac{1}{n}} \tag{4.11}$$

with

$$f_{2D} = \frac{2}{3}\left(\frac{B'}{W_{eff}}\right)^2 \frac{54.95}{S\left(\frac{\Delta}{0.5d}\right)^{2.377}} \tag{4.12}$$

$$f_{3D} = \left(\frac{1 - b_1 S_\Delta}{1 + b_1 S_\Delta}\right) - 2b_1 \left(\frac{S - S_\Delta}{1 + b_1 S_\Delta}\right) \frac{1}{1 + b_1 S_\Delta} \tag{4.13}$$

where S_Δ=S when 2Δ/d=2B, and

$$n = \frac{B}{(0.1918 + 0.3308B)} \tag{4.14}$$

$$b_1 = \frac{K_2\left(\frac{\pi}{2B}\right)}{K_o\left(\frac{\pi}{2B}\right)} \tag{4.15}$$

Where K_n are modified Bessel functions of order n.

For the comparison, we set B=1 and 5, L_p=15 μm, P_{inlet}=10 cm(water), and P_{exit}=9.5 cm(water). Figure [4.5] shows a comparison for B=1 an B=5. The results show a reason-

able agreement with Weinbaum's exact analysis, and the error was within 30% for mosr cases.

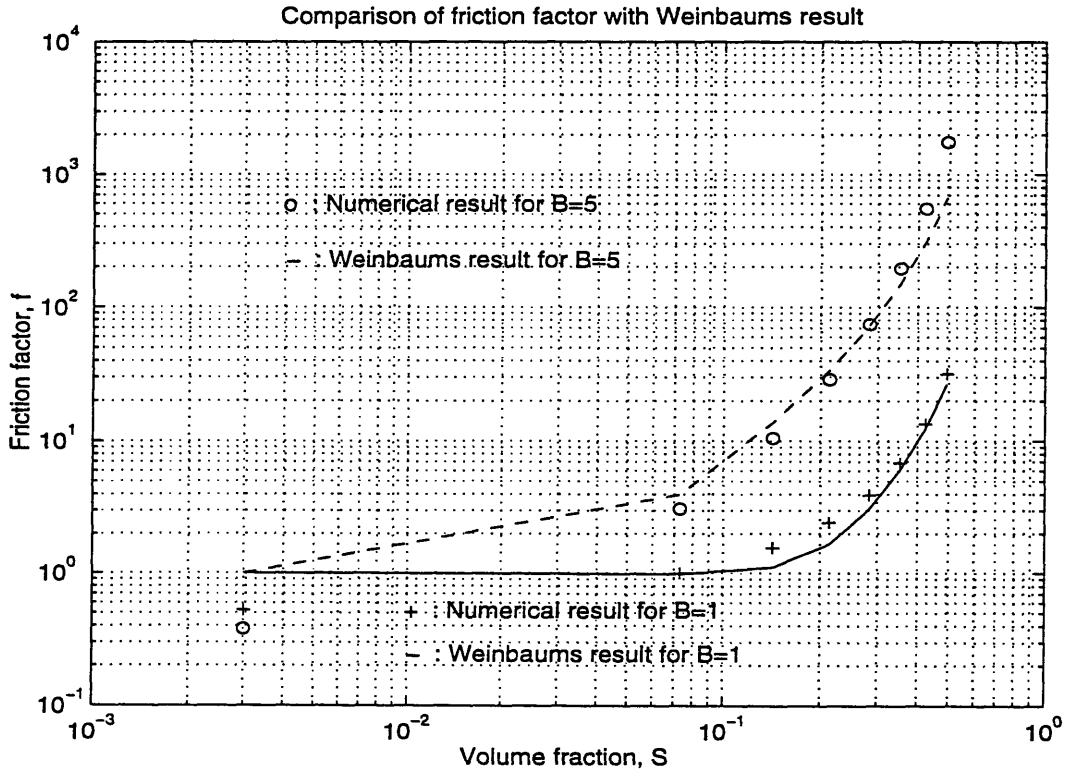

Figure 4.5: Friction factor comparison with Weinbaum's model

A note about the friction factor computation from the Tube-model

The exact analysis of Tsay and Weinbaum for a rigid cross-bridged fibre matrix provide a good test for comparing the capillary and junction resistance in the tube model. While the results presented in this thesis were obtained using resistance estimates described in chapter 3 (K_p=0.4 and estimation of hydraulic diameter assuming an elliptical cross-section), we were able to improve the resistance estimate by setting K_p=0.25 and by computing the capillary resistance by assuming a rectangular axial cross section in order to determine the hydraulic diameter at locations along the capillary. This improved the friction factor comparison with Weinbaum's results (Figure [4.5]), and thus allowed for a better estimate of the junction and capillary resistance.

We now proceed to present the results obtained from the tube-flow model. First, results for the dynamics associated with breathing are presented, followed by results for static cases under various conditions (spatial variability and capillary blockage).

4.3.2 The dynamics induced due to breathing.

Having established that the flow-rates obtained from the static sheet-flow model and the static capillary-network model are in good agreement, we can now proceed to calculations pertaining to the dynamic effects associated with breathing.

Breathing is examined under 3 conditions, namely, *(i)* no statistical variability in α and h_0, *(ii)* statistical variability in the parameters, and finally, *(iii)* no variability but with the blockage of 2 capillaries. Our interest in is exploring the extent of pressure and flow-rate oscillations induced within the septum resulting from time-dependent deformations of the septum and variations in the volume compliance, $\beta(t)$ (see ch. 3), with breathing.

Since our interest lies in the flow-rates observed in capillaries and the pressure oscillations at the junctions, we have developed a method to conveniently represent all of the time-varying flow-rates and pressures on a single chart. With this approach, flows in individual capillaries are plotted vs time, and the plot for each capillary is placed at a location corresponding to the location of the given capillary in the network. Similarly, pressures at each of the junctions are represented by individual time history plots, and each time history plot is placed onto a location on the chart that corresponds to the physical location of the given junction. The time-axis for each of the plots ranges from 0-5 seconds.

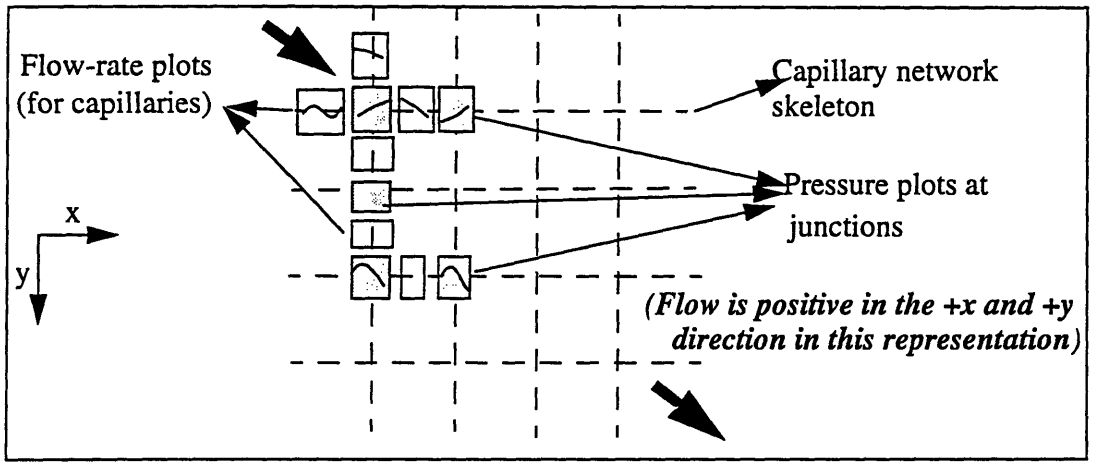

Figure 4.6: Method to show time-dependent pressures and capillary flow-rates on a single chart.Time-history plots are placed at every junction and capillary in the network.

The results in this section are presented in the following order

Pressure range (cms of water)	Statistical variability?	Capillary blockage?
10-9.5	N	N
1.0-0.0	N	N
10.0-9.5	Y	N
1.0-0.0	Y	N
10.0-9.5	N	Y
1.0-0.0	N	Y
10.0-9.5	Y	Y
1.0-0.0	Y	Y
10-9.5. 5% Pulsatile	N	N

Table 4.3: Presentation of results for the dynamic cases

Note that the pressure gradient was increased for cases with low mean pressures. This was done in order to maintain the same flow-rate through each septum. Approaching the venular side from the arteriolar side, the local blood pressure decreases monotonically,

thereby causing the capillaries toward the venular side to be less distended than those on the arteriolar side. On average, however, they must carry the same flow rate and therefore require a greater pressure drop at lower mean pressures.

Dynamic case with no spatial variability and no capillary blockage

We now proceed to present the results for the case with no spatial-variability. The computations were done at two conditions of inlet-exit pressures (given in table [4.3]). Figures [4.7] and [4.8] show the results obtained for these cases.

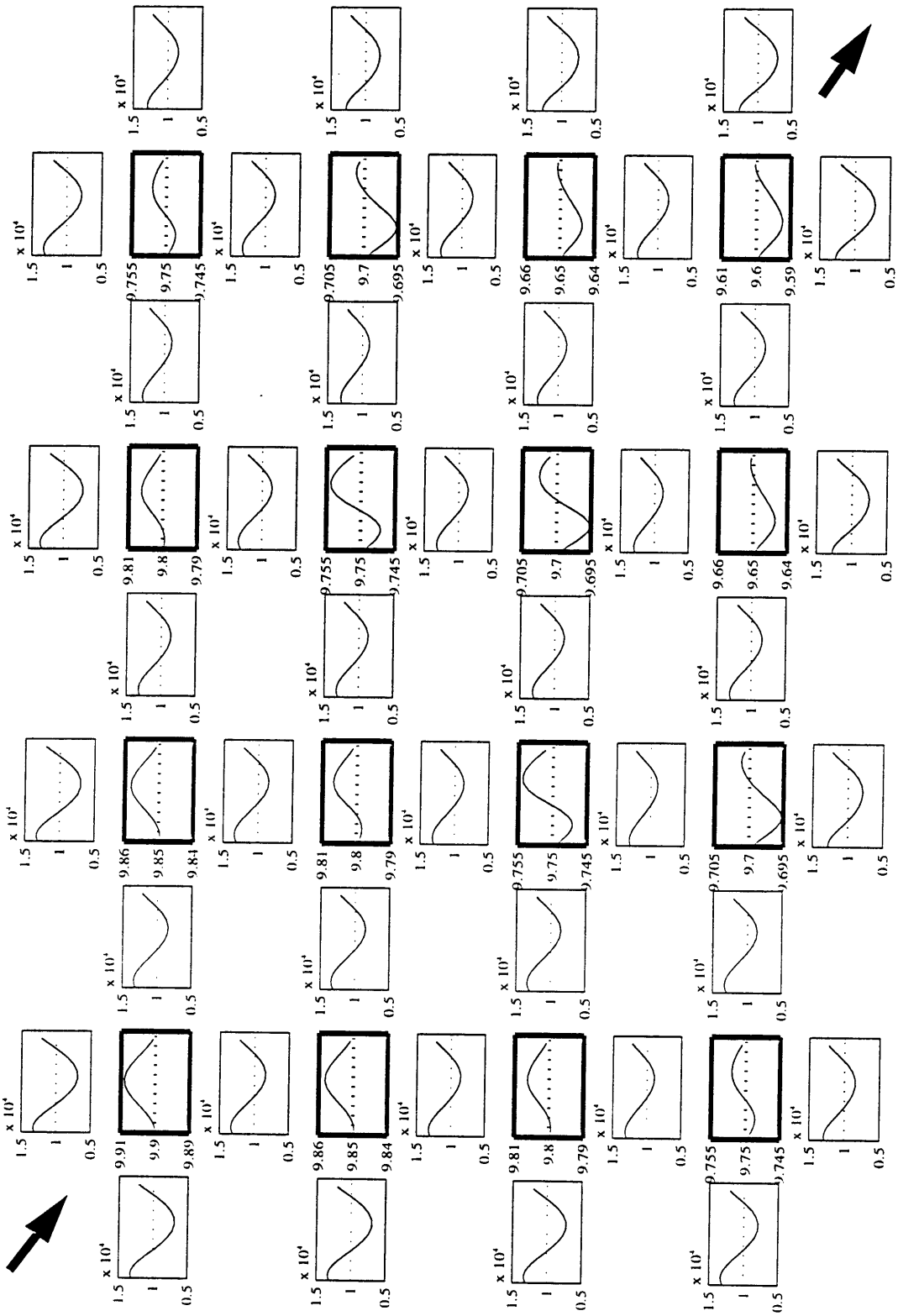

Figure 4.7: Case with no statistical spatial variability in h_o &α. P 10-9.5 cm of water.

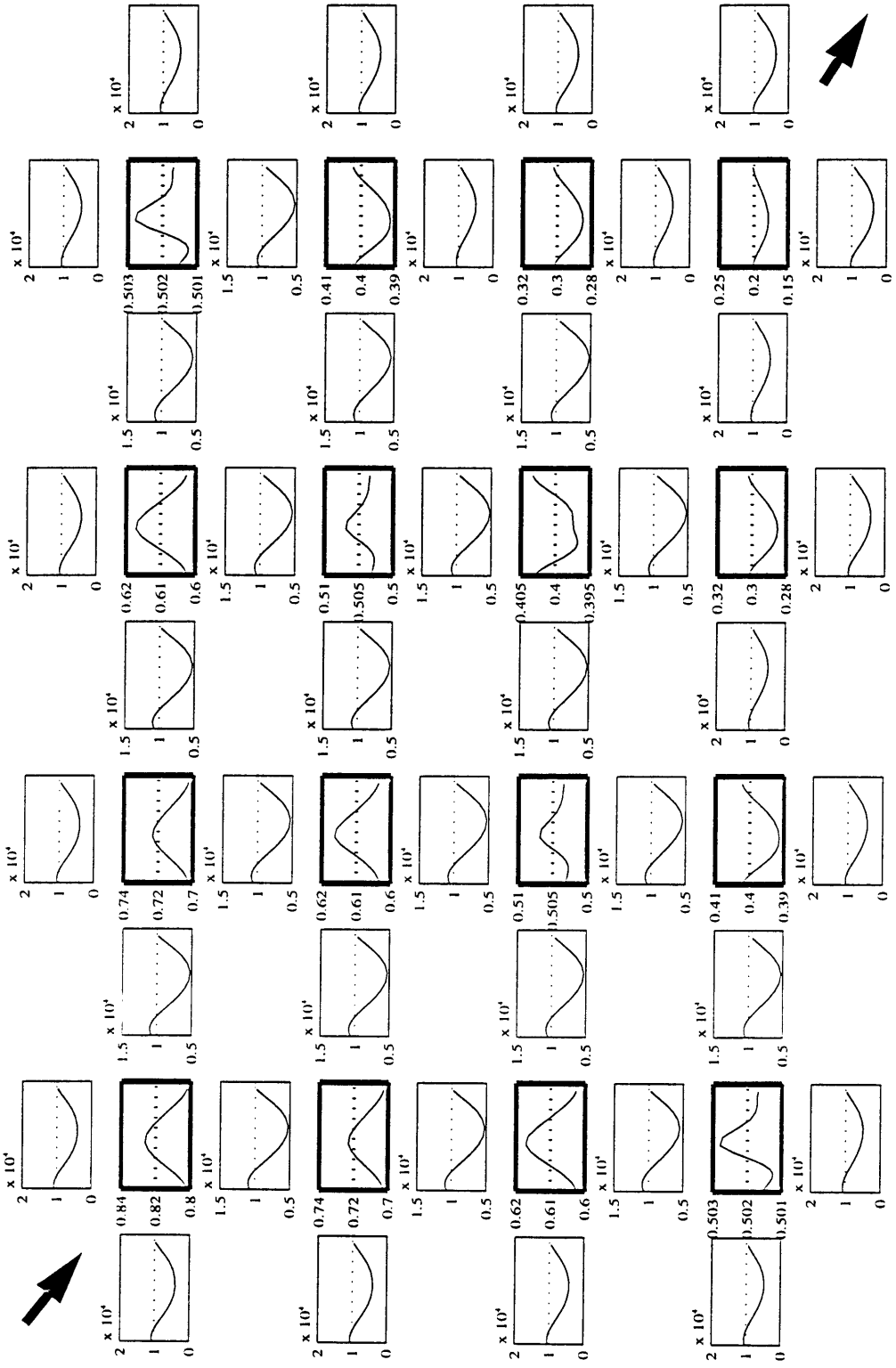

Figure 4.8: Dynamic case with no statistical variability and a lower inflow and outflow pressure boundary condition (P_{in}=1 cm(H_2O), P_{out}=0.0 cm (H_2O))

Figures [4.7] and [4.8] show that the dynamics induced due to breathing have a significant influence on flow-rates but much less in pressures in the capillary bed. Figure [4.5] indicates that in a homogenous sheet (no spatial variability), the flow rates within the capillaries may oscillate by as much as 50% during a breathing cycle. The relatively large oscillations in flow-rates is important, and will play a key role in determining the transit of RBC's. Further, typical pressure oscillations at the junctions are relatively small. This may be misleading, however, since it is largely due to the fact that the overall pressure-drop across the capillary bed is fixed while the flow rate is allowed is allowed to vary. Conversely, if flow-rates were specified at the boundaries, the pressure fluctuations would be greater by comparison. Perhaps a better way to view this result is in terms of segmental resistance which changes due to the changing septal dimensions. Since the swings in the junction-pressures are small, the resistance must vary significantly in order to produce the observed changes in flow-rates. Therefore, both the geometry and viscosity of blood in the capillary bed play a key role in determining plasma (and possibly RBC and PMN) transit.

This effect of viscosity is even more pronounced for the case of homogenous properties but a lower pressure range (1.0-0.0 cms of water, figure [4.8]), where the capillaries are less distended. In this situation, since the low-pressures result in smaller capillary distensions, the overall dimensions of the capillaries remains small, allowing for the non-linear effects of the blood viscosity to become more prominent; these non-linear effects may be observed in the behavior of junction pressures in figure [4.6]. This situation with lower capillary distensions also results in a more pronounced time-dependent gradient in pressures (say between adjacent junctions). Since the overall force on a cell (RBC or PMN say) within a capillary depends on this gradient in pressure, these dynamic pressures will

play a key role in mechanically mobilizing a PMN (or a capillary blocked by an RBC). Pressure differences between junctions across a blocked capillary may be critical in either mechanically mobilizing or activating a blocked PMN, depending on its sensitivity to changes in surrounding pressures.

Dynamic cases with Spatial variability in parameters and with no capillary blockage

We now proceed to present results for the dynamic cases with spatial variability in parameters. We are interested in looking at the spatial distribution of flow-rates as a result of spatial variability in parameters, and also in making a comparison between how sensitive the effect of spatial variability is on the values of inlet-exit pressures. Time and spatially averaged flow-rates are compared in order to make this comparison.

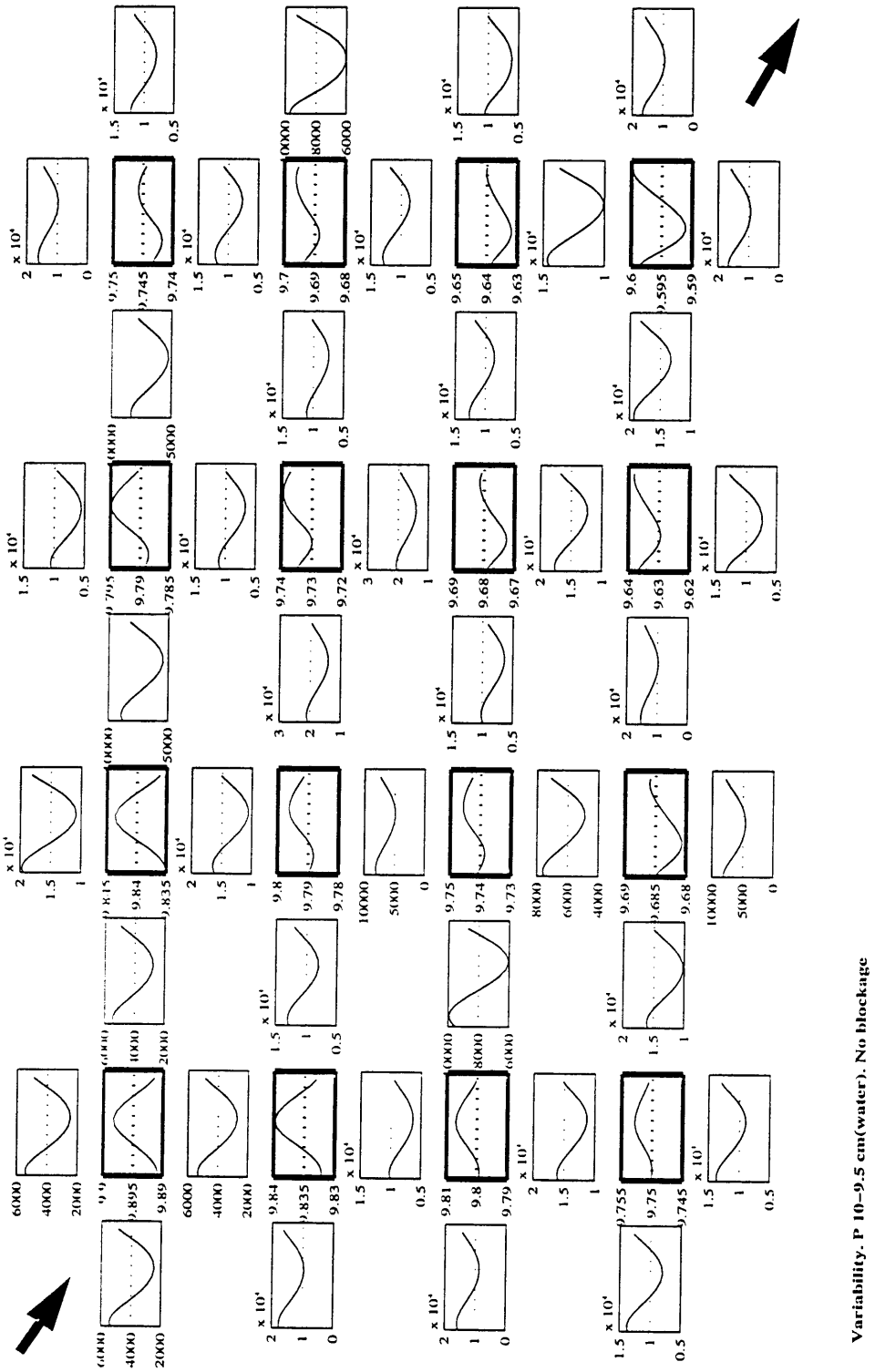

Figure 4.9: Case with 40% statistical variability(std. deviation, uniform probability distribution) in compliance, α, and 40% variability(std. deviation, uniform distribution) h_o.

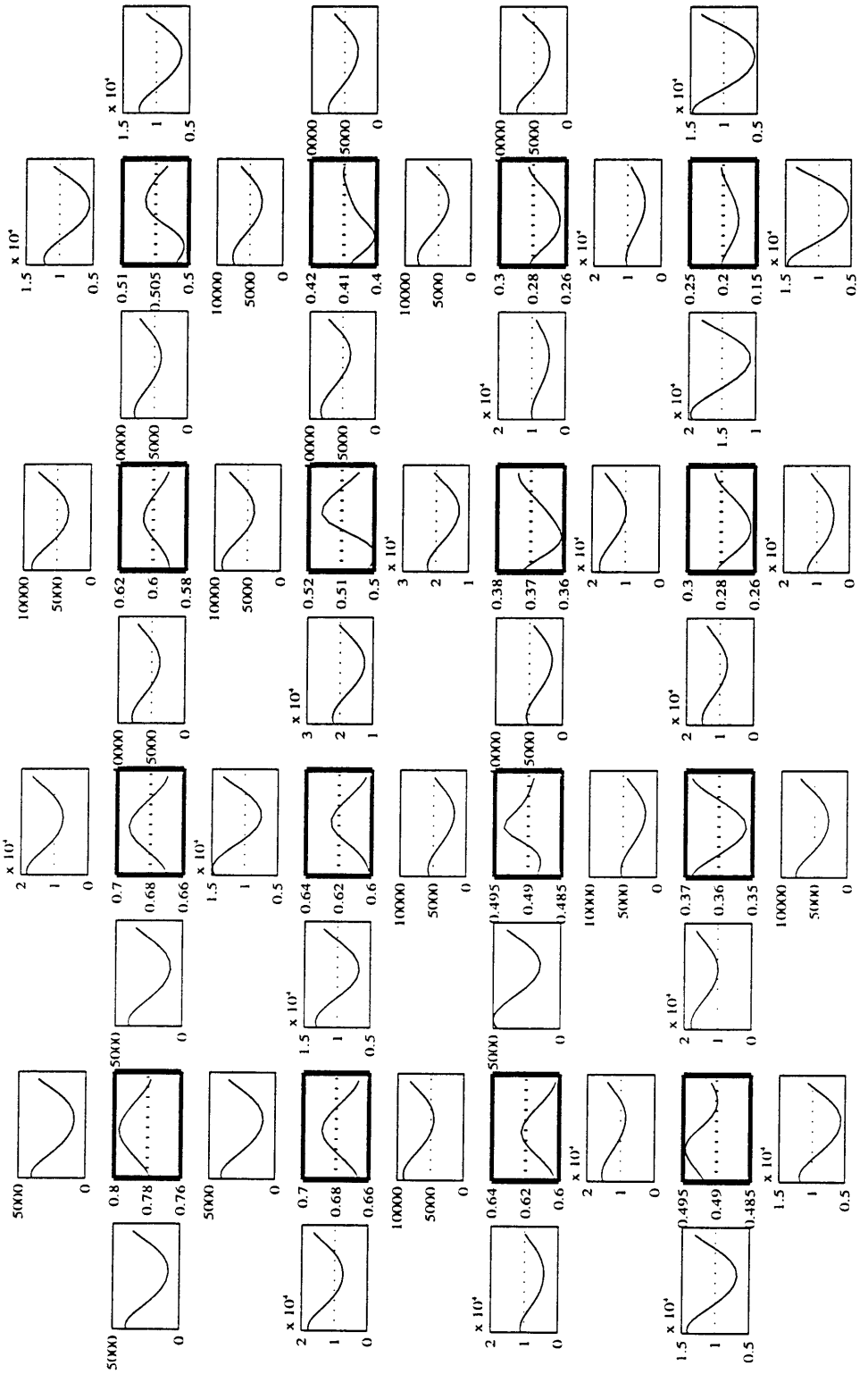

Figure 4.10: Variability in parameters. P 1-0.0 cms of water

Statistical variability clearly plays an important role in determining the dynamics of blood flow in the septum. Although the following sections will primarily deal with issues such as the overall distribution of flows, a few observations from the previous two plots may be made. Similar to previous observations, the non-linear effects become more prominent for a lower range of pressure. The dynamics or "oscillations" in the capillary flow-rates follow similar trends as the case with no variability, with an important difference being in the extent of spatial distribution in the mean flow-rates. Even though introducing randomness does not change the time-dependent flow rate wave forms (they appear similar to the case with no variability), a key aspect introduced as a result of spatial variability is the spatial distribution of mean flows and flow-rate amplitudes; figures [4.9]and [4.10] indicate the spatial discrepancies in flow-rates (magnitude of oscillations, range of oscillations etc.); see figures [4.9] and [4.10]

Dynamic cases to demonstrate the effect of capillary blockage under homogenous and spatially variable sheet properties

The effect of capillary blockage coupled with the spatial variability in the parameters is presented in this section. We are interested in understanding the effect of capillary blockage on the overall flow distribution in the septum.

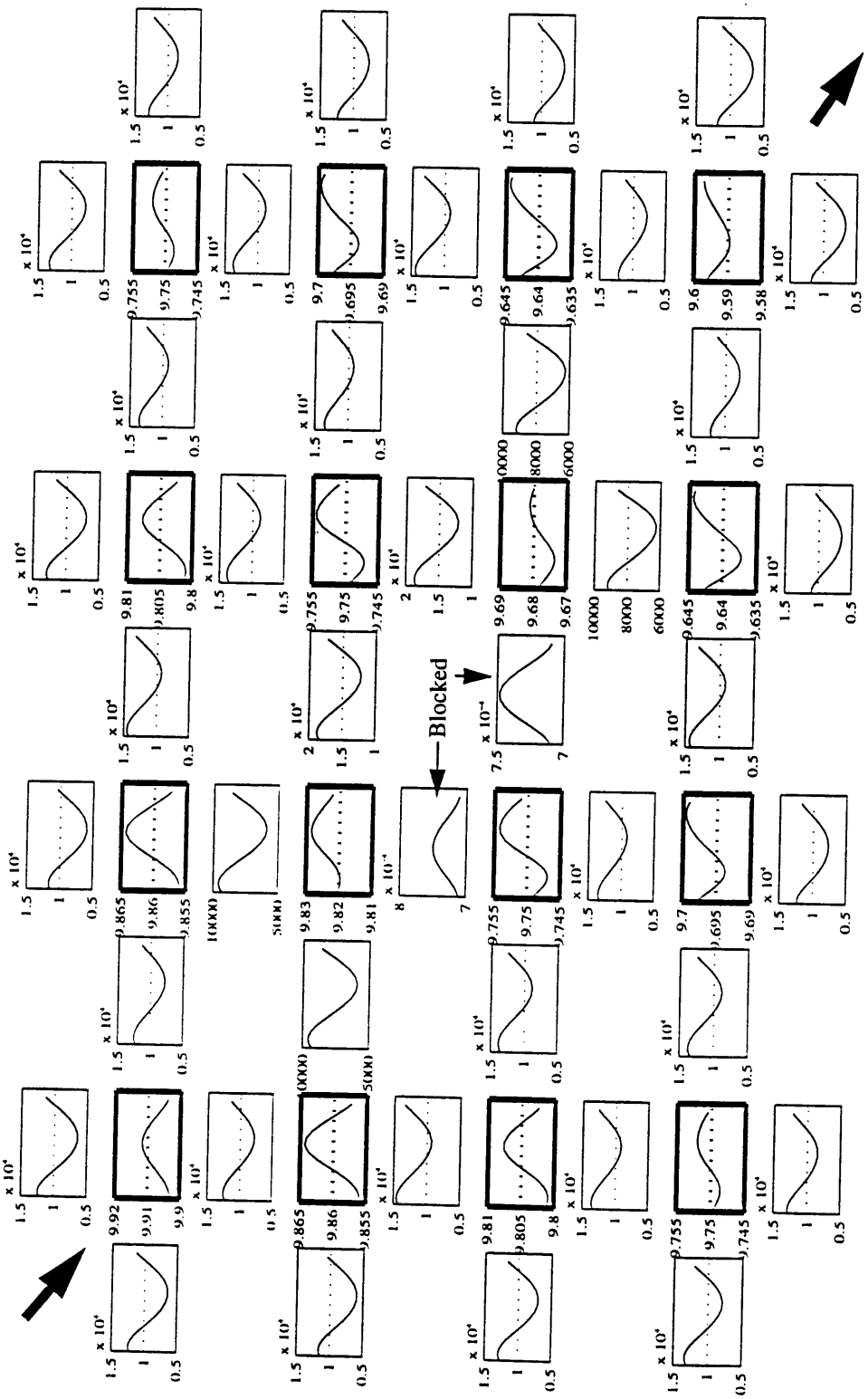

Figure 4.11: Case with uniform properties and blockage of 2 capillaries.

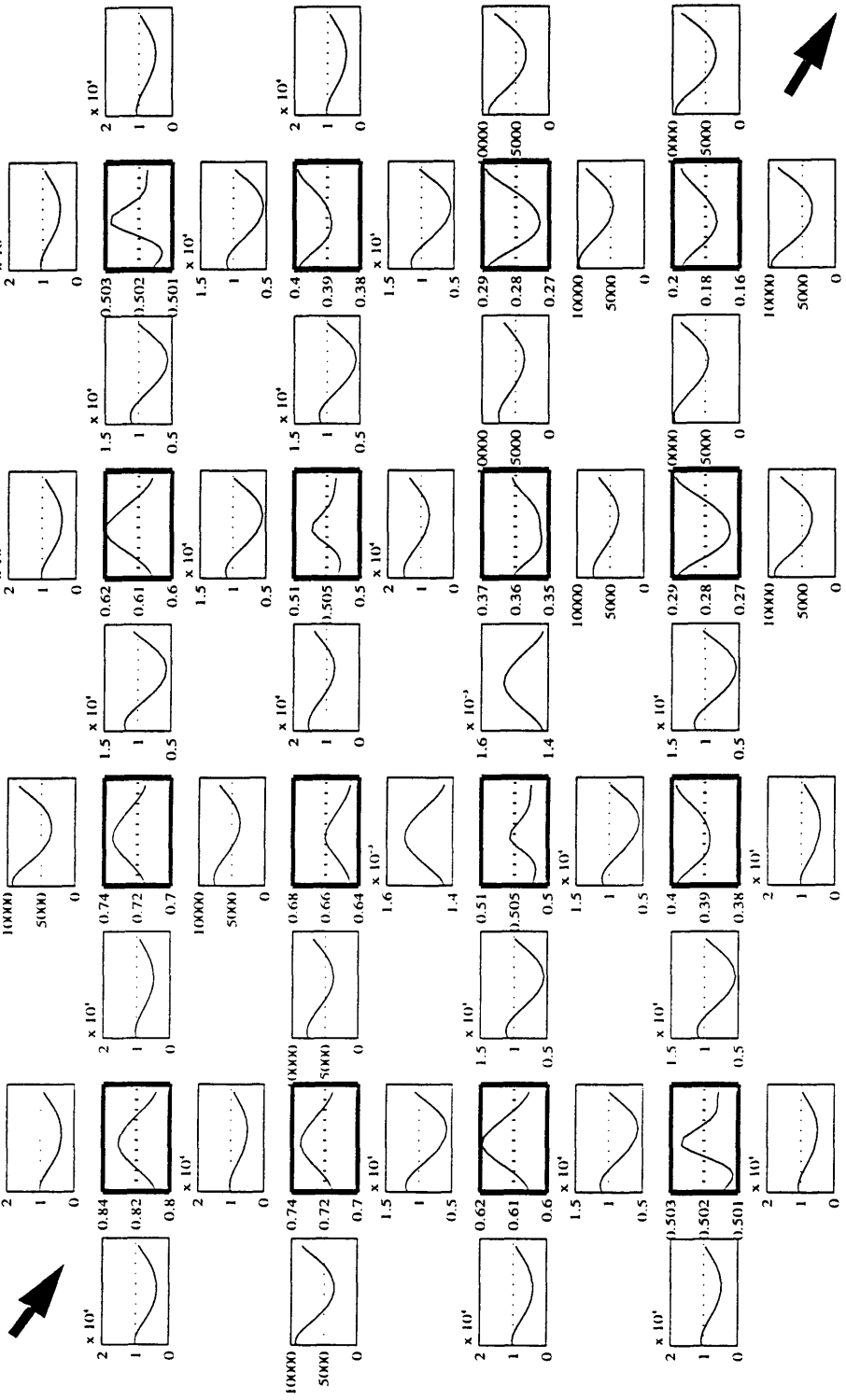

Figure 4.12: 2 capillaries blocked. P 1.0-0.0 cm of water

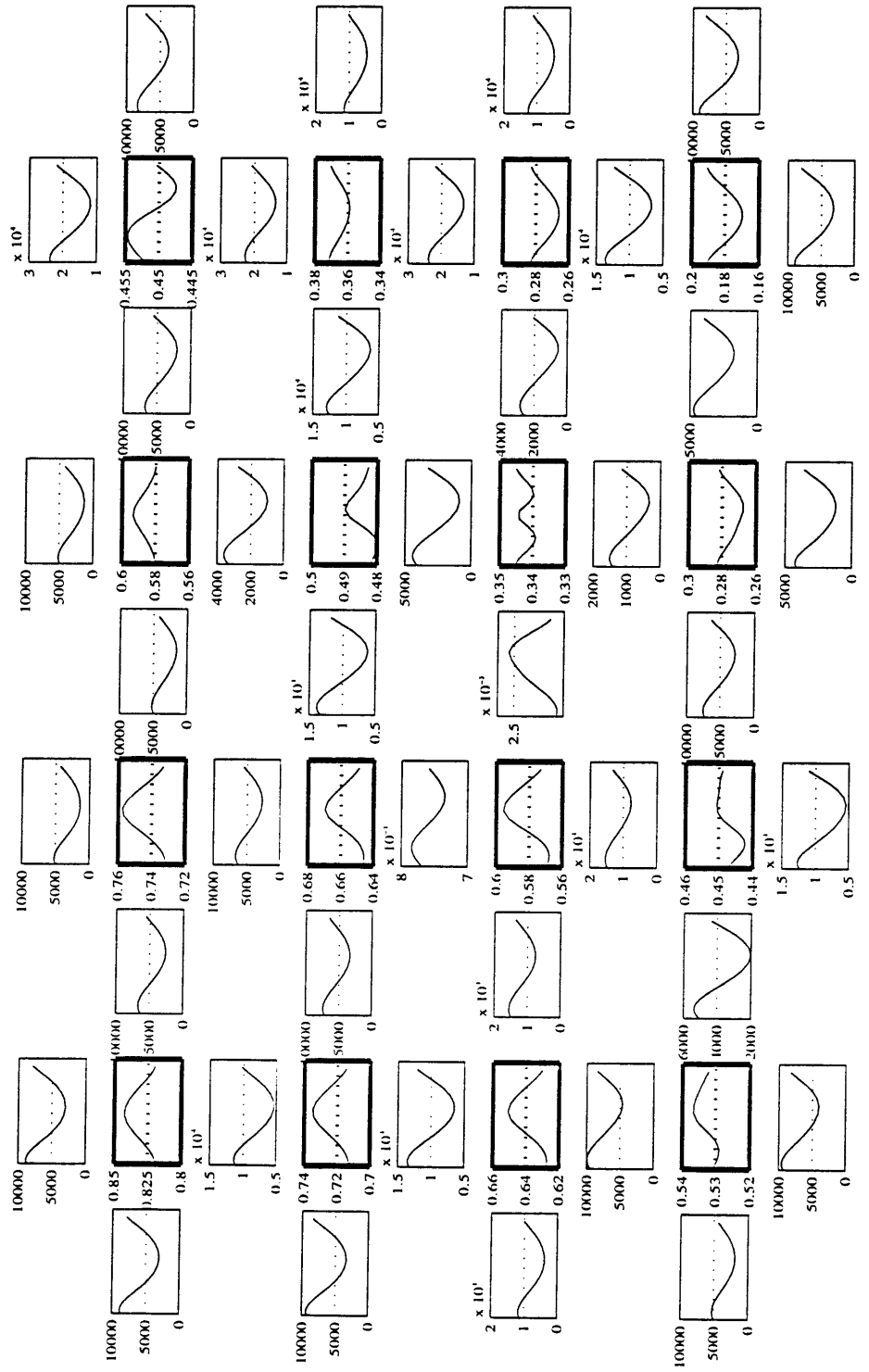

Figure 4.13: 2 capillaries blocked. variable properties. P 10-9.5 cm of water

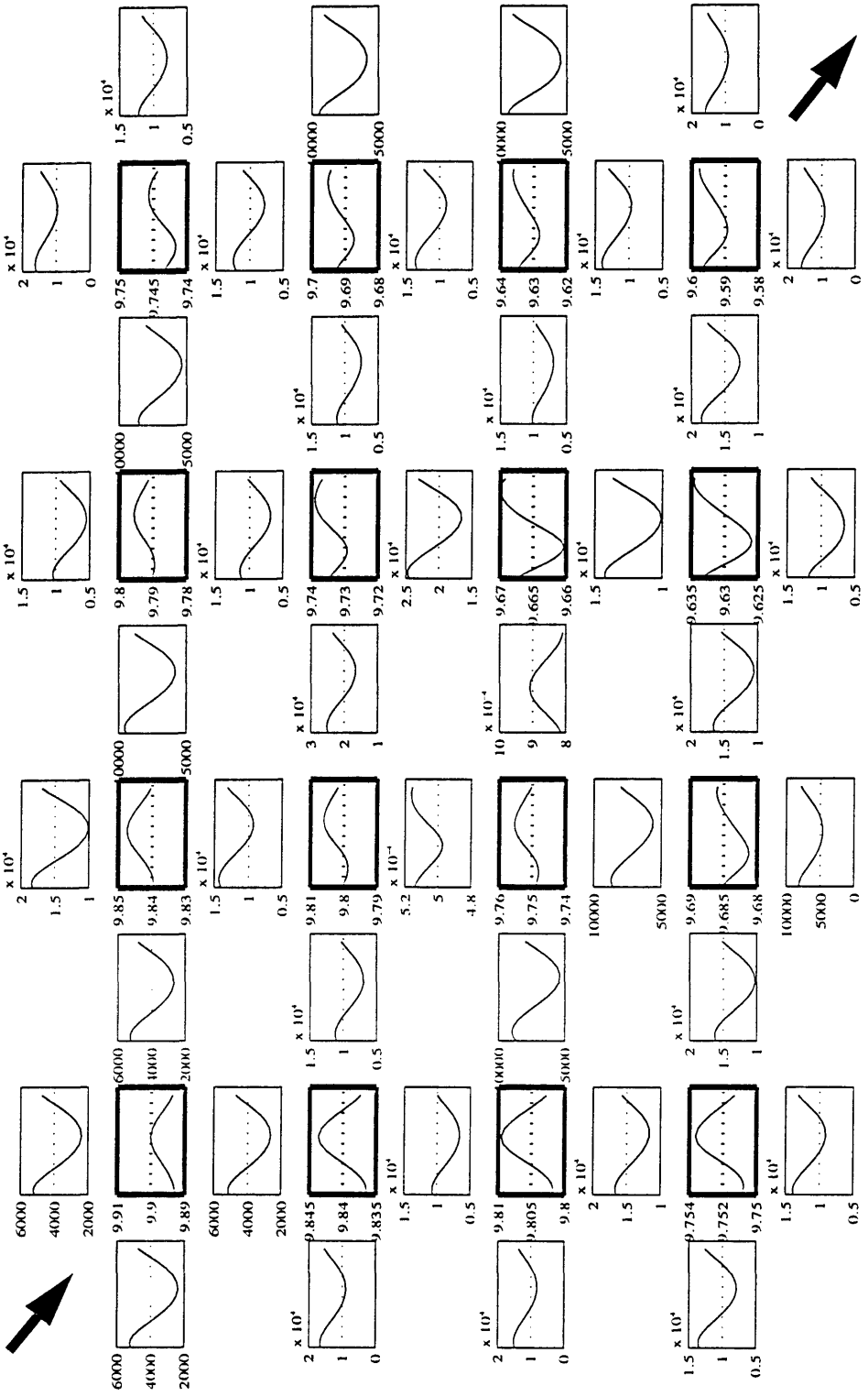

Figure 4.14: 2 capillaries blocked. Variable properties. 1.0-0.0 cm of water

Effect of pulsatility in boundary pressures

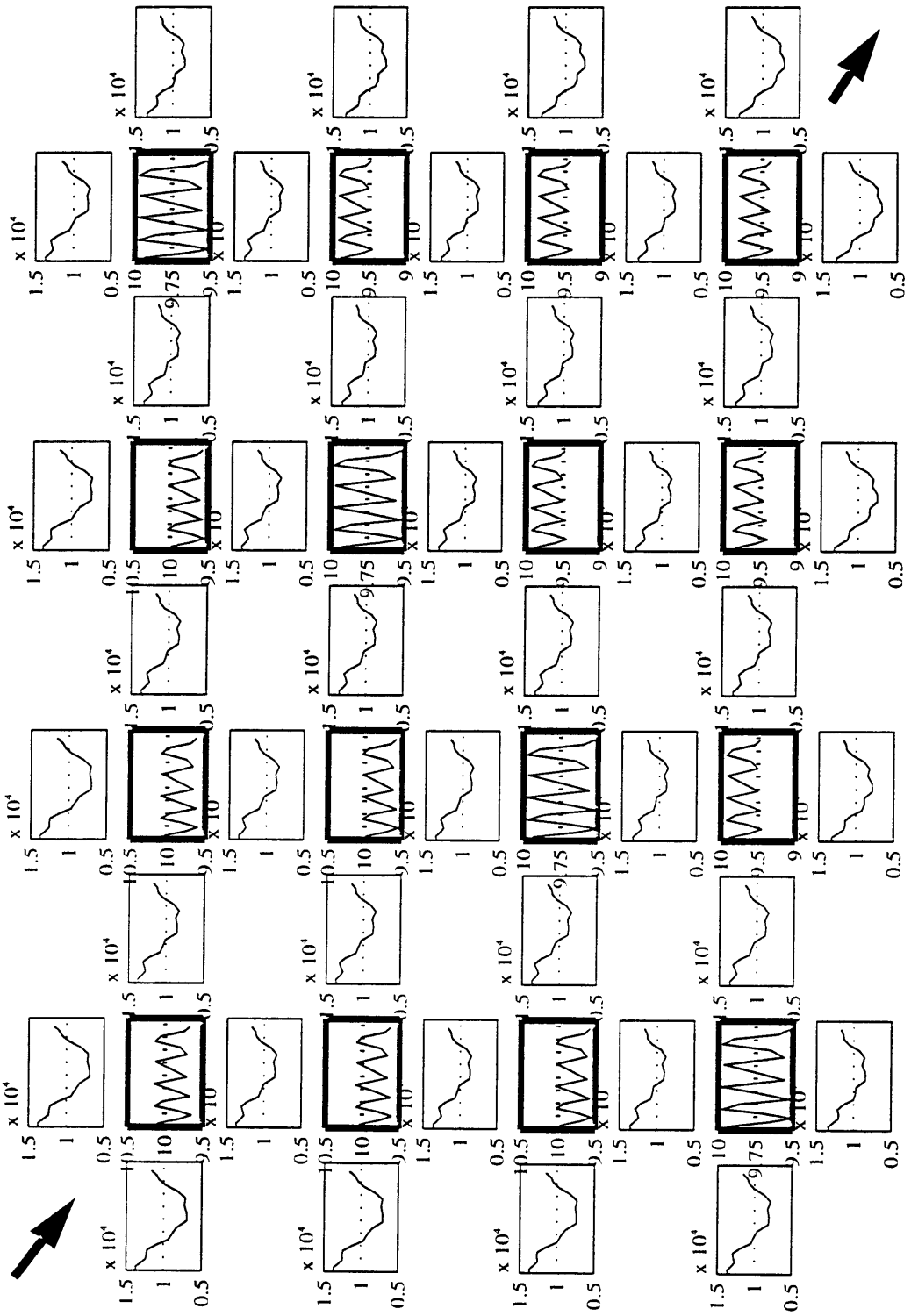

Figure 4.15: Case with 5% time-dependent sinusoidal pulsatility in the boundary pressures at cardiac frequency (taken as 60 beats/minute)

Capillary blockage affects the distribution of flows predominantly in the immediate vicinity the area of capillary blockage. The blockage of 2 capillaries introduces flow-rates in neighboring capillaries that vary in the extent of oscillation, as well as in the mean values, even for the case of uniform properties. This effect is quantified in more detail in the following two sections; however, the important point to note here is that capillary blockage did not introduce any appreciable effects in the neighboring region. The non-linearities become prominent at the lower pressure range, just as in the previous cases.

One of the questions we were interested in pursuing was "does variability, capillary blockage, or breathing introduce a condition of flow reversal during a breathing cycle?" Certainly, one could imagine a situation where a physically feasible boundary condition (pressure profile) coupled with blockage and variability would yield flow reversal in the bed. "Flow-reversal" will be of interest in determining RBC transit and also in addressing issues such as the transient force on a blocked PMN. However, for the cases considered, with the linear drop in pressure as the boundary profile, we failed to observe a reversal in flow.

Effect of pressure pulsatility

The pulsatile boundary pressures were imposed by using a mean profile of linear variation in pressures (as shown in figure [3.11]) and a 5% magnitude oscillation about the mean pressures; the oscillations being imposed at the cardiac frequency and with no phase lag around the boundary. A slight pulsatility in the boundary pressures at the cardiac frequency caused the pressures in the septum to oscillate at the cardiac frequency. However, the high-frequency oscillations induced in the septum were of a small magnitude compared to the extent of oscillations in the capillary resistance (which mimics the frequency

of sheet distension or the breathing frequency). As a result, capillary flow-rate waveforms primarily followed the breathing frequency. The magnitude of pressure oscillation amplitudes (~0.5 cm of water) are significantly larger than the pressure oscillation amplitudes for the case with no pulsatility. These pressure oscillations will be important is mobilizing RBC's and obstructing neutrophils in the capillary bed.

4.3.3 Results for static cases

Spatial variations in the sheet compliance, α, and the resting segment height represents the heterogeneity found in the septal-bed, and play a key role in the overall distribution of flows in the septal bed. In this section, we approach the problem with a more statistical view, and present results for several static cases to demonstrate the effects of spatial variability. It should be noted that other factors too can influence the degree of randomness seen physiologically. However, the extent to which these mimic the real variability seen in of pulmonary-blood flow suggest that they may be the most important factors.

There is a point to be made about the justification for our choosing to do static runs to study this phenomenon. We have seen from the dynamic cases discussed previously that the effect of breathing is important in causing large flow-rate oscillations within capillaries. However, we also observed that introducing randomness with the dynamic simulations does not change the character of oscillations introduced earlier, it introduces a spatial distribution in mean dynamic flows. Further, we obtained in chapter 2 that the time-scale for the equilibration of pressures was of the order of 10^{-3} seconds, which is small compared to the externally imposed time scales of the problem (~5 seconds for breathing or ~1 sec for cardiac pulsatility). Therefore, for purposes of exploring just the degree of spatial

variability, it is appropriate to study the phenomenon with static runs - the effects are well demonstrated in fig. [4.14].

The method adopted for choosing a random spatial distribution has been discussed previously in chapter 3. However, since we want to specifically see the effect the degree of randomness in α, and how it couples with the effects associated with degree of randomness in h_0, we made an initial selection of three spatially random distributions for each of the two quantities in order to make a comparative study; in other words, an initial selection of 3 randomly selected spatial distributions for 0%, 15% and 30% variability in h_0, in conjunction with an initial selection of 3 randomly selected spatial distributions for 0%, 25%, and 50% variability in α was made. In order to study the effect of each of the parameters, combinations from this set of selections were explored. Further, in order to get an idea for the overall distribution in the capillary flow-rates, we computed the overall spatial mean and standard deviation of the capillary flow rates (obtained for static runs).

The method for presenting the results was chosen as follows. Static runs (no breathing) result in steady state capillary and junction flow-rates. These flow-rates are then mapped onto the physical geometry of the capillary bed, with the greyscale shading along capillaries representing corresponding flow-rates. This method provides an easy way to visualize the network and the overall flow-distribution. Figure [4.16] demonstrates this method of visualization by showing a sample graph

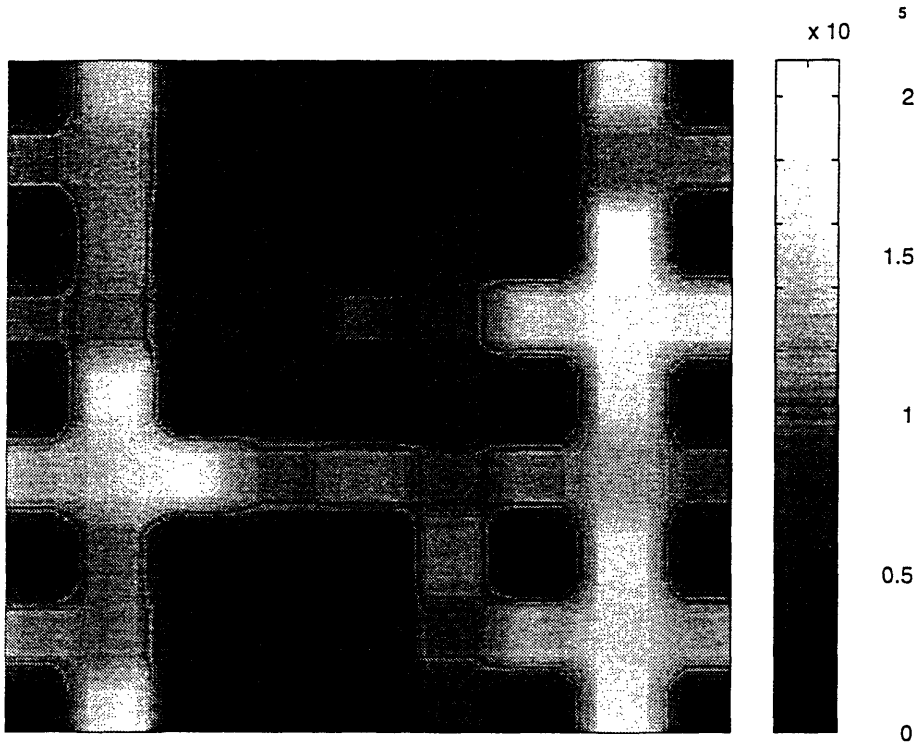

Figure 4.16: A Sample graph demonstrating the visualization of the capillary bed and the flow-rate distribution in the network.

The effect of spatial variability in h_0 and α.

The above plot presents a sample calculation for the flow-rate distribution in a static capillary network with statistical variability in h_0 and α. Figure [4.17] presents a series of plots showing the effect of increasing randomness in each of the two parameters. From the figure, it is evident that the flow distributions are more sensitive to the degree of randomness in h_0 than the degree of randomness in α. This is easily seen by noting that of the two terms in equation [3.4] that determine the vertical dimension *h*, the first term (h_0) is typically about 3 times larger than the second ($\alpha\Delta P$). Therefore, its effect on the flow distribution should be roughly three times as great.

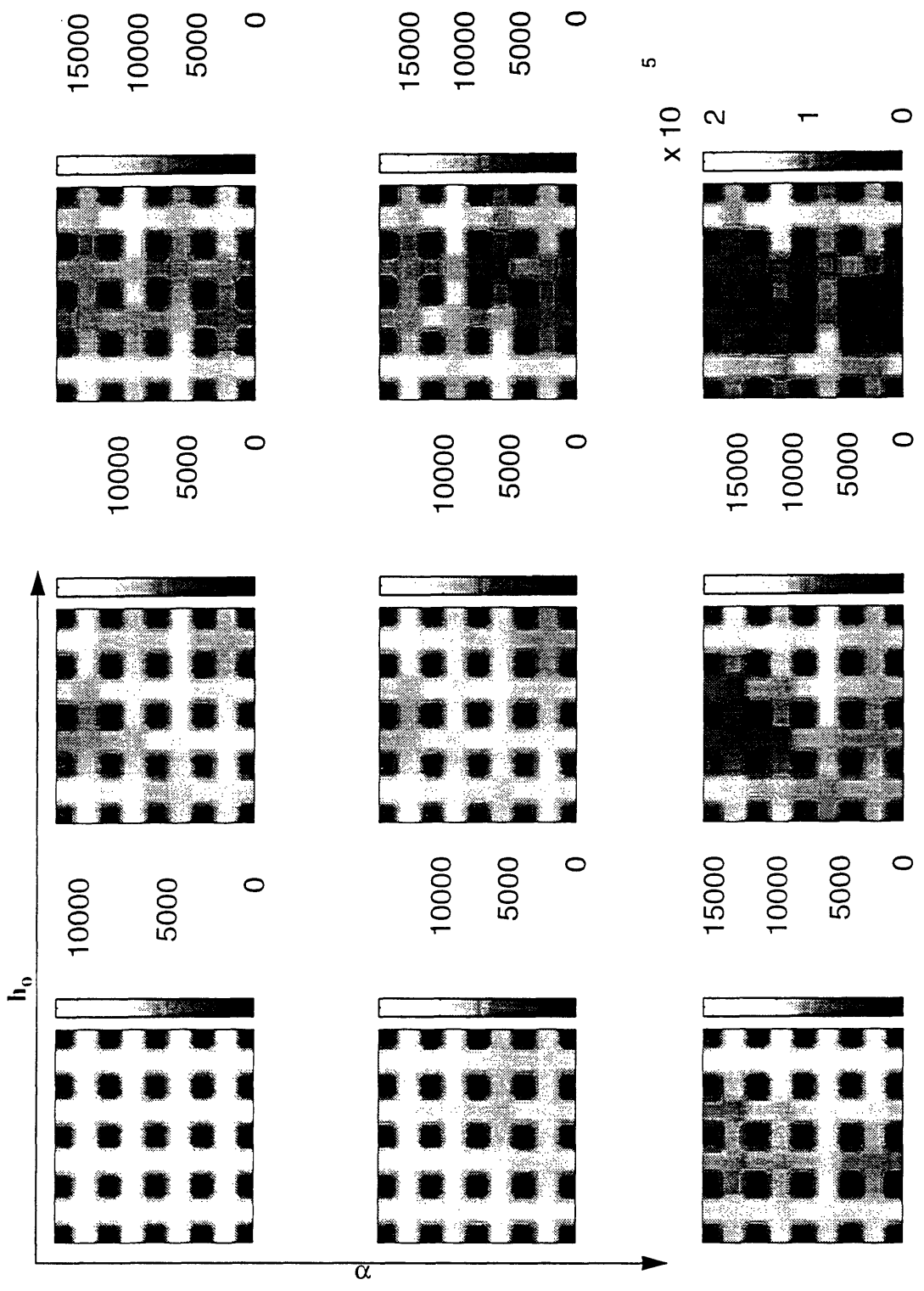

Figure 4.17: Effect of randomness in α and ho. The extent of variability in each of the variables increases in the direction of the arrows shown. Flow rates in μm^3/sec

Table 4.4: Mean flow rates (spatial mean) in cubic microns/sec & associated standard deviation of the flows

% Variability	h_0=0%	h_0=15%	h_0=30%
alpha=0%	1.109e+04, 52.6963	1.1057e+04 1.9871e+03	1.1159e+04 2.5301e+03
alpha=25%	1.1601e+04 1.1063e+03	1.1664e+04 1.8868e+03	1.1559e+04 2.9998e+03
alpha=50%	1.0876e+04 2.4100e+03	1.0857e+04 3.522e+03	1.0873E04 4.3348E03

(* Values listed as (mean,std) in cubic-microns/sec)

Table 4.5: Coefficient of variation (std/mean)

% Variability	h_0=0%	h_0=15%	h_0=30%
alpha=0%	0.0048	0.1797	0.2267
alpha=25%	0.0954	0.1618	0.2595
alpha=50%	0.2216	0.3244	0.3987

4.3.4 Effect of capillary blockage.

Capillary blockage, a condition of little or no flow through a capillary, may occur due to several reasons in a capillary bed - there may be a region of collapsed capillaries or a region where one or more capillaries have been blocked mechanically (RBC's, PMN's). We are interested in how capillary blockage influences the overall distribution of flows and pressures in the capillary bed, and also in how the blockage influences pressures and flows in neighbouring capillaries. In addition, we would like to examine the coupled effect of blockage and randomness in the parameters.

This section presents the results in much the same way as in the previous section pertaining to the effect of randomness. Figure [4.18] is a sample plot, demonstrating the effect of segment blockage on flow-rates in a situation where the properties of the septum are uniformly distributed.

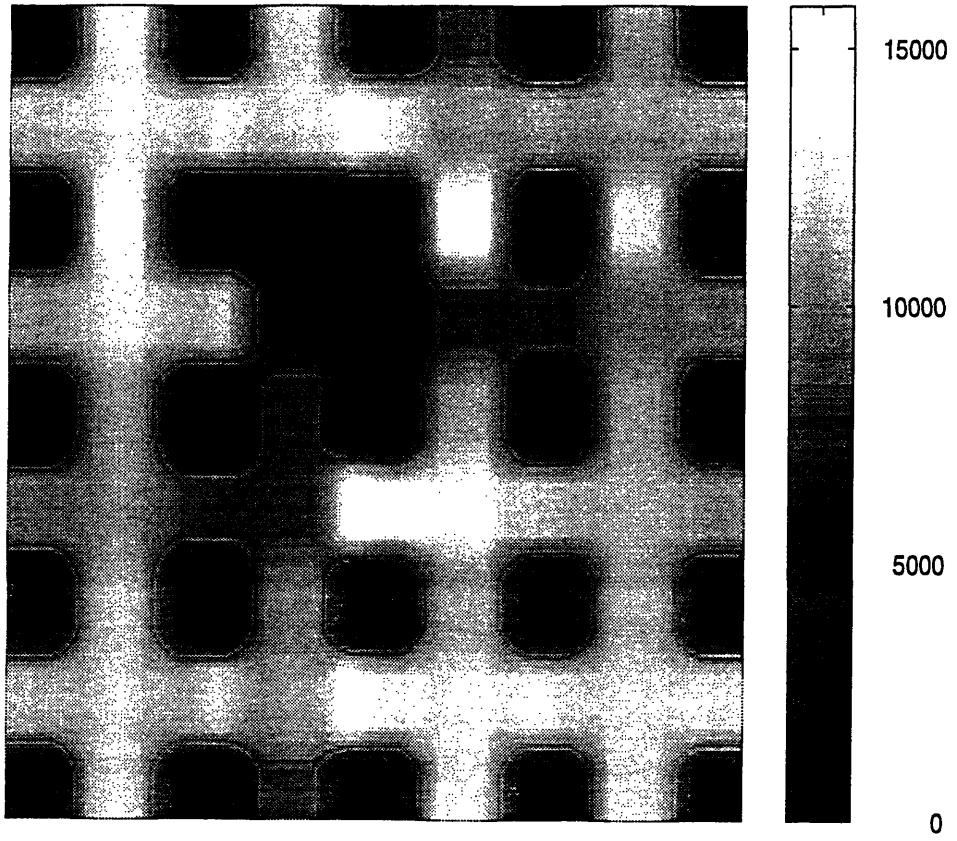

Figure 4.18: Example of a graph showing the flow-rate distribution in a case with uniform properties but two capillary segments blocked. Flow rates in cubic-microns/sec

Statistically speaking, it is clear from the above figure that the blockage of capillaries introduces an appreciable spatial distribution in the flow-rates (see also mean and standard deviation values in table [4.6]). However, the disturbances introduced are mostly local to the region of blockage. Introducing randomness in the variables coupled with capillary-blockage increases the spatial variability in the computed flow-rates, as expected. Capil-

lary blockage also couples with the effect of spatial variability to produce "patchy" flow-regions, or, regions of high and low flow-rates (Figure [4.22]).

Table 4.6: Demonstration of the effect of capillary-blockage: Mean flow rates (spatial mean) in cubic microns/sec & associated standard deviationof the flows

% Variability	h_0=0%	h_0=15%	h_0=30%
alpha=0%	1.0841E4 1.6518E3	1.0987E04 2.6920E3	1.0789E4 2.9659E3
alpha=25%	1.1101E4 1.9003E3	1.1406E4 2.6508E3	1.0846E4 3.2936E3
alpha=50%	1.0813E4 2.8949E3	1.0914E4 3.9127E3	1.0739E4 4.6209E3

(* Values listed as (mean,std))

Table 4.7: Coefficient of variation (std/mean)

% Variability	h_0=0%	h_0=15%	h_0=30%
alpha=0%	.1523	0.2450	0.2749
alpha=25%	.1712	0.2324	0.3037
alpha=50%	.2677	0.3585	0.4303

One method of quantitatively addressing the question of the spatial extent of capillary blockage is to consider the following plots which make a comparison of flow rates in capillaries in the 'blocked case' to the flow-rates in corresponding capillaries in the 'unblocked case' with the same degree of variability in h_0 and α. This comparison is made by computing ing a 'relative deviation from the unblocked case, f_r' for each capillary, and plotting this fraction vs. the spatial separation of that capillary determined by the shortest number of capillaries that need to be traversed from the 'blockage junction' in order to reach the given capillary. These plots may be obtained for any of the 'blocked cases' (with

different degrees of randomness). Figure [4.19] further illustrates how the plots are generated, based on the skeletal capillary network.

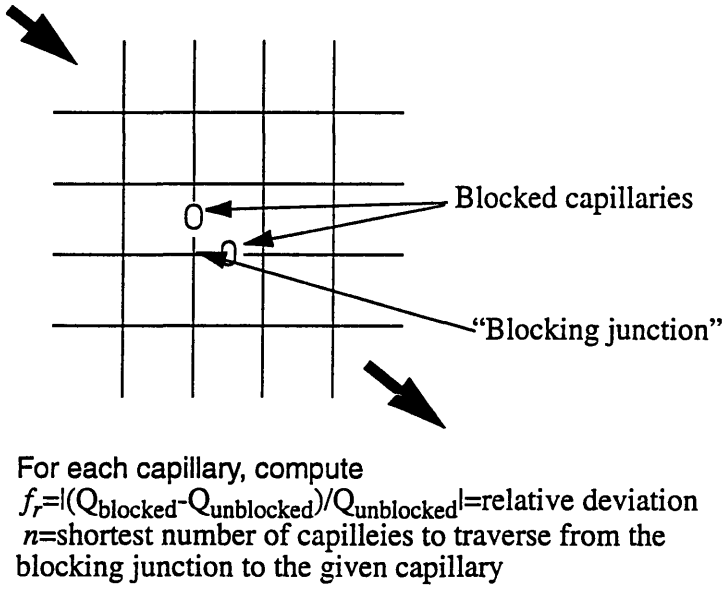

Figure 4.19: Demonstration of plots to show the spatial extent of capillary blockage.

Based on the above figure, the following plots were generated for the *(i)* No variability case, *(ii)* the '15% h_0 and 25% α variability' case, and finally,*(iii)* the '30% h_0 and 50% α variability' case. Figure [4.20] shows a plot of the parameter f_r as a function of n (for the blocking junction), the minimum number of capillary segments needed to traverse from any given capillary segment to that "blocking junction".

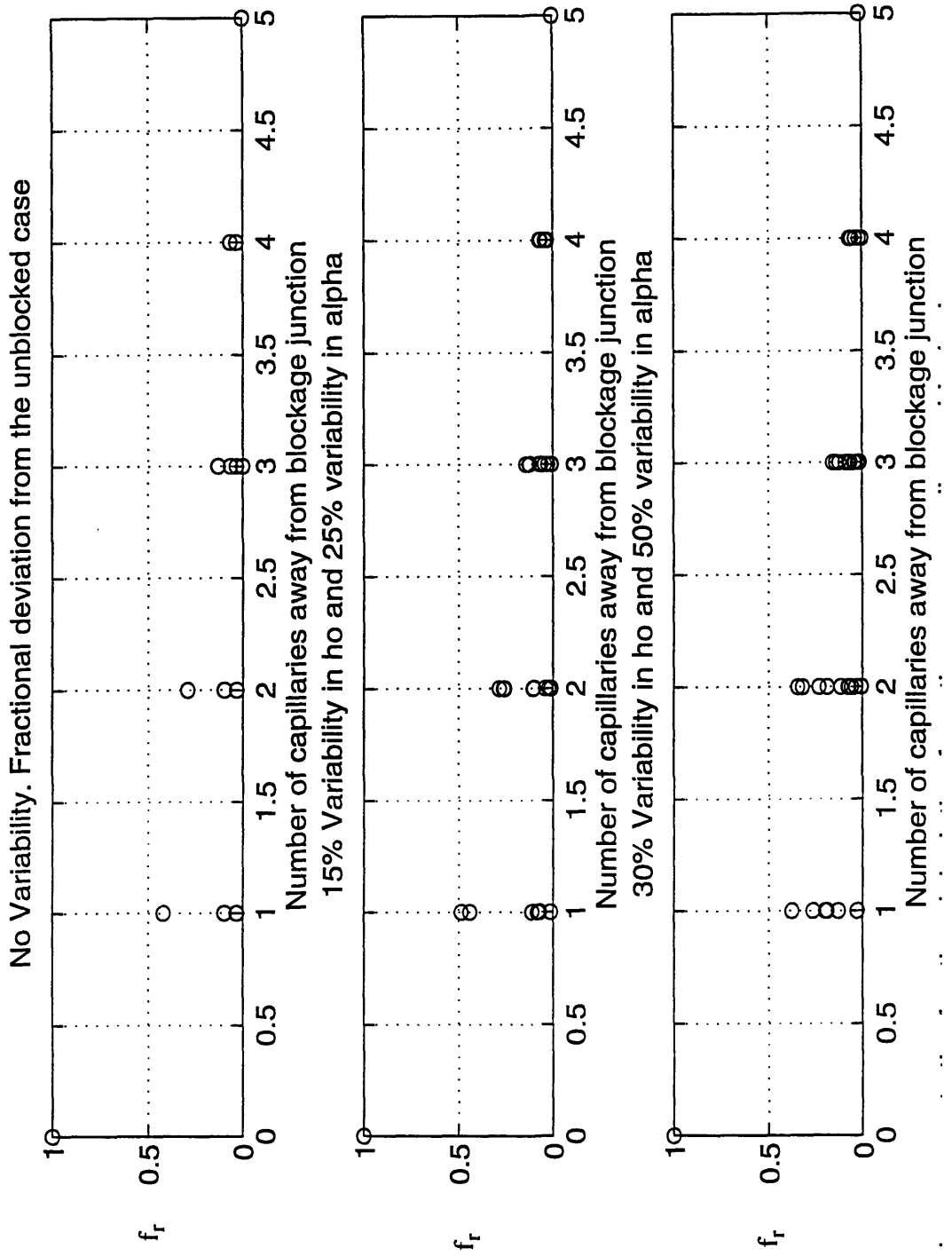

Figure 4.20: Spatial extent of capillary blockage

Based on the previous plot, we may also find the mean 'f_r' for each n in every plot. The

mean "for each n' would then represent the mean deviation of flow-rates for that value of n (e.g. for n=2 capillaries away from the blocking junction, then mean $(f_r)\,|_{n=2}$ would indicate the spatial extent of the capillary blockage at capillaries with n=2).The results are shown in figure [4.21].

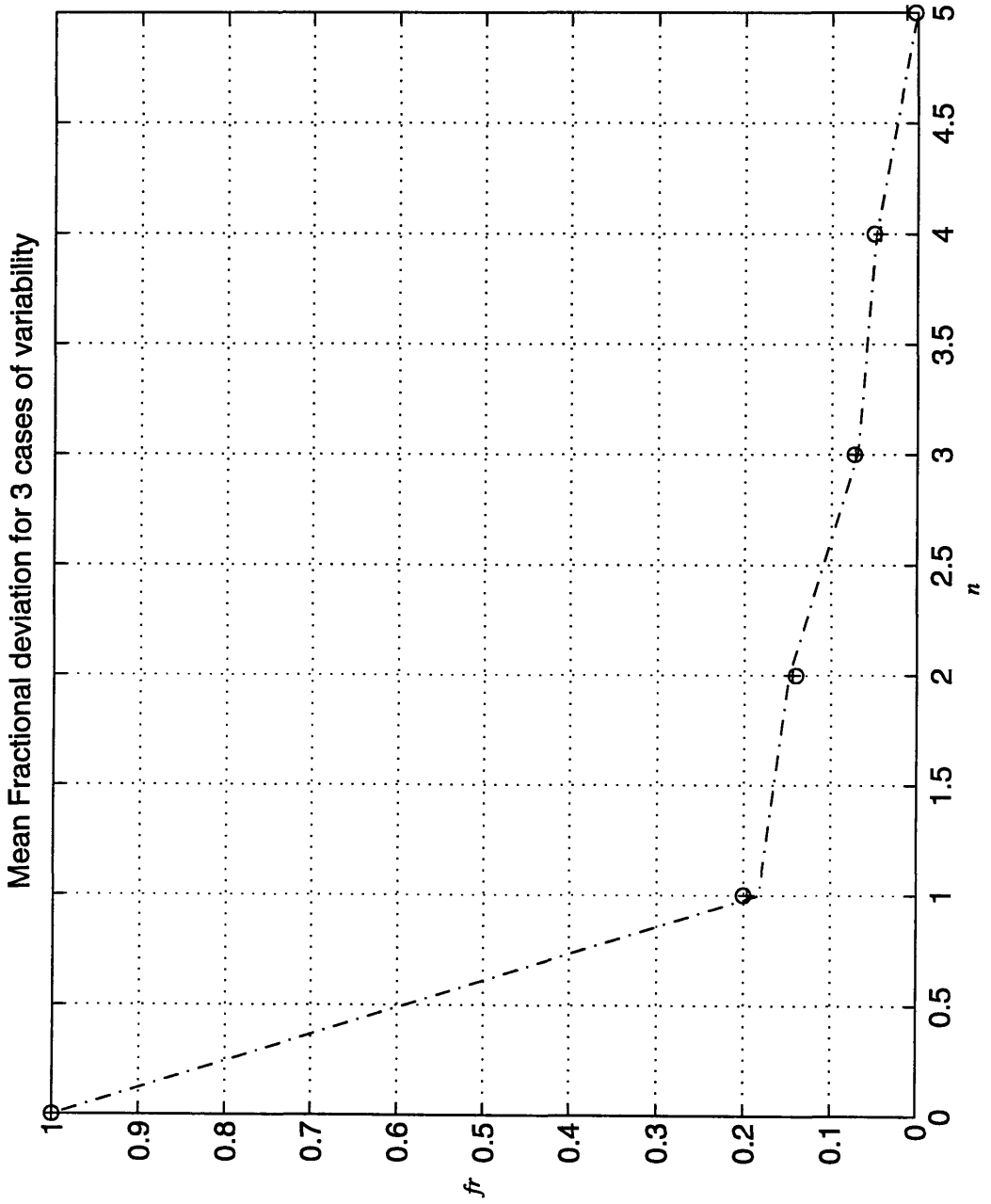

Figure 4.21: Mean 'f_r' for the three cases

It is clear from the above two plots that the extent of capillary blockage on the flow-rates is a 'local phenomenon', with the spatial effect of capillary blockage (or *f*) diminishing rapidly within 1-2 capillary segments away from the "blockage junction". Further, the mean values of *f* for the 3 cases of "0", "mid", and "maximum" variability in h_0 and α were almost identical, implying that spatial variability in h_0 and α does not significantly influence the local effects associated with of capillary blockage (figure [4.21]).

It is interesting to point to a comparison of corresponding numbers in table [4.5] and [4.7]. The similarity in the coefficient of variation between corressponding cases of randomness increases, becoming almost identical for the case with maximum randomness. This implies that capillary blockage has less of an effect on the overall flow as the degree of randomness increases.

Tables [4.6] and [4.7] present the statistical description of results obtained by blocking capillaries. From a statistical view, capillary blockage by itself gives rise to an appreciable spatial distribution in perfusion (flow-rates) relative to a case with no-blockage but with randomness (say h_0=15%variable, alpha=0%variable in table [4.5]). However, the spatial extent of this effect is clearly local, as seen in figure [4.18] and figure [4.22].

Further, a careful comparison between tables [4.5] and [4.7] shows that the effect of capillary blockage on the spatial flow-distribution diminishes with an increase in randomness; this is seen by comparing minimum and maximum entries in the values of coefficient of variation. While at low degree of randomness, there is a large difference in the coef. of variations (indicating that blockage has a dominant effect), the coefficients of variations at large degrees of randomness appear much more comparable, indicating that randomness is more dominating effect than capillary blockage in determining overall perfusion patterns.

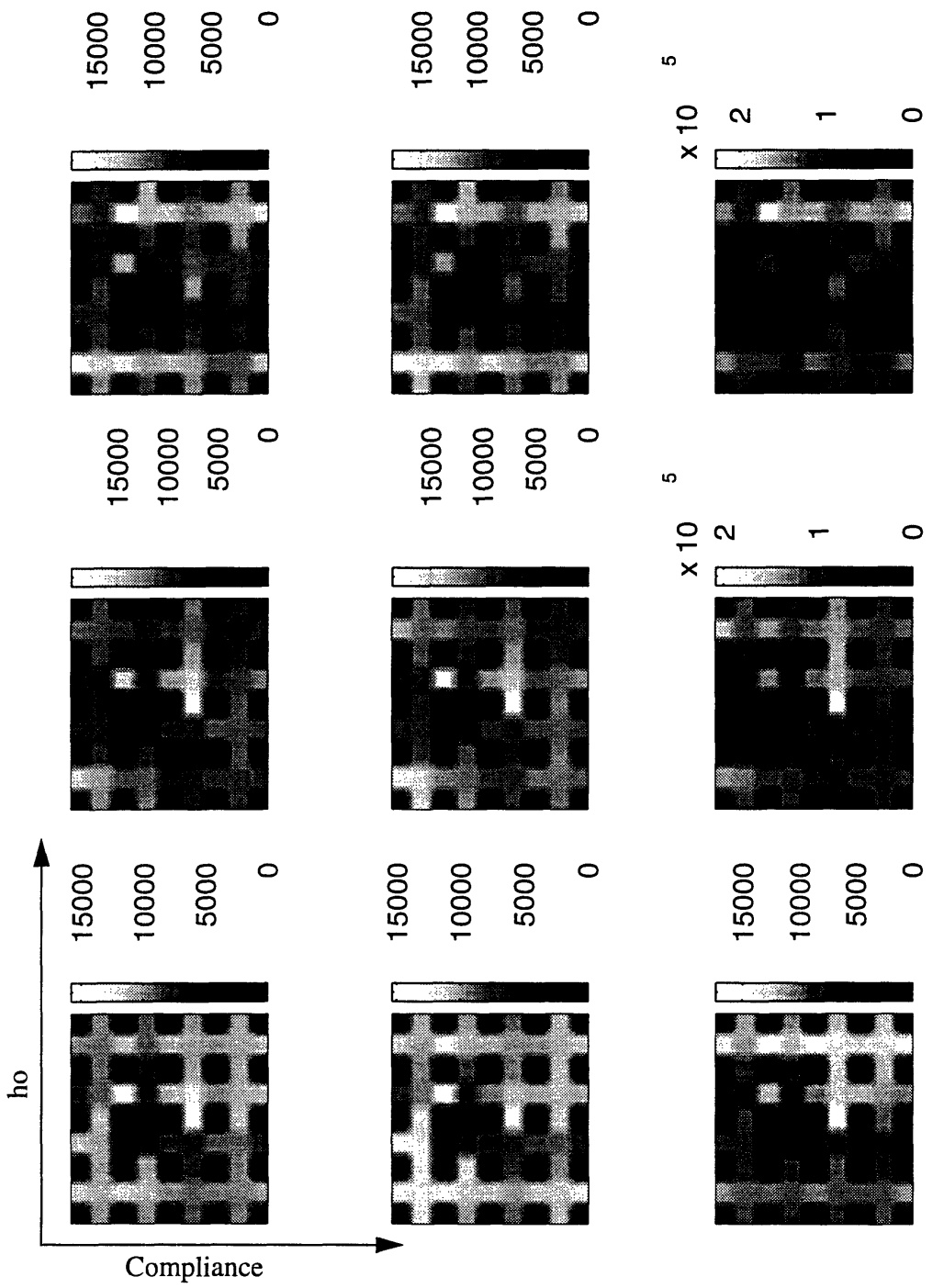

Figure 4.22: Effect of capillary blockage coupled with randomness in parameters. Randomness increases in the direction of the arrows in the figure. Flow rates in $\mu m^3/sec$

Spatially correlated randomness

A random selection with a specified spatial correlation changes the distribution of flows. Figure [4.23] shows a sample run to demonstrate the "patchiness" in flow-rates resulting from a case with high spatial-correlation. The flow-rate distribution shows similar trends as the previous cases. Since our attempt here is to choose the randomness in a manner that makes more sense physiologically, actual morphometric data for the compliance and ho would be useful in exploring the effects of randomness, specifically, spatially-correlated "randomness". In addition, this sample run for correlated randomness confirms our earlier observation that the effect of randomness is to create preferentially perfused regions in the septum (Figure [4.23]).

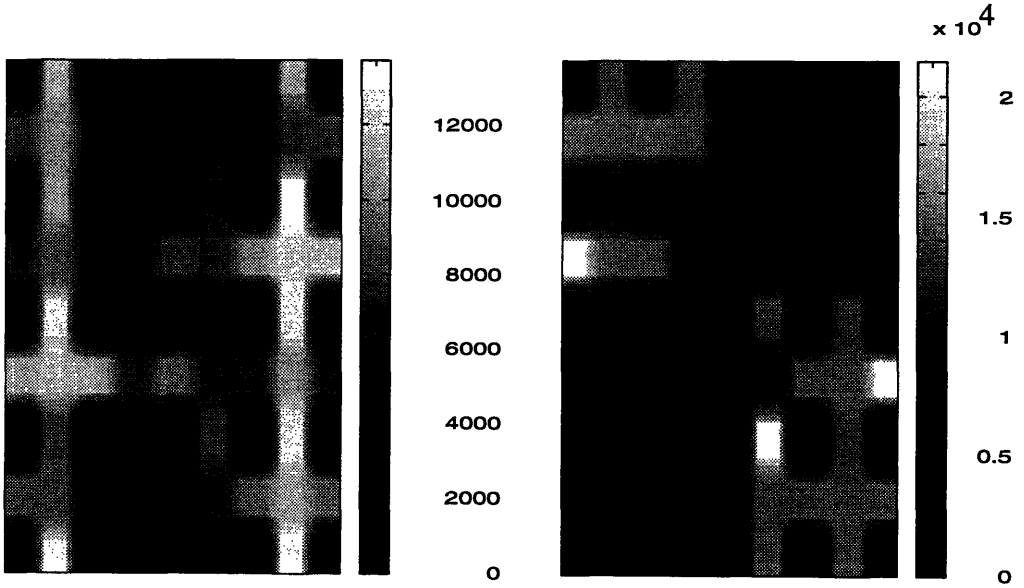

Spatially uncorrelated

Spatially correlated

Figure 4.23: Effect of spatially correlated randomness

Chapter 5

Conclusions

5.1 Recapitulation of goals and findings

The primary goal of this thesis was to develop a computational model that would simulate the dynamics of blood flow in the alveolar septum. With the help of this model, we aimed at addressing the following questions: How does breathing affect the dynamics of blood flow in the septum, and to what quantitative extent ? What is the effect of spatial variability in h_o and the compliance, α? What kind of flow patterns, if any, might such a variability induce in the septum? What is the effect of capillary blockage in the septum? With these questions as motivation, we sought to couple the essential physical elements to obtain a realistic simulation of blood flow in the pulmonary microvessels. The underlying goal behind the model development was to address the problem of RBC and PMN transit in the septal capillary bed, and, as a first-step in this direction, quantify the general blood-flow characteristics.

Our first approach was to develop an enhanced version of Fung's sheet-flow model to incorporate breathing. While this was achieved, it was realized that although Fung's model does an excellent job at predicting "bulk quantities" such as overall flow-rates and pressure-flow behavior, the model was not appropriate for our goal of predicting RBC and neutrophil transit along a tortuous path in the septum. As a result, the tube-flow model was developed, which used some of the same underlying principles as Fung's model, but which also captured the physical details at the spatial-scale of interest to us - the scale of capillaries and RBC dimensions.

The tube-model compared well with flow-rate predictions from Fung's model when the friction factor f in Fung's model was set to one. It was also possible to compute a friction from the tube-model and make a comparison with the exact analysis for the friction factor by Tsay and Weinbaum [44]; these results compared favourably, and further allowed us to improve the method of junction and capillary resistance in the tube-model.

The dynamic simulations showed that breathing was important in describing the capillary flow-rates, and resulted in capillary flow-rate oscillations as high as 40% about a mean. Further, breathing also introduced pressure oscillations at the junctions, although the magnitude of pressure oscillations was relatively small due to the way the boundary conditions were imposed. The "true" boundary condition is probably between the two extremes of constant flow-rate and constant-pressure, and the result of this 'true' boundary condition is probably that breathing gives rise to variations in pressure and flow-rates of comparable relative-magnitude. Just as expected, it was observed that the non-linear effects became more noticeable at a lower range of boundary pressures, where the capillaries were less distended and the segmental resistances were more sensitive to small variations in h. Introducing a spatial variability in the compliance and h_o (based on a random selection from a normal distribution) with the dynamic effects of breathing resulted in a spatial distribution of the mean flows, although the variability did not influence the capillary flow-rate waveforms. As a result, it was deemed sufficient at this stage to perform static-runs (no breathing) to study the effect of spatial variability in the parameters.

Spatial variability in the parameters had a drastic change on the overall flow-rate distribution, with the presence of "preferential pathways" being observed for several of the cases presented. The variability also resulted in regions of high and low flow, giving the

overall distribution of flows as "patchy". In addition, the flow-rate patterns were more sensitive to variabiliy in h_0 than the variability in compliance, α.

Capillary blockage in itself changes the statistical distribution of flow-rates within the septum, even for the case of no variability in parameters. However, the disturbances remained relatively localized to the area of blockage, with its effect dropping to about 20% within capillaries that were a distance of one capillary from the blocked junction. An increase in randomness in the parameters, coupled with blockage, resulted in well defined "preferential pathways" and regions of low flow. However, it was observed that capillary blockage has less of an effect on perfusion patterns than did the degree of randomness.

Therefore, some of the key features that influence the flow-distribution and the dynamics of blood flow in the septum were identified. These findings will be useful in addressing the problem of RBC and PMN transit in the septal bed.

5.2 Future considerations

The underlying motivation for this work is to develop a means of simulating RBC and PMN transit through the alveolar capillary network with an aim toward understanding the role of purely mechanical or geometrical effects on RBC or PMN transit times, and PMN margination. Although the model developed in this thesis is more appropriate to blood-flow, some of the aspects of RBC mechanics have been incorporated in the modelling.

The present model, however, represents an initial step towards our long-range goal and will require further extensions. First, with the current model, it will be useful to utilize some of the dynamic flow-rates to conduct numerical experiments that would allow the simulation of RBC transit times. However, to do that requires a probability distribution to

describe how a RBC chooses among several paths exiting from a bifurcation (or a junction).

The current model does not yet incorporate the change in hematocrit at a bifurcation (or at a junction), and this would be required to obtain a more accurate description of flows, and to make the model more representative of RBC motion. Morphometric measurements of compliance (α or β) and h_0 (or V_0), if made available, are essential in specifying a realistic distribution of spatial variability. The issue of morphometric measurements raises the question of the degree of accuracy in measurements. The numerical simulations indicate that the flow distributions are more sensitive to randomness in h_o than to randomness in the compliance; as a result, one would expect a higher level of accuracy in the measurements for h_0 (or V_o) than the measurements in α (or β). In addition, the time-dependence of these two quantities as functions of lung-volume (obtained experimentally) would be extremely useful for the model under conditions of breathing comparing static cases at different lung volumes or pressures. Although the current model fails to incorporate the effect of variable capillary lengths, it could be modified within the same basic framework in order to incorporate such effects. Eventually, the capillary dimensions could be obtained from morphometric data in order to construct a more realistic geometry of the capillary network.

A more accurate model for the transit of PMN's and RBC's through the capillaries is a more complicated problem, one that requires a coupling between fluid-dynamic calculations and an accurate description of PMN (or RBC) mechanics. The present model gives us useful information about the general behavior of the fluid-dynamics associated within the septum.

Appendix A

Sheet Flow model

A.1 FORTAN 77 Code for the solution of the transformed sheet-flow equations

The following FORTRAN code for the dynamic solution of the transformed sheet-flow equations was developed in order to integrate the equations anemically.

```
C REAL NAME :  SOURCED FROM
C SHEET_1_3.f CHANGED CORNER POINT BC


C-----------------------------------------------------------------
C
C   SHEET FLOW : OCT 21 1993
C   A NUMERICAL COMPUTATION OF THE UNSTEADY EQUATIONS OF FLUID MOTION
C   IN THE ALVEOLAR SEPTUM
C
C
C                AMIT S DHADWAL
C                  M I T
C
C
C-----------------------------------------------------------------

C-----------------------------------------------------------------
C
C  VARIABLES USED IN THE CODE:
C
C   AFTER THE EQNS HAVE BEEN TRANSFORMED (DROP THE STAR NOTATION)
C
C    INDEX I : X DIRECTION
C    INDEX J : Y DIRECTION
C    INDEX K : TIME DERECTION
C
C    THREE DIMENSIONAL VARIABLES
C    X (I), Y(J) (TRANSFORMED, THUS NO TIME)
C    U(I,J,K), V(I,J,K), P(I,J,K), H(I,J,K)
C
C    USES 3RD ORDER ADAMS BASHFORTH FOR TIME INTEG.
C    CODE USES CENTRAL, FORWARD AND BACKWARD DIFF EXPRESSIONS WITH
C    SECOND ORDER ACCURACY (FOR THE SPATIAL DERIVATIVES)
C-----------------------------------------------------------------

      PARAMETER (IMAX=6, JMAX=6, DX=1.0/IMAX,DY=1.0/JMAX)
      PARAMETER (KMAX1=200,KMAX2=2*KMAX1)
      PARAMETER (KMAX=KMAX2)
      PARAMETER( WR_STEP=1)
      PARAMETER (DT1=0.00001,DT2=0.00001,KSTEP=KMAX1/4)
      PARAMETER (NCYCLES=3,KKMAX=(5*NCYCLES/(DT2*KMAX1)))
```

```
      PARAMETER (AVS_STEP=KMAX1/1)  !AVS TIME STEP TO WRITE
      PARAMETER (AVS_STP=IMAX/5)    !AVS NODE  STEP (6x6 points)
      PARAMETER (AVS_START=1.0*5.0) ! STARTING TIME FOR AVS (secs)
      PARAMETER (AVS_CLK_STEP=.25)  ! time (sec) step for avs

      REAL U(0:IMAX,0:JMAX,0:KMAX+1), V(0:IMAX,0:JMAX,0:KMAX+1)
      REAL X(0:IMAX),Y(0:JMAX)
      REAL H(0:IMAX,0:JMAX,0:KMAX+1)
      REAL P(0:IMAX,0:JMAX,0:KMAX+1)
      REAL TIME,AVS_CLOCK

      REAL G(0:IMAX,0:JMAX,0:KMAX+1)  ! VARIABLE TO INTEGRATE USING ADAMS-BASH
      REAL L1,L1D,L2,L2D
      REAL ALPHA,MU,KE,F,VC,UC,H0,PO
      REAL DP ! DELTA P ACROSS SHEET AS A FUNC OF TIME
      REAL HEXIT,HINLET
      REAL PINLET,PEXIT

      REAL CENT,FORW,BACK,DELTA
      REAL EULER,ADAMS

      REAL D1,D2,D3,D4,D5,D6,D7,D8,D9,D10 ! DUMMY VARS
      REAL C1,C2,C3,C4,C5,C6,C7,C8       ! DUMMY VARIABLES
      REAL A1,A2,A3,A4,A5,A6 ! DUMMY VARIABLES
      REAL E1,E2,E3,E4,E5 ! DUMMYS
      REAL EU1,EU2,EU3,EU4
      REAL CA1,CA2,CA3,CA4

      INTEGER I,J,K,S1,S2,S3
      INTEGER I1,J1,K1,NREC
      INTEGER AVS_CTR

      REAL HA,PA,UA,VA
      PI=4.000*ATAN(1.00)

      OPEN(UNIT=2, FILE='H.DAT', STATUS='UNKNOWN')
      OPEN(UNIT=3, FILE='U.DAT',STATUS='UNKNOWN')
      OPEN(UNIT=4, FILE='V.DAT',STATUS='UNKNOWN')
      OPEN(UNIT=5,FILE='P.DAT',STATUS='UNKNOWN')
      OPEN(UNIT=7,FILE='BIN.OUT',STATUS='NEW',
     + ACCESS='DIRECT',RECL=1,FORM='UNFORMATTED')
      OPEN(UNIT=8, FILE='AVS.INFO',STATUS='UNKNOWN')
      OPEN(UNIT=9, FILE='BEGIN_TIME',STATUS='UNKNOWN')
C---------------------------------
C  DEFINE VARIABES & REF VALUES
C---------------------------------

      KE=12.00
      ALPHA=1.29592E-10
      H0=3.5E-6
      HO=H0
      UC=1.0
      VC=1.0

      PINLET=12.5 ! CMSof water
      PINLET=PINLET*98.00*ALPHA/H0

      PEXIT=12.0 !cms of water
      PEXIT=PEXIT*98.00*ALPHA/H0
```

```
      HINLET=1.00+PINLET-PO(0)
      HEXIT=1.00+PEXIT-PO(0)

      WRITE (*,*) PINLET,PEXIT,HINLET,HEXIT

      WRITE (*,*) ' INPUT SCR,MAT,BIN'
      READ(*,*)  OUT_SCR,OUT_MAT,OUT_BIN

C---------------------------------
C GENERATE GRID X(I,J), Y(I,J)
C---------------------------------

      X(0)=-0.5
      Y(0)=-0.5

      DO 2 I=1,IMAX
        X(I)=X(I-1)+DX
  2   CONTINUE

      DO 3 J=1,JMAX
        Y(J)=Y(J-1)+DY
  3   CONTINUE

C---------------------------------
C  END GRID GENERATION
C---------------------------------


C---------------------------------
C  SET INITIAL CONDITIONS
C---------------------------------
      DO 5 K=0,KMAX1
      DO 5 J=0,JMAX
      DO 4 I=0,IMAX

        H(I,J,K)=HINLET-2.0*(HINLET-HEXIT)*X(I)
        P(I,J,K)=PINLET-2.0*(PINLET-PEXIT)*X(I)
        V(I,J,K)=0.0
        U(I,J,K)=-(HO*HO*HO)*H(I,J,K)*H(I,J,K)*2.0*
     +   (HEXIT-HINLET)/(ALPHA*MU(H(I,J,K))*KE*F(H(I,J,K)))

        U(I,J,K)=2.0E-4

    4 CONTINUE
    5 CONTINUE

C-----------------------------------------------------
C      START MAIN PROGRAM
C-----------------------------------------------------
      TIME=-dt
      CTR=0
      nrec=0
      AVS_CLOCK=-DT

     DO 3001 KK=0,KKMAX
      DO 3000 K=KMAX1,KMAX2

      CTR=CTR+1
```

```
      IF (CTR.LE.1000) THEN
       DT=DT1
      ENDIF

      IF (CTR.GT.1000) THEN
       DT=DT2
      ENDIF

       TIME = TIME+DT
       AVS_CLOCK=AVS_CLOCK+DT
C-------------------------------------
C      INTERIOR POINT COMPUTATION OF H
C-------------------------------------

       DO 2000 J=1,JMAX-1
        DO 1000 I=1,IMAX-1

         A=H(I-1,J,K)*U(I-1,J,K)
         B=H(I+1,J,K)*U(I+1,J,K)
         DELTA=DX
         D1=(UC/L1(TIME))*CENT(A,B,DELTA)

         A=H(I,J-1,K)*V(I,J-1,K)
         B=H(I,J+1,K)*V(I,J+1,K)
         DELTA=DY
         D2=(VC/L2(TIME))*CENT(A,B,DELTA)

C        A=H(I-1,J,K)*X(I-1)
C        B=H(I+1,J,K)*X(I+1)
C        DELTA=DX
C        D3=(L1D(TIME)/L1(TIME))*CENT(A,B,DELTA)
         D3=(L1D(TIME)/L1(TIME))*H(I,J,K)

C        A=H(I,J-1,K)*Y(J-1)
C        B=H(I,J+1,K)*Y(J+1)
C        DELTA=DY
C        D4=(L2D(TIME)/L2(TIME))*CENT(A,B,DELTA)
         D4=(L2D(TIME)/L2(TIME))*H(I,J,K)

         G(I,J,K)=-(D1+D2+D3+D4)

         IF (CTR.LE.4) THEN !(EULER SCHEME TO INTEGRATE)
          H(I,J,K+1)=EULER(H(I,J,K),G(I,J,K),DT)
         ENDIF

         IF (CTR.GT.4) THEN ! ADAMS BASHFORTH METHOD
          H(I,J,K+1)=ADAMS(H(I,J,K),G(I,J,K),G(I,J,K-1),DT)
         ENDIF

 1000    CONTINUE
 2000    CONTINUE !  END GETTING H(N+1) FOR INTERIOR POINTS

C--------------------------------------
C OBTAIN H ON THE BOUNDARY 1: OK
C--------------------------------------

      J=0
      DO 2001 I=1,IMAX-1
```

```
      A=H(I-1,J,K)*U(I-1,J,K)
      B=H(I+1,J,K)*U(I+1,J,K)
      DELTA=DX
      D1=(UC/L1(TIME))*CENT(A,B,DELTA)

      A=H(I,J,K)*V(I,J,K)
      B=H(I,J+1,K)*V(I,J+1,K)
      C=H(I,J+2,K)*V(I,J+2,K)
      DELTA=DY
      D2=(VC/L2(TIME))*FORW(A,B,C,DELTA)

C     A=H(I-1,J,K)*X(I-1)
C     B=H(I+1,J,K)*X(I+1)
C     DELTA=DX
C     D3=(L1D(TIME)/L1(TIME))*CENT(A,B,DELTA)
      D3=(L1D(TIME)/L1(TIME))*H(I,J,K)

C     A=H(I,J,K)*Y(J)
C     B=H(I,J+1,K)*Y(J+1)
C     C=H(I,J+2,K)*Y(J+2)
C     DELTA=DY
C     D4=(L2D(TIME)/L2(TIME))*FORW(A,B,C,DELTA)
      D4=(L2D(TIME)/L2(TIME))*H(I,J,K)

      G(I,J,K)=-(D1+D2+D3+D4)

      IF (CTR.LE.4) THEN
       H(I,J,K+1)=EULER(H(I,J,K),G(I,J,K),DT)
      ENDIF

      IF (CTR.GT.4) THEN ! ADAMS BASHFORTH
       H(I,J,K+1)=ADAMS(H(I,J,K),G(I,J,K),G(I,J,K-1),DT)
      ENDIF

 2001  CONTINUE

C---------------------------------------
C  OBTAIN H ON BOUNDARY 3: OK
C---------------------------------------

     J=JMAX
     DO 2002 I=1,IMAX-1

      A=H(I-1,J,K)*U(I-1,J,K)
      B=H(I+1,J,K)*U(I+1,J,K)
      DELTA=DX
      D1=(UC/L1(TIME))*CENT(A,B,DELTA)

      A=H(I,J-2,K)*V(I,J-2,K)
      B=H(I,J-1,K)*V(I,J-1,K)
      C=H(I,J,K)*V(I,J,K)
      DELTA=DY
      D2=(VC/L2(TIME))*BACK(A,B,C,DELTA)

C     A=H(I-1,J,K)*X(I-1)
C     B=H(I+1,J,K)*X(I+1)
C     DELTA=DX
C     D3=(L1D(TIME)/L1(TIME))*CENT(A,B,DELTA)
```

```
      D3=(L1D(TIME)/L1(TIME))*H(I,J,K)

C     A=H(I,J-2,K)*Y(J-2)
C     B=H(I,J-1,K)*Y(J-1)
C     C=H(I,J,K)*Y(J)
C     DELTA=DY
C     D4=(L2D(TIME)/L2(TIME))*BACK(A,B,C,DELTA)
      D4=(L2D(TIME)/L2(TIME))*H(I,J,K)

      G(I,J,K)=-(D1+D2+D3+D4)

      IF (CTR.LE.4) THEN
       H(I,J,K+1)=EULER(H(I,J,K),G(I,J,K),DT)
      ENDIF

      IF (CTR.GT.4) THEN
       H(I,J,K+1)=ADAMS(H(I,J,K),G(I,J,K),G(I,J,K-1),DT)
      ENDIF
2002   CONTINUE

C-------------------------------------------------
C  BOUNDARY CONDITIONS ON 1,2,3,4
C-------------------------------------------------


C-----------------------------------
C BOUNDARY CONDITION ON 4
C-----------------------------------

     I=0
     DO 2005 J=0,JMAX
      W=0.2*2.0*3.1416
      P(I,J,K+1)=PINLET*(1.0+0.05*(SIN(5.0*W*TIME)))
2005   CONTINUE

C---------------------------------------
C BOUNDARY CONDITION ON 2
C---------------------------------------

     I=IMAX
     DO 2006 J=0,JMAX
      W=0.2*2.0*3.1416
      P(I,J,K+1)=PEXIT*(1.0+0.05*(SIN(5.0*W*TIME)))
2006   CONTINUE

C-----------------------------------------
C BOUNDARY CONDITION ON 1 (include corners)
C-----------------------------------------

     J=0
     DO 2007 I=0,IMAX
      V(I,J,K+1)=0.0
2007   CONTINUE

C-----------------------------------
C BOUNDARY CONDITION ON 3
C-----------------------------------

     J=JMAX
```

```
      DO 2008 I=0,IMAX
       V(I,J,K+1)=0.0
 2008   CONTINUE

C-----------------------------------------------

C---------------------------------------
C NEW : FIND H ON THE INLET AND EXIT
C---------------------------------------

      I=0
      DO 2009 J=0,JMAX
       H(I,J,K+1)=1.0+P(I,J,K+1)-PO(TIME+DT)
 2009  CONTINUE

      I=IMAX
      DO 2010 J=0,JMAX
       H(I,J,K+1)=1.0+P(I,J,K+1)-PO(TIME+DT)
 2010  CONTINUE

C-----------------------------------------------
C  DONE WITH OBTAINING H(N+1) EVERYWHERE
C-----------------------------------------------

C-----------------------------------------
C UPDATE U,V (N+1)'S FOR INTERIOR POINTS:OK
C-----------------------------------------

      DO 2200 J=1,JMAX-1
       DO 2300 I=1,IMAX-1

       A=H(I-1,J,K+1)
       B=H(I+1,J,K+1)
       DELTA=DX
       D1=H(I,J,K+1)*H(I,J,K+1)*CENT(A,B,DELTA)
       C1=-L1(TIME+DT) * ALPHA * MU(H(I,J,K+1))
       C1=C1* KE * F(H(I,J,K+1))*UC
       U(I,J,K+1)=(D1*H0*H0*H0)/(C1) - L1D(TIME+DT)*X(I)/UC

       A=H(I,J-1,K+1)
       B=H(I,J+1,K+1)
       DELTA=DY
       D1=H(I,J,K+1)*H(I,J,K+1)*CENT(A,B,DELTA)
       C1=-L2(TIME+DT)*ALPHA*MU(H(I,J,K+1))*KE*F(H(I,J,K+1))*VC
       V(I,J,K+1)=(H0*H0*H0*D1)/(C1) - L2D(TIME+DT)*Y(J)/VC

 2300    CONTINUE
 2200    CONTINUE

C-----------------------------------------
C OBTAIN U,V ON BOUNDARY 1:  OK
C-----------------------------------------

      J=0
      DO 2201 I=1,IMAX-1

C       V ON 1 IS SPECIFIED

       A=H(I-1,J,K+1)
```

```
        B=H(I+1,J,K+1)
        DELTA=DX
        D1=H(I,J,K+1)*H(I,J,K+1)*CENT(A,B,DELTA)
        C1=-L1(TIME+DT)*ALPHA*MU(H(I,J,K+1))*KE*F(H(I,J,K+1))*UC

        U(I,J,K+1)=(D1*H0*H0*H0)/(C1) - L1D(TIME+DT)*X(I)/UC

 2201   CONTINUE

C-----------------------------------------
C OBTAIN  U,V ON BOUNDARY 3: OK
C-----------------------------------------

C   V ON 3 IS SPECIFIED

      J=JMAX
      DO 2202 I=1,IMAX-1

        A=H(I-1,J,K+1)
        B=H(I+1,J,K+1)
        DELTA=DX
        D1=H(I,J,K+1)*H(I,J,K+1)*CENT(A,B,DELTA)
        C1=-L1(TIME+DT)*ALPHA*MU(H(I,J,K+1))*KE*F(H(I,J,K+1))*UC
        U(I,J,K+1)=(D1*H0*H0*H0)/(C1) - L1D(TIME+DT)*X(I)/UC

 2202   CONTINUE

C-----------------------------------------
C OBTAIN U,V ON BOUNDARY 2
C-----------------------------------------

      I=IMAX
       DO 2203 J=0,JMAX

C       ------ U VELS . CORNERS OK --------

        A=H(I-2,J,K+1)
        B=H(I-1,J,K+1)
        C=H(I,J,K+1)
        D1=H(I,J,K+1)*H(I,J,K+1)*BACK(A,B,C,DX)
        C1=-L1(TIME+DT)*ALPHA*MU(H(I,J,K+1))*KE*F(H(I,J,K+1))*UC

        U(I,J,K+1)=(H0*H0*H0*D1)/(C1)-L1D(TIME+DT)*X(I)/UC

C       ----- V VELOCITIES ----------

        C1=-L2(TIME+DT)*ALPHA*MU(H(I,J,K+1))*KE*F(H(I,J,K+1))*VC

        IF (J.EQ.0) THEN
          A=H(I,J,K+1)
          B=H(I,J+1,K+1)
          C=H(I,J+2,K+1)
          D1=H(I,J,K+1)*H(I,J,K+1)*FORW(A,B,C,DY)
        ENDIF

        IF (J.EQ.JMAX) THEN
          A=H(I,J-2,K+1)
          B=H(I,J-1,K+1)
          C=H(I,J,K+1)
```

```
        D1=H(I,J,K+1)*H(I,J,K+1)*BACK(A,B,C,DY)
       ENDIF

       IF(J.GT.0 .AND. J.LT.JMAX) THEN
        A=H(I,J-1,K+1)
        B=H(I,J+1,K+1)
        D1=H(I,J,K+1)*H(I,J,K+1)*CENT(A,B,DY)
       ENDIF

       V(I,J,K+1)=(H0*H0*H0*D1/C1)-L2D(TIME+DT)*Y(J)/VC
C  -------------------
C  ADD CORNER CONDITION
C  -------------------

       IF (J.EQ.0.OR.J.EQ.JMAX) THEN
        V(I,J,K+1)=0.0
       ENDIF

 2203  CONTINUE

C-----------------------------------------
C OBTAIN U,V ON BOUNDARY 4
C-----------------------------------------

      I=0
      DO 2204 J=0,JMAX

       A=H(I,J,K+1)
       B=H(I+1,J,K+1)
       C=H(I+2,J,K+1)
       D1=H(I,J,K+1)*H(I,J,K+1)*FORW(A,B,C,DX)
       C1=-L1(TIME+DT)*ALPHA*MU(H(I,J,K+1))*KE*F(H(I,J,K+1))*UC
       U(I,J,K+1)=(H0*H0*H0*D1/C1)-L1D(TIME+DT)*X(I)/UC

       C1=-L2(TIME+DT)*ALPHA*MU(H(I,J,K+1))*KE*F(H(I,J,K+1))*VC

       IF (J.EQ.0) THEN
        A=H(I,J,K+1)
        B=H(I,J+1,K+1)
        C=H(I,J+2,K+1)
        D1=H(I,J,K+1)*H(I,J,K+1)*FORW(A,B,C,DY)
       ENDIF

       IF (J.EQ.JMAX) THEN
        A=H(I,J-2,K+1)
        B=H(I,J-1,K+1)
        C=H(I,J,K+1)
        D1=H(I,J,K+1)*H(I,J,K+1)*BACK(A,B,C,DY)
       ENDIF

       IF (J.GT.0 .AND. J.LT.JMAX) THEN
        A=H(I,J-1,K+1)
        B=H(I,J+1,K+1)
        D1=H(I,J,K+1)*H(I,J,K+1)*CENT(A,B,DY)
       ENDIF

       V(I,J,K+1)=(H0*H0*H0*D1/C1)-L2D(TIME+DT)*Y(J)/VC

C      -------------------
```

```
C      ADD CORNER CONDITIONS
C      ---------------------
       IF (J.EQ.0.OR.J.EQ.JMAX)THEN
        V(I,J,K+1)=0.0
       ENDIF

 2204    CONTINUE

C---------------------------------------
C COMPUTE PRESSURE VALUES EXCEPT AT I=0,IMAX
C---------------------------------------


       DO 2207 I=1,IMAX-1
        DO 2207 J=0,JMAX

        P(I,J,K+1)=H(I,J,K+1)+PO(TIME+DT)-1.00

        IF (P(I,J,K+1).LT.PO(TIME+DT)) THEN
       WRITE (*,*) 'ALARM....Po is too low: soln not possible'
            WRITE(*,*) 'AT (I,J,K)',I,J,CTR
            STOP
       ENDIF

 2207   CONTINUE

C---------------------------------------
C SWAP ARRAYS
C---------------------------------------

       DO 2205 S1=0,KMAX1
        DO 2205 S2=0,JMAX
         DO 2205 S3=0,IMAX

        U(S3,S2,S1)=U(S3,S2,S1+KMAX1+1)
        V(S3,S2,S1)=V(S3,S2,S1+KMAX1+1)
        H(S3,S2,S1)=H(S3,S2,S1+KMAX1+1)
        P(S3,S2,S1)=P(S3,S2,S1+KMAX1+1)

 2205  CONTINUE

C--------------------------------
C  OUTPUT RESULTS
C--------------------------------

      IF (OUT_SCR.EQ.1) THEN
       WRITE(*,*) 'CTR= ',CTR

C      WRITE (*,*) ' P VALUES       '
C      DO 2400 J=JMAX,0,-WR_STEP
C         WRITE(*,*)  (P(I,3,K+1)*(H0/ALPHA)/98.0, I=0,IMAX,WR_STEP)
C         WRITE(*,*)  (H(I,J,K+1), I=0,IMAX,WR_STEP)
 2400    CONTINUE

       WRITE (*,*) ' U VELOCITIES'
       do 2401 j=jmax,0,-1
        WRITE (*,*) (U(I,J,K+1) ,I=0,IMAX,WR_STEP)
 2401   CONTINUE
```

```
C      WRITE(*,*) '  V VELOCITIES '
C      DO 2402 J=JMAX,0,-1
C       WRITE(*,*) (V(I,J,K+1), I=0,IMAX,2)
C 2402   CONTINUE
       ENDIF

 3000  CONTINUE

       IF (OUT_MAT.EQ.1) THEN
         J=6
         DO 2404 KUO=1,KMAX1,KSTEP
          WRITE (*,*) KUO,CTR,TIME
          WRITE(2,*) (H(I,J,KUO+1)*H0/(1.0E-6), I=0,IMAX,2)
          WRITE(5,*) (P(I,J,KUO+1)*(H0/ALPHA)/98.00, I=0,IMAX,2)
          WRITE(3,*) (U(I,J,KUO+1),I=0,IMAX,2)
          WRITE(4,*) (V(I,J,KUO+1),I=0,IMAX,2)
 2404   CONTINUE
       ENDIF

       IF (OUT_BIN.EQ.1.AND.TIME.GT.AVS_START) THEN
        IF (AVS_CLOCK.GE.AVS_CLK_STEP) THEN

        AVS_CLOCK=0.0

        write (8,*) TIME

        DO 2405 K1=0,KMAX1,AVS_STEP
         AVS_CTR=AVS_CTR+1
c         write (*,*) 'AVS-CTR',AVS_CTR
         DO 2405 J1=0,JMAX,AVS_STP
          DO 2405 I1=0,IMAX,AVS_STP

         UA=U(I1,J1,K1)
         VA=V(I1,J1,K1)
         HA=H(I1,J1,K1)*H0/(1.0E-6)
         PA=P(I1,J1,K1)*(H0/ALPHA)/98.00

         nrec=nrec+1
         write(7,rec=nrec)UA
         nrec=nrec+1
         write(7,rec=nrec)VA
         nrec=nrec+1
         write(7,rec=nrec)HA
         nrec=nrec+1
         write(7,rec=nrec)PA

 2405  CONTINUE
       ENDIF
       ENDIF

 3001  CONTINUE

       WRITE (8,*) '# OF XxY POINTS',IMAX/(AVS_STP)+1
       WRITE (8,*) '# OF TIME STEPS',AVS_CTR

       CLOSE(2)
       CLOSE(3)
       CLOSE(4)
       END
```

```
C-----------------------------------------------------
C BEGIN FUNCTION DEFINITIONS
C-----------------------------------------------------


C-----------------------------------------
C    DIFF. FUNCTIONS
C
C    CONVENTION: THE LOWEST INDEX IS A
C            THEN B AND THEN C
C-----------------------------------------

      REAL FUNCTION CENT(A,B,DELTA)
      CENT = (B-A)/(2.0*DELTA)
      RETURN
      END

      REAL FUNCTION FORW(A,B,C,DELTA)
      FORW = (-3.0*A + 4.0*B - C) / (2.0*DELTA)
      RETURN
      END

      REAL FUNCTION BACK(A,B,C,DELTA)
      BACK=( 3.0*C -4.0*B + A) / (2.0*DELTA)
      RETURN
      END

      REAL FUNCTION EULER(EU1,EU2,EU3)
      EULER= EU1+EU2*EU3
      RETURN
      END

      REAL FUNCTION ADAMS(CA1,CA2,CA3,CA4)
      ADAMS=CA1+(CA4/2.0)*(3.0*CA2-CA3)
      RETURN
      END

C-----------------------------------------
C    BEGIN OTHER FUNCTIONS
C-----------------------------------------


      REAL FUNCTION L1D(TIME)
      W=0.2*2.0*3.1416
c     L1D=0.5*(75.0E-6)*0.2*0.33*0.5*W*SIN(W*TIME)*
c    + (0.5*(1.01-COS(W*TIME)))**(-0.66)

      L1D=(75.0E-6)*W*0.1*SIN(W*TIME)
C     L1D=0.0
C     WRITE (*,*) 'L1D',L1D
      RETURN
      END


      REAL FUNCTION L2D(TIME)
      W=0.2*2.0*3.1416
c     L2D=0.5*(75.0E-6)*0.2*0.33*0.5*W*SIN(W*TIME)*
c    + (0.5*(1.01-COS(W*TIME)))**(-0.66)
```

```
      L2D=(75.0E-6)*0.1*W*SIN(W*TIME)
C     L2D=0.0
C     WRITE(*,*) 'L2D',L2D
      RETURN
      END

      REAL FUNCTION L1(TIME)
      W=0.2*2.0*3.1416
c     L1=0.5*(75.0E-6)*(1.00+0.2*(0.5*(1.01-COS(W*TIME)))**(0.33))
      L1=(75.0E-6)*(1.00+0.1*(1.0-COS(W*TIME)))
c     L1=(75.0E-6)*0.5
C     WRITE(*,*) 'L1',L1
      RETURN
      END

      REAL FUNCTION L2(TIME)
      W=0.2*2.0*3.1416
c     L2=0.5*(75.0E-6)*(1.00+0.2*(0.5*(1.01-COS(W*TIME)))**(0.33))
      L2=(75.0E-6)*(1.00+0.1*(1.0-COS(W*TIME)))
C     L2=(75.0E-6)*0.5
C     WRITE (*,*) 'L2',L2
      RETURN
      END


      REAL FUNCTION PO(TIME)
      REAL FACTOR,ALPHA,HO
      HO=3.5E-6
      ALPHA=1.2959E-10
      FACTOR=98.0*ALPHA/HO
      PO=1.0 ! 1 cm of water
c     PO=PO*FACTOR
      PO=-PO*(FACTOR)*SIN(0.2*2.0*3.141*TIME)
C     THE AVLEOLAR PRESSURE IS OUT OF PHASE BY 180 DEG, THEREF THE - SIGN
      RETURN
      END

      REAL FUNCTION F(C,D)
      F=4.0
      RETURN
      END

      REAL FUNCTION MU(DUMMY)


      REAL MUR,MUP,HD,D,UUC,DELT,SAM1,SAM2,DM
      Ho=3.5E-6
      ALPHA=1.2959E-10
      d=DUMMY
      d=d*Ho ! change to real sheet ht
      d=d/0.000001 ! convert to micron
      Hd=.45
      uuc=2.71828**(0.48+2.35*Hd)
      delt=2.03-2.0*Hd
      Mup=1.7
      Dm=2.7
      SAM1=(1.0 - (1.0-mup/uuc)*((1-2.0*delt/d)**(4.0)))**(-1.0)
      SAM2=(1.0-(Dm/d)**(4.0))**(-1.0)
      mur=SAM1*SAM2 ! Mu relative
```

```
MU=mup*mur ! in Centippoise. Mup=1.7 cP

MU=MU/1000.00 ! in PA-SEC
RETURN
END
```

Appendix B

Capillary-matrix Model

B.1 Segment geometry and segment-volume approximations

The volume of a given junction and the neighbouring 4 half-segments needs to be approximated in order to determine an equivalent volume compliance, β, and V_o. This is done as follows.

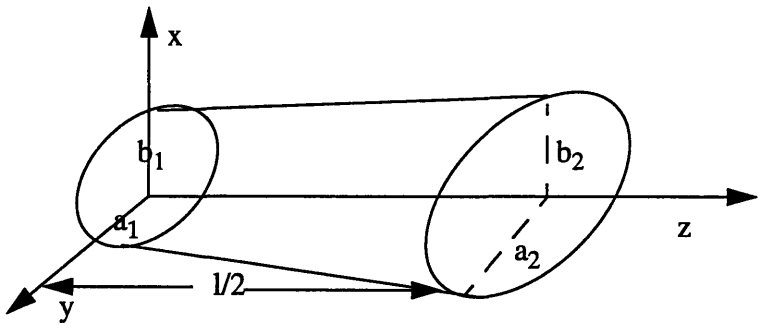

Figure 2.1: Volume approximation for half-segment

$$V = \pi \int_0^{\frac{l}{2}} x(z)\, y(z)\, dz \tag{B.1}$$

$$V = \pi \left[a_1 b_2 + a_2 b_1 + 2 (a_1 b_1 + a_2 b_2) \right] \quad \text{(For one segment)} \tag{B.2}$$

but $b_1=h_1$, $b_2=h_5$ (B.3)

$$\therefore V_{Segment} = \pi \frac{L}{12} \left[h_1 (a_2 + 2a_1) + h_2 (a_1 + 2a_2) \right] \tag{B.4}$$

$a_1=(L_p-d)/2$, $a_2=L_p/2$ (d=post diameter, L_p=spacing between center of posts) (B.5)

also, $h=h_o+\alpha(P-Po)$ (i=1 or 2) (B.6)

Using the above equations, we may derive the equavalent Volume-compliance law

$$V_{CV} = A_c h_o + \sum_{j=1}^{4} \Pi \frac{d}{8} (2L_p - d) h_o + \Delta P \left[\sum_{j=1}^{4} \Pi \frac{d}{8} (2L_p - d) \alpha_j + \alpha A_c \right] \quad \text{(B.7)}$$

(*Subscripts 'j'=1,2,3,4 represent the 4 directions (North, East, South & West) around a junction)

B.2 MATLAB Code

The MATLAB code developed for the Capillary matrix model is structured to utilize several user-defined subroutines; further, it was completely vectorized (all operations are performed by manipulation of quantities represented in matrix form, as opposed to manipulalation of each quantities individually; for e.g., the task of computing the resistance of all the capillaries in the network is performed in one step as opposed to finding the resistance of each of the individual capillaries in several steps). The figure below describes the structure of the subroutines:

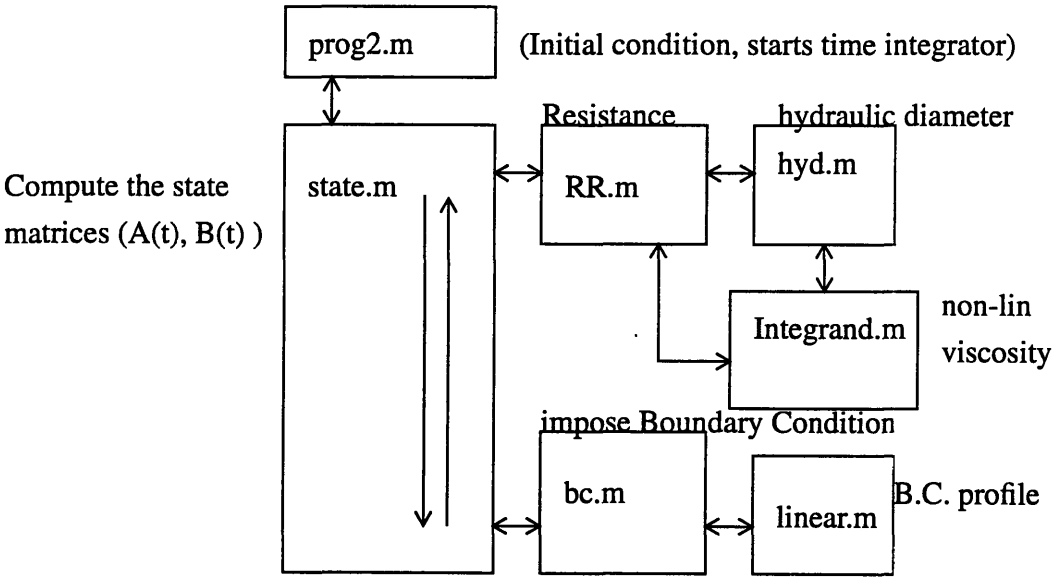

Figure B.1: Schematic of MATLAB Code subroutine layout

The following MATLAB code was used in order to make the computations.

prog2.m

```
% MAIN PROGRAM THAT INITIATES THE TUBE MODEL clear all global
global ALPHA_RAND alpha1 X_X Y_Y alpha_save RE RW RN RS hb_save pin pout ho_rand w hnom1
imax=4; jmax=4; ijmax=imax*jmax;
RAN=[1.1 1.0 0.1 0.2 1.2 1.1 0.05 0.3 0.3 0.1 0.9 1.0 0.25 0.11 1.2 0.8];
% Multiply random by p/50 where p=percent variation)
ask=input('Alpha random ? 1=yes, 25=25%, 50=50%, 100=max, 2=no')
if (ask==1) alpha1=normrnd(.127, 0.50*.127,4,4); ALPHA_RAND=(alpha1-0.127*ones(4,4)) ./ (.127); elseif (ask==25)
load alpha25.dat alpha1=alpha25; ALPHA_RAND=(alpha1-0.127*ones(4,4)) ./ (.127); elseif (ask==50) load alpha50.dat
alpha1=alpha50; ALPHA_RAND=(alpha1-0.127*ones(4,4)) ./ (.127); elseif (ask==100) load alpha_max_corr.dat
alpha1=alpha_max_corr; ALPHA_RAND=(alpha1-0.127*ones(4,4)) ./ (.127); else alpha1=0.127 .* ones(4);
ALPHA_RAND=zeros(4); end
ask=input('Ho Rand ? 1=yes, 15=15%, 30=30%,100=max, 2=no') if (ask==1) hnom1=normrnd(3.5,0.3*3.5,4,4);
%ho_rand=(rand(4)-0.5).*(40/50); for i1=1:4, for j1=1:4, if (hnom1(i1,j1) <= 2.7) hnom1(i1,j1)=2.75; end if
(hnom1(i1,j1) >= 6.55) hnom1(i1,j1)=6.55 end end end ho_rand=(hnom1-3.5.*ones(4)) ./ (3.5);
elseif (ask==15) load ho15.dat hnom1=ho15; ho_rand=(hnom1-3.5.*ones(4)) ./ (3.5); elseif (ask==30) load ho30.dat
hnom1=ho30; ho_rand=(hnom1-3.5.*ones(4)) ./ (3.5); elseif (ask==100) load ho_max_corr.dat hnom1=ho_max_corr;
ho_rand=(hnom1-3.5.*ones(4)) ./ (3.5); else hnom1=3.5.*ones(4,4); ho_rand=zeros(4); end
ALPHA_RAND,alpha1 ho_rand, hnom1
%ASSIGN TIME scale %w=0.2*2.0*3.1416; w=0.0; dt=0.1; t0=0.0; tfinal=0.15;
pin=10.0; pout=9.5;
% ASSIGN GRID X_X=[-0.5:1/(imax+2-1):0.5]'; Y_Y=[-0.5:1/(jmax+2-1):0.5]';
% Assign Initial Condition
for i=1:imax, for j=1:jmax, V(i,j)=(pin+pout)/2; %V(i,j)=0.0; end end end
% CREATE LINEAR Initial V0 Array for j=1:jmax, for i=1:imax, V0=[V0 ; V(i,j)]; end end % END OF INITIAL CONDITION
tol=7.0E-7; tic [t,y1]=ode45('state',t0,tfinal,V0,tol,1); toc
% Done integration. Now Convert into a 6x6 array
y1=y1';
% RECONSTRUCT the BOUNDARY CONDITION IN ORDER TO % RUN THRU THE ENTIRE BC kmax=length(t);
sst=20;
for k=1:kmax/sst:kmax
time=t(k,1); VV=bc(pin,pout,X_X,imax,jmax,time,w);
for i=1:imax+2, for j=1:jmax+2,
if (i==1) P(i,j)=VV(i,j); end
if (i==imax+2) P(i,j)=VV(i,j); end
if (j==1) P(i,j)=VV(i,j); end
if (j==jmax+2) P(i,j)=VV(i,j); end
if (i>1 & i<imax+2 & j>1 & j<jmax+2) m=i-1+(j-2)*imax; P(i,j)=y1(m,k); end
end end Pf=[Pf ; P]; end
save Pf.dat Pf -ascii save P.dat P -ascii save time.dat t -ascii save alpha_save.dat alpha_save -ascii save hb_save.dat hb_save -ascii
save ho_rand.dat ho_rand -ascii
% FINISHED CREATING THE ENTIRE TIME HISTORY % NOW CREATE THE MOVIE
!zwrite adhadwal < done stop
ax=[1 6 1 6 0 2.0]'; axis(ax)
i=0; Mo=moviein(kmax/sst/3); for k=1:3*6:length(Pf), i=i+1; tmp=Pf(k:k+5,:); mesh (tmp) Mo(:,i)=getframe; end
!zwrite adhadwal < done
```

state.m

```
function ydot=state(t,y1) global alpha1 ALPHA_RAND X_X Y_Y alpha_save RE RW RN RS hb_save pin pout ho_rand w
hnom1
% DETERMINE THE STATE MATRICES
imax=4; jmax=4; ijmax=imax*jmax;
```

```
onn=ones(imax); oonn=ones(imax+2);
% PUT w in prog2.m %w=0.2*2.0*3.1416; w=0.0;
vmean=3.5; vtidal=1.0; kk=vtidal/(2.0*vmean); %vol=vmean-(vtidal/2).* cos(w .* t); lo=75; kkk=(1-kk)^(1/3); L=(lo/kkk) .* (1 - kk .* cos(w .* t)).^(1/3); % Include the factor (1-kk) since we want L=75 microns at w=0 DLdt=(lo/kkk.*3).*((1 - kk .* cos(w .* t)).^ (-2/3)) .* kk .* w .* sin(w .* t);
dx=(X_X(2)-X_X(1))*L; % LENGTH OF A SEGMENT Ddxdt=(X_X(2)-X_X(1)).*DLdt;
% ASSIGN VARIABLES & DERIVATIVES %alpha=(onn + ALPHA_RAND).* 0.127; %alpha=0.127 .* onn; alpha=alpha1;
do=7.5 .* onn; dok=7.5 .* oonn;
ddo=(dx/15) .* (do); Dddodt=(X_X(2)-X_X(1)) .* (do ./ 15) .* DLdt; ddok=(dx/15) .* (dok);
%hnom=(onn+ho_rand).*3.5; %hnom=(onn).*3.5; hnom=hnom1;
dnom=do; ho=((hnom.*dnom.*dnom)./ (ddo .* ddo)) .* onn; Dhodt=(( -2*(hnom.*dnom.*dnom) .* (Dddodt)) ./ (ddo .* ddo .* ddo)) .* onn;
%ho=hnom .* onn; %Dalphadt=0.0 .* onn: LATER.
Po=-sin(w*t) .* onn; DPodt= -w .* cos(w*t) .* onn;
Ac=(dx.*onn-ddo) .* (dx.*onn-ddo) .* onn; %DAcdt=(2.0*(1.0+0.2*(1-cos(w*t)))*0.2*w*sin(w*t)*dx*dx) .* onn
DAcdt=2.*(dx.*onn - ddo).*(Ddxdt.*onn - Dddodt);  % do is the nominal post diameter. 15 is the 15 micron nominal spacing
V=reshape(y1,4,4);
%  Assign Alpha and are Ac(i,j) for sheet %  then recompute Alpha at the center
k_c=1.0 .* onn; k_e=1.0 .* onn; k_w=1.0 .* onn; k_n=1.0 .* onn; k_s=1.0 .* onn;
alpha_c = alpha .* k_c; alpha_e = alpha .* k_e; alpha_w = alpha .* k_w; alpha_n = alpha .* k_n; alpha_s = alpha .* k_s;
alpha=alpha_c+alpha_e+alpha_w+alpha_n+alpha_s;
h=ho+alpha_c .* (V-Po);
onnb=ones(imax+2); alphab_c=1.0*.127 .* onnb; alphab_e=1.0*.127 .* onnb; alphab_w=1.0*.127 .* onnb; alphab_n=1.0*.127 .* onnb; alphab_s=1.0*.127 .* onnb;
hob=3.5 .* onnb; Pob=-sin(w*t) .* onnb;
%alphab=alphab_c+alphab_e+alphab_w+alphab_n+alphab_s; alphab=alphab_c+alphab_e+alphab_w+alphab_n;
% Create *b for boundary value variables
%ASSIGN BOUNDARY CONDITIONS VV VV=bc(pin,pout,X_X,imax,jmax,t,w);
% WAS . CHANGED BELOW. hb=hob+alphab_c .* (VV-Pob); hb=hob+alphab_c .* (VV-Pob);
% END BOUNDARY CONDITIONS % COMPUTE RESISTANCES: CREATE 6x6 ARRAY OF h FIRST (NOT 4x4) % CALL THIS 6x6 ARRAY hk. Same for alphak_c, alphak_e,w,n,s strip=[1 1 1 1 1 1 ; 1 0 0 0 0 1; 1 0 0 0 0 1; 1 0 0 0 0 1;1 0 0 0 0 1;  1 1 1 1 1 1];
hk1=zeros(imax+2); hk1(2:imax+1,2:jmax+1)=h; hk=hb.*strip+hk1;
alc1=zeros(imax+2); alc1(2:imax+1,2:jmax+1)=alpha_c; alphak_c=strip .* alphab_c + alc1;
ale1=zeros(imax+2); ale1(2:imax+1,2:jmax+1)=alpha_e; alphak_e=strip .* alphab_e + ale1;
alw1=zeros(imax+2); alw1(2:imax+1,2:jmax+1)=alpha_w; alphak_w=strip .* alphab_w + alw1;
aln1=zeros(imax+2); aln1(2:imax+1,2:jmax+1)=alpha_n; alphak_n=strip .* alphab_n + aln1;
als1=zeros(imax+2); als1(2:imax+1,2:jmax+1)=alpha_s; alphak_s=strip .* alphab_s + als1;
al1=zeros(imax+2); al1(2:imax+1,2:jmax+1)=alpha; alphak=strip .* alphab + al1;
Vk1=zeros(imax+2); Vk1(2:imax+1,2:jmax+1)=V; Vk=strip .* VV + Vk1;
Po1=zeros(imax+2); Po1(2:imax+1,2:jmax+1)=Po; Pok=strip .* Pob + Po1;
ho1=zeros(imax+2); ho1(2:imax+1,2:jmax+1)=ho; hok=strip .* hob + ho1;
hk_c=hok+alphak_c .* (Vk-Pok); hk_n=hok+alphak_n .* (Vk-Pok); hk_s=hok+alphak_s .* (Vk-Pok); hk_e=hok+alphak_e .* (Vk-Pok); hk_w=hok+alphak_w .* (Vk-Pok);
alpha_save=alphak; hb_save=hk_c;
RE=zeros(4); RW=zeros(4); RN=zeros(4); RS=zeros(4); [RE,RW,RN,RS]=RR(hk_c,hk_e,hk_w,hk_n,hk_s,ddok,dx);
%RE(2,2)=1E2; %RW(3,2)=100; %RN(2,2)=1E2; %RS(2,3)=1E2;
% NOW DEFINE BETA, DBETADT, VO, DVODT: THE NEW STUFF %bet=Ac .* alpha; %C=bet; %Dbetdt=DAcdt .* alpha + Ac .* Dalphadt; %Dvodt=DAcdt .* ho + Ac .* Dhodt
diam=ddo .* onn; leng=dx .* onn;
bet_c=Ac .* alpha_c; bet_e=(pi/8) .* (2 .* diam .* leng - diam .* diam) .* alpha_e; bet_w=(pi/8) .* (2 .* diam .* leng - diam .* diam) .* alpha_w; bet_n=(pi/8) .* (2 .* diam .* leng - diam .* diam) .* alpha_n; bet_s=(pi/8) .* (2 .* diam .* leng - diam .* diam) .* alpha_s; bet=bet_c + bet_e + bet_w + bet_n + bet_s; C=bet;
d1=diam; Dd1=Dddodt; dx1=leng; Ddx1=Ddxdt .* onn; Dalphadt=0.0 .* onn; Dbetf=(2.*d1.*dx1.*Dalphadt - 2.0.*d1.*alpha_c.*Dd1 - d1.*d1.*Dalphadt);
```

```
Dbet_c=DAcdt .* alpha_c + Ac .* Dalphadt; Dbet_e=(pi/8).*(Dbetf+2.*d1.*alpha_e.*Ddx1 + 2.0.*dx1.*alpha_e.*Dd1);
Dbet_w=(pi/8).*(Dbetf+2.*d1.*alpha_w.*Ddx1 + 2.0.*dx1.*alpha_w.*Dd1); Dbet_n=(pi/8).*(Dbetf+2.*d1.*alpha_n.*Ddx1 +
2.0.*dx1.*alpha_n.*Dd1); Dbet_s=(pi/8).*(Dbetf+2.*d1.*alpha_s.*Ddx1 + 2.0.*dx1.*alpha_s.*Dd1);
Dbetdt=Dbet_c+Dbet_e+Dbet_w+Dbet_n+Dbet_s;
p8=pi/8; Dvodt_c=DAcdt .* ho + Ac .* Dhodt; Dvodt_e=p8.*((2.*dx1.*ho-2.*ho.*d1).*Dd1+(2.*d1.*dx1-
d1.*d1).*Dhodt+2.*d1.*ho.*Ddx1); Dvodt_w=p8.*((2.*dx1.*ho-2.*ho.*d1).*Dd1+(2.*d1.*dx1-
d1.*d1).*Dhodt+2.*d1.*ho.*Ddx1); Dvodt_n=p8.*((2.*dx1.*ho-2.*ho.*d1).*Dd1+(2.*d1.*dx1-
d1.*d1).*Dhodt+2.*d1.*ho.*Ddx1); Dvodt_s=p8.*((2.*dx1.*ho-2.*ho.*d1).*Dd1+(2.*d1.*dx1-
d1.*d1).*Dhodt+2.*d1.*ho.*Ddx1); Dvodt=Dvodt_c+Dvodt_e+Dvodt_w+Dvodt_n+Dvodt_s;
% Assign Ak(i,k) for i=1 to 4
a1=-((1 ./ RE) + (1 ./ RN) + (1 ./ RS) + (1 ./ RW) + Dbetdt ); a2=1 ./ RW; a3=1 ./ RE; a4=1 ./ RS; a5=1 ./ RN; a6=zeros(imax);
b=zeros(imax);
iii=[1:imax]'; jjj=[1:jmax]'; ioi=ones(1,imax); joj=ones(1,jmax);
a2(1,jjj)=0.0 .* ioi; a6(1,jjj)=1.0 .* joj; b(1,1:jmax)=(1 ./ RW(1,1:jmax)) .* VV(1,2:jmax+1);
a3(imax,jjj)=0.0 .* ioi; a6(imax,jjj)=1.0 .* joj; b(imax,1:jmax)=(1 ./ RE(imax,1:jmax)) .* VV(imax+2,2:jmax+1);
a4(iii,1)=0.0 .* ioi'; a6(iii,1)=1.0 .* ioi'; b(1:imax,1)=(1 ./ RS(1:imax,1)) .* VV(2:imax+1,1);
a5(iii,jmax)=0.0 .* ioi'; a6(iii,jmax)=1.0 .* ioi'; b(1:imax,jmax)=( 1 ./ RN(1:imax,jmax)) .* VV(2:imax+1,jmax+2);
i=1; j=jmax; b(1,jmax)=(1/RN(1,jmax))*VV(2,jmax+2)+(1/RW(1,jmax))*VV(1,jmax+1);
i=imax; j=jmax; b(i,j)=(1/RN(i,j))*VV(imax+1,jmax+2)+(1/RE(i,j))*VV(imax+2,jmax+1);
i=imax; j=1; b(i,j)=(1/RE(i,j))*VV(imax+2,2)+(1/RS(i,j))*VV(imax+1,1);
i=1; j=1; b(i,j)=(1/RW(i,j))*VV(1,2)+(1/RS(i,j))*VV(2,1);
temp=Po .* Dbetdt + bet .* DPodt - Dvodt + b .* a6;
bb=reshape(temp,imax*jmax,1); CC=reshape(C,imax*jmax,1); aa1=reshape(a1,imax*jmax,1); aa2=reshape(a2,imax*jmax,1);
aa3=reshape(a3,imax*jmax,1); aa4=reshape(a4,imax*jmax,1); aa5=reshape(a5,imax*jmax,1);
MP=diag(1 ./CC); aa2=aa2(2:ijmax,1); aa3=aa3(1:ijmax-1,1); aa4=aa4(imax+1:ijmax,1); aa5=aa5(1:ijmax-imax,1); B=bb;
%THESE FORM THE DIAGONALS of the A matrix  AT1=diag(aa1);  AT2=diag(aa2,-1);  AT3=diag(aa3,1);  AT4=diag(aa4,-
4);  AT5=diag(aa5,4);  A=AT1+AT2+AT3+AT4+AT5; %END FORMING A 16x16 A MATRIX
AA=MP*A; BB=MP*B;
ydot=AA*y1+BB;
```

RR.m

```
function [RE,RW,RN,RS]=RR(hk_c,hk_e,hk_w,hk_n,hk_s,ddok,dx);
%le=ddok=diameter of post %l=dx-ddo=hor spacing between the posts at the ctr %dx=spacing between centers of posts
le=ddok; l=dx-ddok;
a=dx; b=hk_c; dh_c=hyd(a,b);
a=0.5 .* (dx+l); b=hk_e; dh_e=hyd(a,b);
a=0.5 .*(dx+l); b=hk_w; dh_w=hyd(a,b);
a=0.5 .*(dx+l); b=hk_n; dh_n=hyd(a,b);
a=0.5 .* (dx+l); b=hk_s; dh_s=hyd(a,b);
%xx=[0:dx/8.0:dx/2]; xx=[0:le/4.0:le]; %dh3 is a 4x4 matrix
dh3_e(1:4,1:4)=hyd(l(2:5,2:5),0.5*(hk_e(2:5,2:5)+hk_w(3:6,2:5)));
dh3_w(1:4,1:4)=hyd(l(2:5,2:5),0.5*(hk_w(2:5,2:5)+hk_e(1:4,2:5)));
dh3_n(1:4,1:4)=hyd(l(2:5,2:5),0.5*(hk_n(2:5,2:5)+hk_s(2:5,3:6)));
dh3_s(1:4,1:4)=hyd(l(2:5,2:5),0.5*(hk_s(2:5,2:5)+hk_n(2:5,1:4)));
func_c=integrand(dh_c); func_e=integrand(dh_e); func_w=integrand(dh_w); func_n=integrand(dh_n); func_s=integrand(dh_s);
func3_e=integrand(dh3_e); func3_w=integrand(dh3_w); func3_n=integrand(dh3_n); func3_s=integrand(dh3_s);
RC=integrand2(hk_c(2:5,2:5));
% CHECKED FOR VALIDITY WITH THE FOR_NEXT SCHEME u1=reshape(func_c(2:5,2:5),1,16);
u2=reshape(func_e(2:5,2:5),1,16); u3=reshape(func3_e(1:4,1:4),1,16); u4=reshape(func_w(3:6,2:5),1,16);
u5=reshape(func_c(3:6,2:5),1,16); fe=[u1' u2' u3' u4' u5']; %size(xx') %size(fe') RE=trapz(xx',fe');
RE=reshape(RE,4,4)+RC;
u1=reshape(func_c(2:5,2:5),1,16); u2=reshape(func_w(2:5,2:5),1,16); u3=reshape(func3_w(1:4,1:4),1,16);
u4=reshape(func_e(1:4,2:5),1,16); u5=reshape(func_c(1:4,2:5),1,16); fe=[u1' u2' u3' u4' u5']; RW=trapz(xx',fe');
RW=reshape(RW,4,4)+RC;
```

```
u1=reshape(func_c(2:5,2:5),1,16); u2=reshape(func_n(2:5,2:5),1,16); u3=reshape(func3_n(1:4,1:4),1,16);
u4=reshape(func_s(2:5,3:6),1,16); u5=reshape(func_c(2:5,3:6),1,16); fe=[u1' u2' u3' u4' u5']; RN=trapz(xx',fe');
RN=reshape(RN,4,4)+RC;
u1=reshape(func_c(2:5,2:5),1,16); u2=reshape(func_s(2:5,2:5),1,16); u3=reshape(func3_s(1:4,1:4),1,16);
u4=reshape(func_n(2:5,1:4),1,16); u5=reshape(func_c(2:5,1:4),1,16); fe=[u1' u2' u3' u4' u5']; RS=trapz(xx',fe');
RS=reshape(RS,4,4)+RC;
```

bc.m

```
function WW=bc(pin,pout,X_X,imax,jmax,t,w); VV=zeros(imax+2);
d_d=X_X';
%wp=5*w; wp=0.0; fac=1+(0.05/2)*sin(wp*t);
% BOUNDARY 4 %VV(1,:)=fac.*linear((pin+pout)/2,pin,d_d); VV(1,:)=linear(pin,pin,d_d);
% BOUNDARY 2 %VV(imax+2,:)=fac.*linear(pout,(pin+pout)/2,d_d); VV(imax+2,:)=linear(pout,pout.d_d);
d_d=X_X; %BOUNDARY 1 %VV(:,1)=fac.*linear(0.5*(pin+pout),pout,d_d); VV(:,1)=linear(pin,pout,d_d);
% BOUNDARY 3 %VV(:,jmax+2)=fac.*linear(pin,0.5*(pout+pin),d_d); VV(:,jmax+2)=linear(pin,pout,d_d);
WW=VV;
```

2.2.1 MATLAB codes for data processing and visualization.

Program to demonstrate the dynamic results: flowplot.m

```
clear all global !cv global DH_CT DH_ET DH_WT DH_NT DH_ST DH3_ET DH3_WT DH3_ST DH3_NT
rc=input('R Center ? 1=yes, 2=no') block=input('Blocked ? 1=yes, 2=no') imax=4; jmax=4; onn=ones(imax);
oonn=ones(imax+2);
ppat=path; path(ppat,'/mit/matlab/Matlab4.2/toolbox/contrib/graphics/plotyy');
X_X=[-0.5:1/(imax+2-1):0.5]';
xax=X_X; yay=X_X; mes=meshdom(xax,yay);
xax=mes; yay=mes';
load Pfv.dat Pf=Pfv; load Pv.dat; P=Pv; load tv.dat; ti=tv; load alphav.dat load hov.dat
alpha=alphav; alp=alpha./4; alp(2:5,2:5)=alp(2:5,2:5) .* 4 ./ 5; alpha=alp;
hnom=(onn+hov).*3.5; hnom6=3.5 .*oonn; hnom6(2:5,2:5)=hnom; alpha, hnom,hnom6
sst=20; kmax=length(ti);
%---------------------------- % SAMPLE THE TIME VECTOR for i=1:kmax/sst:kmax tt=ti(i); time=[time ; tt]; end %----------
----------
% For now, keep only one alpha, and not alpha_c etc etc %alpha= 0.127 .* ones(imax+2);
w=0.2*2.0*3.1416; %w=0.0;
vmean=3.5; vtidal=1.0; kk=vtidal/(2.0*vmean); kkk=(1-kk)^(1/3);
lo=75;
do=7.5 .* onn; dok=7.5 .* oonn; dnom=do; dnom6=dok;
% START MAIN CYCLE HERE
i=0; for ii=7:6:length(Pf), i=i+1; t=time(i);
PP=Pf(ii:ii+5,:); Po=-sin(w*t) .* ones(6);
% COMPUTE TOTAL LENGTH OF SHEET, L, Po,Dpodt L=(lo/kkk) .* (1 - kk .* cos(w .* t)).^(1/3); DLdt=(lo/kkk.*3).*((1 -
kk .* cos(w .* t)).^ (-2/3)) .* kk .* w .* sin(w .* t);
dx=(X_X(2)-X_X(1))*L; %LENGTH OF A SEGMENT  Ddxdt=(X_X(2)-X_X(1)).*DLdt;
ddo=(dx/15) .* (do); Dddodt=(X_X(2)-X_X(1)) .* (dok ./ 15) .* DLdt; ddok=(dx/15) .* (dok);
ho=((hnom*dnom*dnom)./ (ddo .* ddo)) .* onn; %CHANGE TO 6x6 ho=((hnom6.*dnom6.*dnom6)./ (ddok .* ddok)) .*
ones(6);
Dalphadt=0.0 .* oonn; Dhodt=(( -2*(hnom6.*dnom6.*dnom6) .* (Dddodt)) ./ (ddok .* ddok .* ddok)) .* oonn;
```

```
Ac=(dx.*oonn-ddok) .* (dx.*oonn-ddok) .* oonn; DAcdt=2.*(dx.*oonn - ddok).*(Ddxdt.*oonn - Dddodt);  h=ho+ alpha .* (PP-Po); hsave=[hsave ; h];
%plot3(xax,yay,PP','+')
hk_c=h; hk_n=h; hk_s=h; hk_e=h; hk_w=h;
[RE,RW,RN,RS]=RRflow(hk_c,hk_e,hk_w,hk_n,hk_s,ddok,dx,rc);
if (block==1) RE(2,2)=1E2; RW(3,2)=100; RN(2,2)=1E2; RS(2,3)=1E2; end
RET=[RET ; RE]; RWT=[RWT ; RW]; RNT=[RNT ; RN]; RST=[RST ; RS];
for jj=2:5, for iii=2:5,
i1=iii-1; j1=jj-1;
%QE(i1,j1)=(PP(iii,jj)-PP(iii+1,jj))./ RE(i1,j1); %QW(i1,j1)=(PP(iii,jj)-PP(iii-1,jj))./ RW(i1,j1); %QN(i1,j1)=(PP(iii,jj)-PP(iii,jj+1))./ RN(i1,j1); %QS(i1,j1)=(PP(iii,jj)-PP(iii,jj-1))./ RS(i1,j1);
QE(i1,j1)=(PP(iii,jj)-PP(iii+1,jj))./ (RE(i1,j1)); QW(i1,j1)=(PP(iii,jj)-PP(iii-1,jj))./ (RW(i1,j1)); QN(i1,j1)=(PP(iii,jj)-PP(iii,jj+1))./ (RN(i1,j1)); QS(i1,j1)=(PP(iii,jj)-PP(iii,jj-1))./ (RS(i1,j1));
end end
for jj=1:4, for iii=1:4,
ka=iii+(jj-1)*(imax); qe(ka,i)=QE(iii,jj); qw(ka,i)=QW(iii,jj); qn(ka,i)=QN(iii,jj); qs(ka,i)=QS(iii,jj); re(ka,i)=RE(iii,jj); rn(ka,i)=RN(iii,jj); hs(ka,i)=h(iii+1,jj+1); ps(ka,i)=PP(iii+1,jj+1); end end
end
m2=[11 13 15 17 29 31 33 35 47 49 51 53 65 67 69 71]; m2p=[65 67 69 71 47 49 51 53 29 31 33 35 11 13 15 17];
tit=time(1:19,1);
for i=1:1:16 ii=m2p(i);
 subplot(9,9,ii) plot(tit,ps(i,:)) set(gca,'FontName','times','FontSize',8,'LineWidth',2.5,'XTickLabels',[]) uu=get(gca,'YLim'); u1=uu(1); u3=uu(2); u2=(u1+u3)/2; u=[u1 u2 u3]; set(gca,'YTickMode','manual','YTick',u,'LineStyleOrder','--'); grid
subplot(9,9,ii+1); plot(tit,qe(i,:)); set(gca,'FontName','times','FontSize',8,'XTickLabels',[]) grid
 subplot(9,9,ii+9); plot(tit,qs(i,:)); set(gca,'FontName','times','FontSize',8,'XTickLabels',[]) grid
if (ii>=11 & ii<=17) subplot(9,9,ii-9); plot(tit,-qn(i,:)); set(gca,'FontName','times','FontSize',8,'XTickLabels',[]) grid end
end
for j=1:4:16, ii=m2p(j); subplot(9,9,ii-1); plot(tit,-qw(j,:)); set(gca,'FontName','times','FontSize',8,'XTickLabels',[]) grid end
aa=input('TEXT PLEASE','s'); [m1 m2]=ginput(1)
text(m1,m2,aa,'FontName','times','FontSize',9,'FontWeight','bold') orient landscape
```

Program to "visualize" the capillary bed with flow rates iunder static conditions:

flowmean.m

```
clear all global !cv global DH_CT DH_ET DH_WT DH_NT DH_ST DH3_ET DH3_WT DH3_ST DH3_NT
rc=input('R Center ? 1=yes, 2=no')
imax=4; jmax=4; onn=ones(imax); oonn=ones(imax+2);
ppat=path; path(ppat,'/mit/matlab/Matlab4.2/toolbox/contrib/graphics/plotyy');
X_X=[-0.5:1/(imax+2-1):0.5]';
xax=X_X; yay=X_X; mes=meshdom(xax,yay);
xax=mes; yay=mes';
load Pfv.dat Pf=Pfv; load Pv.dat; P=Pv; load tv.dat; ti=tv; load alphav.dat load hov.dat
ask=input('Blocked=1  open=2')
alpha=alphav; alp=alpha./4; alp(2:5,2:5)=alp(2:5,2:5) .* 4 ./ 5; alpha=alp;
hnom=(onn+hov).*3.5; hnom6=3.5 .*oonn; hnom6(2:5,2:5)=hnom; alpha, hnom,hnom6
sst=20; kmax=length(ti);
%---------------------------- % SAMPLE THE TIME VECTOR for i=1:kmax/sst:kmax tt=ti(i); time=[time ; tt]; end %----------
---------
% For now, keep only one alpha, and not alpha_c etc etc %alpha= 0.127 .* ones(imax+2);
%w=0.2*2.0*3.1416; w=0.0;
vmean=3.5; vtidal=1.0; kk=vtidal/(2.0*vmean); kkk=(1-kk)^(1/3);
lo=75;
```

```
do=7.5 .* onn; dok=7.5 .* oonn; dnom=do; dnom6=dok;
% START MAIN CYCLE HERE
i=0; for ii=7:6:length(Pf), i=i+1; t=time(i);
PP=Pf(ii:ii+5,:); Po=-sin(w*t) .* ones(6);
% COMPUTE TOTAL LENGTH OF SHEET, L, Po,Dpodt L=(lo/kkk) .* (1 - kk .* cos(w .* t)).^(1/3); DLdt=(lo/kkk.*3).*((1 -
kk .* cos(w .* t)).^ (-2/3)) .* kk .* w .* sin(w .* t);
dx=(X_X(2)-X_X(1))*L; %LENGTH OF A SEGMENT  Ddxdt=(X_X(2)-X_X(1)).*DLdt;
ddo=(dx/15) .* (do); Dddodt=(X_X(2)-X_X(1)) .* (dok ./ 15) .* DLdt; ddok=(dx/15) .* (dok);
ho=((hnom*dnom*dnom)./ (ddo .* ddo)) .* onn; %CHANGE TO 6x6 ho=((hnom6.*dnom6.*dnom6)./ (ddok .* ddok)) .*
ones(6);
Dalphadt=0.0 .* oonn; Dhodt=(( -2*(hnom6.*dnom6.*dnom6) .* (Dddodt)) ./ (ddok .* ddok .* ddok)) .* oonn;
Ac=(dx.*oonn-ddok) .* (dx.*oonn-ddok) .* oonn; DAcdt=2.*(dx.*oonn - ddok).*(Ddxdt.*oonn - Dddodt);   h=ho+ alpha .* (PP-
Po); hsave=[hsave ; h];
%plot3(xax,yay,PP','+')
hk_c=h; hk_n=h; hk_s=h; hk_e=h; hk_w=h;
[RE,RW,RN,RS]=RRflow(hk_c,hk_e,hk_w,hk_n,hk_s,ddok,dx,rc);
if (ask==1)  RE(2,2)=1E2; RW(3,2)=100; RN(2,2)=1E2; RS(2,3)=1E2; end
RET=[RET ; RE]; RWT=[RWT ; RW]; RNT=[RNT ; RN]; RST=[RST ; RS];
for jj=2:5, for iii=2:5,  i1=iii-1;  j1=jj-1;  QE(i1,j1)=(PP(iii,jj)-PP(iii+1,jj))./ (RE(i1,j1));  QW(i1,j1)=(PP(iii,jj)-PP(iii-1,jj))./
(RW(i1,j1));  QN(i1,j1)=(PP(iii,jj)-PP(iii,jj+1))./ (RN(i1,j1));  QS(i1,j1)=(PP(iii,jj)-PP(iii,jj-1))./ (RS(i1,j1));
DPE(i1,j1)=(PP(iii,jj)-PP(iii+1,jj));  DPW(i1,j1)=(PP(iii,jj)-PP(iii-1,jj));  DPN(i1,j1)=(PP(iii,jj)-PP(iii,jj+1));
DPS(i1,j1)=(PP(iii,jj)-PP(iii,jj-1)); end end
for jj=1:4, for iii=1:4,
ka=iii+(jj-1)*(imax);
 qe(ka,i)=QE(iii,jj);  qw(ka,i)=QW(iii,jj);  qn(ka,i)=QN(iii,jj);  qs(ka,i)=QS(iii,jj);
qc(ka,i)=QE(iii,jj)+QW(iii,jj)+QN(iii,jj)+QS(iii,jj);
 re(ka,i)=RE(iii,jj);  rn(ka,i)=RN(iii,jj);  hs(ka,i)=h(iii+1,jj+1);  ps(ka,i)=PP(iii+1,jj+1);
 dps(ka,i)=DPS(iii,jj);  dpn(ka,i)=DPN(iii,jj);  dpe(ka,i)=DPE(iii,jj);  dpw(ka,i)=DPW(iii,jj);
end end
end
m2=[11 13 15 17 29 31 33 35 47 49 51 53 65 67 69 71]; tit=time(1:19,1);
for jj=1:4, for ii=1:4,
k=ii+(jj-1)*4;
hm(ii,jj)=mean(hs(k,:)); pm(ii,jj)=mean(ps(k,:)); qem(ii,jj)=mean(qe(k,:)); qwm(ii,jj)=mean(qw(k,:)); qnm(ii,jj)=mean(qn(k,:));
qsm(ii,jj)=mean(qs(k,:)); qcm(ii,jj)=mean(qc(k,:));
end end
H=[]; for j=1:4 for i=1:4 a1=abs(qwm(i,j)); a3=abs(qnm(i,j)); a4=abs(qem(i,j)); a5=abs(qsm(i,j)); a6=0000.00; a2=mean([a1 a3
a4 a5]);
%a1=a1/abs(a1); %a2=a2/abs(a2); %a3=a3/abs(a3); %a4=a4/abs(a4); %a5=a5/abs(a5); %a6=0.0;
%a1=pm(i,j); %a3=pm(i,j); %a4=a1; %a5=a1; %a6=4.2; %a2=pm(i,j);
B=[ a1 a1 a2 a2   a1 a1 a2 a2   a6 a6 a3 a3   a6 a6 a3 a3]; if i==4 B=[a1 a1 a2 a2 a4 a4   a1 a1 a2 a2 a4 a4   a6 a6 a3 a3 a6 a6
a6 a6  a3 a3 a6 a6]; end if j==4 B=[a6 a6 a5 a5   a6 a6 a5 a5   a1 a1 a2 a2   a1 a1 a2 a2   a6 a6 a3 a3   a6 a6 a3 a3 ]; if i==4
B=[a6 a6 a5 a5  a6 a6   a6 a6 a5 a5  a6 a6   a1 a1 a2 a2 a4  a4   a1 a1 a2 a2 a4  a4   a6 a6 a3 a3 a6  a6   a6 a6 a3 a3 a6  a6];
end end M=[ M  B]; end H= [ M ; H]; M=[] end x22=1:18; y22=1:18; x11=0:.4:20; y11=0:.4:20; [X1,Y1]=meshgrid(x11,y11);
Z1=interp2(x22,y22,H,X1,Y1,'linear');
%subplot(2,1,1)
figure(1) ll=0:1/17:1; pcolor(ll,ll,H); shading interp colormap(hot(128)) set(gca,'FontName','times','FontSize',10)
set(gca,'XTick',[],'YTick',[]) mm=get(colorbar,'Ylim'); ma=mm(2); colorbar set(colorbar,'FontName','times','Fon-
tSize',10,'Ylim',[0 ; ma])
nn=length(Z1)
%subplot(2,1,2) %surfl(Z1) %shading interp %colormap(hot) %grid
%title('Time-averaged Volume flowrate (magnitude): Sample run')
figure(2) mm=input('Fig Number'); subplot(3,3,mm) pcolor(ll,ll,H); shading interp colormap(hot(128)) set(gca,'Font-
Name','times','FontSize',10) %mm=get(colorbar,'Ylim'); %ma=mm(2); colorbar %set(colorbar,'FontName','times','Fon-
tSize',9,'Ylim',[0 ; ma]) set(gca,'XTick',[],'YTick',[]) hold
```

Program to compute the statistical distributions in the flows: flow_hist.m

```
clear all global !cv global DH_CT DH_ET DH_WT DH_NT DH_ST DH3_ET DH3_WT DH3_ST DH3_NT
rc=input('R Center ? 1=yes, 2=no')
imax=4; jmax=4; onn=ones(imax); oonn=ones(imax+2);
ppat=path; path(ppat,'/mit/matlab/Matlab4.2/toolbox/contrib/graphics/plotyy');
X_X=[-0.5:1/(imax+2-1):0.5]';
xax=X_X; yay=X_X; mes=meshdom(xax,yay);
xax=mes; yay=mes';
load Pfv.dat Pf=Pfv; load Pv.dat; P=Pv; load tv.dat; ti=tv; load alphav.dat load hov.dat
alpha=alphav; alp=alpha./4; alp(2:5,2:5)=alp(2:5,2:5) .* 4 ./ 5; alpha=alp;
hnom=(onn+hov).*3.5; hnom6=3.5 .*oonn; hnom6(2:5,2:5)=hnom; alpha, hnom,hnom6
sst=20; kmax=length(ti);
%---------------------------- % SAMPLE THE TIME VECTOR for i=1:kmax/sst:kmax tt=ti(i); time=[time ; tt]; end %----------
----------
% For now, keep only one alpha, and not alpha_c etc etc %alpha= 0.127 .* ones(imax+2);
%w=0.2*2.0*3.1416; w=0.0;
vmean=3.5; vtidal=1.0; kk=vtidal/(2.0*vmean); kkk=(1-kk)^(1/3);
lo=75;
do=7.5 .* onn; dok=7.5 .* oonn; dnom=do; dnom6=dok;
% START MAIN CYCLE HERE
i=0; for ii=7:6:length(Pf), i=i+1; t=time(i);
PP=Pf(ii:ii+5,:); Po=-sin(w*t) .* ones(6);
% COMPUTE TOTAL LENGTH OF SHEET, L, Po,Dpodt L=(lo/kkk) .* (1 - kk .* cos(w .* t)).^(1/3); DLdt=(lo/kkk.*3).*((1 -
kk .* cos(w .* t)).^ (-2/3)) .* kk .* w .* sin(w .* t);
dx=(X_X(2)-X_X(1))*L; %LENGTH OF A SEGMENT  Ddxdt=(X_X(2)-X_X(1)).*DLdt;
ddo=(dx/15) .* (do); Dddodt=(X_X(2)-X_X(1)) .* (dok ./ 15) .* DLdt; ddok=(dx/15) .* (dok);
ho=((hnom*dnom*dnom)./ (ddo .* ddo)) .* onn; %CHANGE TO 6x6 ho=((hnom6.*dnom6.*dnom6)./ (ddok .* ddok)) .*
ones(6);
Dalphadt=0.0 .* oonn; Dhodt=(( -2*(hnom6.*dnom6.*dnom6) .* (Dddodt)) ./ (ddok .* ddok .* ddok)) .* oonn;
Ac=(dx.*oonn-ddok) .* (dx.*oonn-ddok) .* oonn; DAcdt=2.*(dx.*oonn - ddok).*(Ddxdt.*oonn - Dddodt);   h=ho+ alpha .* (PP-
Po); hsave=[hsave ; h];
%plot3(xax,yay,PP','+')
hk_c=h; hk_n=h; hk_s=h; hk_e=h; hk_w=h;
[RE,RW,RN,RS]=RRflow(hk_c,hk_e,hk_w,hk_n,hk_s,ddok,dx,rc);
%RE(2,2)=1E2; %RW(3,2)=100; %RN(2,2)=1E2; %RS(2,3)=1E2;
RET=[RET ; RE]; RWT=[RWT ; RW]; RNT=[RNT ; RN]; RST=[RST ; RS];
for jj=2:5, for iii=2:5, i1=iii-1; j1=jj-1; QE(i1,j1)=(PP(iii,jj)-PP(iii+1,jj))./ (RE(i1,j1)); QW(i1,j1)=(PP(iii,jj)-PP(iii-1,jj))./
(RW(i1,j1)); QN(i1,j1)=(PP(iii,jj)-PP(iii,jj+1))./ (RN(i1,j1)); QS(i1,j1)=(PP(iii,jj)-PP(iii,jj-1))./ (RS(i1,j1));
DPE(i1,j1)=(PP(iii,jj)-PP(iii+1,jj)); DPW(i1,j1)=(PP(iii,jj)-PP(iii-1,jj)); DPN(i1,j1)=(PP(iii,jj)-PP(iii,jj+1));
DPS(i1,j1)=(PP(iii,jj)-PP(iii,jj-1)); end end
for jj=1:4, for iii=1:4,
ka=iii+(jj-1)*(imax);
 qe(ka,i)=abs(QE(iii,jj)); qw(ka,i)=abs(QW(iii,jj)); qn(ka,i)=abs(QN(iii,jj)); qs(ka,i)=abs(QS(iii,jj));
qc(ka,i)=abs(QE(iii,jj)+QW(iii,jj)+QN(iii,jj)+QS(iii,jj));
 re(ka,i)=RE(iii,jj); rn(ka,i)=RN(iii,jj); hs(ka,i)=h(iii+1,jj+1); ps(ka,i)=PP(iii+1,jj+1);
 dps(ka,i)=DPS(iii,jj); dpn(ka,i)=DPN(iii,jj); dpe(ka,i)=DPE(iii,jj); dpw(ka,i)=DPW(iii,jj);
end end
end
tit=time(1:19,1);
for jj=1:4, for ii=1:4,
k=ii+(jj-1)*4;
hm(ii,jj)=mean(hs(k,:)); pm(ii,jj)=mean(ps(k,:)); qem(ii,jj)=mean(qe(k,:)); qwm(ii,jj)=mean(qw(k,:)); qnm(ii,jj)=mean(qn(k,:));
qsm(ii,jj)=mean(qs(k,:)); qcm(ii,jj)=mean(qc(k,:));
end end
```

```
HE=[]; for jj=1:4, for ii=1:4,
a=qem(ii,jj); b=qnm(ii,jj);
ME=[a b]; HE=[ HE  ME]; end end
for ii=1:4 jj=1; ME=qsm(ii,jj); HE=[HE ME]; end
for jj=1:4 ii=1; ME=qwm(ii,jj); HE=[HE ME]; end
size(HE)
mea=mean(HE) st=std(HE) va=st/mea
```

"Dynamic visualization" of the flow-rates in the septum: flowmovie.m

```
clear all global clear  !cv global DH_CT DH_ET DH_WT DH_NT DH_ST DH3_ET DH3_WT DH3_ST DH3_NT
rc=input('R Center ? 1=yes, 2=no')
imax=4; jmax=4; onn=ones(imax); oonn=ones(imax+2);
%ppat=path; %path(ppat,'/mit/matlab/Matlab4.2/toolbox/contrib/graphics/plotyy');
X_X=[-0.5:1/(imax+2-1):0.5]'; xax=X_X; yay=X_X; mes=meshdom(xax,yay);
xax=mes; yay=mes';
load Pfv.dat Pf=Pfv; load Pv.dat; P=Pv; load tv.dat; ti=tv; load alphav.dat load hov.dat
%hov=zeros(4); alpha=alphav; alp=alpha./4; alp(2:5,2:5)=alp(2:5,2:5) .* 4 ./ 5; alpha=alp;
hnom=(onn+hov).*3.5; hnom6=3.5 .*oonn; hnom6(2:5,2:5)=hnom; alpha, hnom,hnom6
sst=20; kmax=length(ti); Moo=[]; Moo=moviein(sst-1); %---------------------------- % SAMPLE THE TIME VECTOR for
i=1:kmax/sst:kmax tt=ti(i); time=[time ; tt]; end %----------------------------
% For now, keep only one alpha, and not alpha_c etc etc %alpha= 0.127 .* ones(imax+2);
w=0.2*2.0*3.1416; %w=0.0;
vmean=3.5; vtidal=1.0; kk=vtidal/(2.0*vmean); kkk=(1-kk)^(1/3);
lo=75;
do=7.5 .* onn; dok=7.5 .* oonn; dnom=do; dnom6=dok;
% START MAIN CYCLE HERE
i=0; for ii=7:6:length(Pf), i=i+1; t=time(i);
PP=Pf(ii:ii+5,:); Po=-sin(w*t) .* ones(6);
% COMPUTE TOTAL LENGTH OF SHEET, L, Po,Dpodt L=(lo/kkk) .* (1 - kk .* cos(w .* t)).^(1/3); DLdt=(lo/kkk.*3).*((1 -
kk .* cos(w .* t)).^ (-2/3)) .* kk .* w .* sin(w .* t);
dx=(X_X(2)-X_X(1))*L; %LENGTH OF A SEGMENT  Ddxdt=(X_X(2)-X_X(1)).*DLdt;
ddo=(dx/15) .* (do); Dddodt=(X_X(2)-X_X(1)) .* (dok ./ 15) .* DLdt; ddok=(dx/15) .* (dok);
ho=((hnom*dnom*dnom)./ (ddo .* ddo)) .* onn; %CHANGE TO 6x6 ho=((hnom6.*dnom6.*dnom6)./ (ddok .* ddok)) .*
ones(6);
Dalphadt=0.0 .* oonn; Dhodt=(( -2*(hnom6.*dnom6.*dnom6) .* (Dddodt)) ./ (ddok .* ddok .* ddok)) .* oonn;
Ac=(dx.*oonn-ddok) .* (dx.*oonn-ddok) .* oonn; DAcdt=2.*(dx.*oonn - ddok).*(Ddxdt.*oonn - Dddodt);   h=ho+ alpha .* (PP-
Po); hsave=[hsave ; h];
%plot3(xax,yay,PP','+')
hk_c=h; hk_n=h; hk_s=h; hk_e=h; hk_w=h;
[RE,RW,RN,RS]=RRflow(hk_c,hk_e,hk_w,hk_n,hk_s,ddok,dx,rc);
RE(2,2)=1E2; RW(3,2)=100; RN(2,2)=1E2; RS(2,3)=1E2;
for jj=2:5, for iii=2:5, i1=iii-1; j1=jj-1; QE(i1,j1)=(PP(iii,jj)-PP(iii+1,jj))./ (RE(i1,j1)); QW(i1,j1)=(PP(iii,jj)-PP(iii-1,jj))./
(RW(i1,j1)); QN(i1,j1)=(PP(iii,jj)-PP(iii,jj+1))./ (RN(i1,j1)); QS(i1,j1)=(PP(iii,jj)-PP(iii,jj-1))./ (RS(i1,j1));
DPE(i1,j1)=(PP(iii,jj)-PP(iii+1,jj)); DPW(i1,j1)=(PP(iii,jj)-PP(iii-1,jj)); DPN(i1,j1)=(PP(iii,jj)-PP(iii,jj+1));
DPS(i1,j1)=(PP(iii,jj)-PP(iii,jj-1)); end end
H=[];
for jj=1:4 for ii=1:4
a1=abs(QW(ii,jj)); a3=abs(QN(ii,jj)); a4=abs(QE(ii,jj)); a5=abs(QS(ii,jj)); a6=0.0; a2=mean([a1 a3 a4 a5]);
B=[a1 a1 a2 a2;   a1 a1 a2 a2;   a6 a6 a3 a3;   a6 a6 a3 a3 ]; if ii==4 B=[a1 a1 a2 a2 a4 a4;   a1 a1 a2 a2 a4 a4;   a6 a6 a3 a3 a6
a6;   a6 a6 a3 a3 a6 a6]; end if jj==4 B=[a6 a6 a5 a5;   a6 a6 a5 a5;   a1 a1 a2 a2;   a1 a1 a2 a2;   a6 a6 a3 a3;   a6 a6 a3 a3]; end
if (ii+jj==8) B=[a6 a6 a5 a5 a6 a6;   a6 a6 a5 a5 a6 a6;   a1 a1 a2 a2 a4 a4;   a1 a1 a2 a2 a4 a4;   a6 a6 a3 a3 a6 a6;   a6 a6 a3 a3
a6 a6]; end  M=[ M  B]; end H= [ M ; H]; M=[]; end
ll=0:1/17:1; pcolor(ll,ll,H); caxis([0 19000]) colorbar shading interp colormap(hot) set(gca,'FontName','times','FontSize',10)
logo; Moo(:,i)=getframe;
```

```
end
```

References

[1] Ambrus, C. M., J. L. Ambrus, G. C. Johnson, E. W. Packman, W. S. Chernick, N. Back, and J.W.E. Harrison. Role of the lungs in the regulation of the white blood cell level. Am. J. Physiol. 178:33-34, 1954.

[2] Barnard, A. C. L., Lopez, L., and Hellums, J. D. (1968). Basic theory of blood flow in capillaries. *Microvascular Research.* **1**: 23-24.

[3] Bhattacharya J. Lung microvascular pressure profile. New kid on the block [editorial]. *American Review of Respiratory Disease.*Nov 1986. **134** (5):pp854-5.

[4] Bhattacharya J., Staub N. C. Direct measurement of microvascular pressure in the isolated perfused dog lung. *Science 1980*; **210**:327-8.

[5] Crystal, R.G., West, J. B. The Lung: Scientific Foundations. Raven Press, 1991.

[6] Doerschuk, C. M., M. F. Allard, B. A. Martin, A. MacKenzie, and J. C. Hogg. Marginated pool of neutrophils in lungs of rabbits. J. Appl Physiol. 63:1806-1815, 1987.

[7] Doerschuk C. M., McLean T, Martin BA, MacKenzie A, Hogg J. C.(1987) Marginated pool of neutrophils in lungs of rabbits. *Journal of Appl Physiology.***63**:1806-1815.

[8] Doerschuk CM, Beyers N, Coxson HO, Wiggs B, Hogg JC (1993).Comparison of neutrophil and capillary diameters and their relation to neutrophil sequestration in the lung. *Journal Of Applied Physiology.***74**: 3040-3045.

[9] Downey GP, Worthen GS. 1988. Neutrophil retention in model capillaries: deformability, geometry, and hydrodynamic forces. *J Appl Physiology.* **65**:1861-1871.

[10] Fahraeus, R. and Lindqvist, T. (1931) The viscosity of the blood innarrow capillary tubes. *American Journal Of Physiology.* **96**:562-568.

[11] Fung, Y. C.(1969). Studies on the blood flow in the lung. In *Proceedings of the Second Canadian Congress of Applied Mechanics*, Waterloo, Canada, pp. 443-545.

[12] Fung, Y. C.(1984). *Biodynamics: Circulation.* Springer-Verlag, New York.

[13] Fung, Y. C.(1969). Theory of sheet flow in lung alveoli. *J. Appl. Physiology.* **26**(4):472-488

[14] Fung, Y. C. and Sobin, S. S. (1972a). Elasticity of the pulmonary alveolar sheet. *Circ. Res.* **30**:451-469.

[15] Fung, Y. C. and Sobin, S. S. (1972b). Pulmonary Alveolar blood flow. *Circ Res.* **30**:470-490.

[16] Hakim, T. S., Michel, R. P., and Chang, H. K. (1982). Partition of pulmonary vascular resistance in dog by arterial and venous occlusion. *J. Appl. Physiol.: Respirat. Environ. Excercise Physiol.* **52:** 710-715.

[17] Halpern, D. and Secomb, T. W. (1989) The sqeezing of red blood cells through capillaries with near-minimal diameters. *J. Fluid Mech.* **203**, 381-400.

[18] Hanger, C. C., W. W. Wagner, Jr., S. J. Janke, T. C. Lloyd, Jr., and R. L Capen. Computer simulation of neutrophil transit through the pulmonary capillary bed. *J. Appl Physiol.* **74**: 1647-1652, 1993.

[19] Hogg J.C.(1987). Neutrophil kinetics and lung injury. *Physiol Review.* **67**:1249-1295.

[20] Hogg J. C., McLean T, Martin B.A., Wiggs B (1988). Erythrocyte transit and neutrophil concentration in the dog lung. *J. Appl Physiology.* **65**:1217-1225.

[21] Johnson, R. L., Jr., J. M. Miller. Distribution of ventilation, blood flow, and gas transfer coefficients in the lung. *J. Appl Physiology.* **25:**1-15, 1968.

[22] Kadowitz P. J., Joiner P. D., Hyman A. L. Influence of sympathetic stimulation and vasoactive substances on the canine pulmonary veins. *Journal of clinical investigation 1975*; 56:354-65.

[23] Kiani M. F., Cokelet. G. R., Sarelius I. H. Effect of diameter variability along a microvessel segment on pressure drop. Microvascular Research **45**, 219-232 (1993).

[24] Kiani, M. and Hudetz, A. (1991). *Biorheology.* **28**:65-73.

[25] Lee. J. S. (1969) Slow viscous flow in a lung alveoli model. *J. Biomechanics.* **2**: 187-198.

[26] Lee. J. S. and Fung, Y. C. (1968). Experiments on blood flow in lung alveoli models. Paper No. 68-WA/BHF-2, American Society of Mech. Engineers. pp. 1-8.

[27] Lee, J. S. & Fung, Y. C. 1969. *J. of Fluid Mechanics.* **37**, 657.

[28] Lien, D. C., W. W. Wagner, Fr., R. L. Capen, C. Haslett, W. L. Hanson, S. E. Hofmeister, P. M. Henson, and G. S. Worthen. Physiologic neutrophil sequestration in the canine pulmonary circulation. *J. Appl. Physiol.* **62**:1236-1243, 1987.

[29] Lien, D. C., G. S. Worthen, R. L. Capen, W. L. hanson, L. L. Checkley, S. J. Janke, P. M. Henson, and W. W. Wagner, Jr. Neutrophil kinetics in the pulmonary microcirculation. Am. Rev. Respir. Dis. **141**: 953-959, 1990.

[30] Lighthill, M. J. (1968). Pressure-forcing of tightly fitting pellets along fluid filled elastic tubes, *J. Fluid Mechanics.* **34**, 113-143.

[31] Martini, P., Pierach, A., and Schreyer, E. (1930) Die Stromung des blutes in engen Gefassen. Eine Abweichung vom Poiseulle'schen Gesetz. *Dtsch. Arch. Klin. Med.* **169**, 212-222.

[32] Needham D, Hochmuth RM.1990. Rapid flow of passive neutrophils into a 4 micron pipet.and measurement of cytoplasmic viscosity. *Journal Of Biomechanic Engineering.* **112**: 269-276.

[33] Permutit, S., Caldini, P., Maseri, A., Palmer, W.H., Sasamori, T., and Zierler, K. L.: Recruitment vs distensibility in the pulmonary vascular bed. *In* The Pulmonary Circulation and Interstitial Space, edited by A. Fishman and H. Hecht. Chicago, University of Chicago Press, 1968, pp 327-338.

[34] Popel AS. 1987. Network Models of peripheral circulation. In *Handbook of Bioengineering* (ed. R. Skalak and S. Chien), pp. 20.1-20.24. New York: McGraw Hill

[35] Pries, A. R., Secomb, T.W., Gaehtgens, P., Gross J.F. (1990) Blood flow in microvascular networks - Experiments and simulation. *Circ Res.* **67**: 826-834.

[36] Pries, A. R, Ley, K., Claasen, M. and Gaehtgens, P. (1989) Red cell distribution at microvascular bifurcations. *Microvascular Research.* **38**, 81-101.

[37] Sangani, A. S. & Acrivos, A. 1982. *Intl Journal of Multiphase Flow.* **8**, 193.

[38] Schmid-Schnobein, G. W, Usami S., Skalak R., Chien S. (1980). Interaction of Leukocytes and erythrocytes in capillary and post-capillary vessels. *Microvasc Res.* **19**:45-70.

[39] Schmid-Schonbein, G. W., Skalak, R., Usami, S. and Chien, S. (1980) Cell distribution in capillary networks. *Microvascular Research.* **19**, 18-44.

[40] Secomb, T. W. (1991) Red Blood cell mechanics and capillary blood rheology. *Cell Biophysics* **18**:231-251.

[41] Secomb, T. W. (1994) Mechanics of blood flow in microcirculation. Biological Fluid Dynamics.

[42] Secomb, T. W. and Gross, J. F. (1983). Flow of red blood cells in narrow capillaries: role of membrane tension. *Int. J. Microcirc. Clin. Exp.* **2**, 229-240., J.

[43] Secomb, T. W., Skalak, R Ozkaya, N., and Gross, J. F. (1986) Flow of axisymetric red blood cells in narrow capillaries, *J. Fluid Mech.* **163**: 405-423

[44] R.-Y. Tsay & S. Weinbaum. Viscous flow in a channel with periodic cross-bridging fibres: exact solutions and Brinkman approximation (1991). *Journal of Fluid Mechanics.* **226**: 125-148.

[45] Wagner W. W., Jr., Latham L. P., Hanson. W. L. *J. Appl Physiology.* 61(4): 1270-1274, 1986..

[46] West, J.B. Respiratory Physiology-the essentials. The Williams and Wilkins Co., 1974.

[47] Wiggs BR, English D, Quinlan WM, Doyle NA, Hogg JC, Doerschuk CM.(1994). The contributions of capillary pathway size and neutrophil deformability to neutrophil transit through Rabbit Lungs. *Journal of Applied Physiology.***77**: 463-470.

[48] Yen, R. T. and Sobin, S. S. (1988). Elasticity of arterioles and venules in postmortem human lungs. *Journal of Applied Physiology.* **64**(2): 611-619.

[49] Zarda, P. R., Chien, S., and Skalak, R. (1977). Interaction of viscous incompressible fluid with elastic body, Computational methods for Fluid-Solid interaction Problems, Belytschko, T. and Geers, T. L., eds., American Society of Mechanical Engineers, New York, pp 65-82.